Assessment and Control of Voltage in Active Distribution Networks

A Thesis Submitted

in Partial Fulfilment of the Requirements

for the Degree of

DOCTOR OF PHILOSOPHY

by

Digamber Kumar

(2018EEZ0002)



DEPARTMENT OF ELECTRICAL ENGINEERING INDIAN INSTITUTE OF TECHNOLOGY ROPAR

July, 2024

Digamber Kumar: Assessment and Control of Voltage Stability in Active Distribution Networks Copyright ©2024 Indian Institute of Technology Ropar All Rights Reserved

Dedicated to My Family and Friends

Declaration of Originality

I hereby declare that the work which is being presented in the thesis entitled Assessment and Control of Voltage Stability in Active Distribution Networks has been solely authored by me. It presents the result of my independent investigation/research conducted during the period from July 2018 to July 2024 under the supervision of Dr. Bibhu Prasad Padhy, Assistant Professor, IIT Ropar. To the best of my knowledge, it is an original work, both in terms of research content and narrative, and has not been submitted or accepted elsewhere, in part or in full, for the award of any degree, diploma, fellowship, associateship, or similar title of any university or institution. Further, due credit has been attributed to the relevant state-of-the-art and collaborations with appropriate citations and acknowledgments, in line with established ethical norms and practices. I also declare that any idea/data/fact/source stated in my thesis has not been fabricated/ falsified/ misrepresented. All the principles of academic honesty and integrity have been followed. I fully understand that if the thesis is found to be unoriginal, fabricated, or plagiarized, the Institute reserves the right to withdraw the thesis from its archive and revoke the associated Degree conferred. Additionally, the Institute also reserves the right to appraise all concerned sections of society of the matter for their information and necessary action. If accepted, I hereby consent for my thesis to be available online in the Institute's Open Access repository, inter-library loan, and the title & abstract to be made available to outside organizations.

Signature Signature

Name: Digamber Kumar Entry Number: 2018EEZ0002

Program: PhD

Department: Electrical Engineering Indian Institute of Technology Ropar

Rupnagar, Punjab 140001

August, 2024

Acknowledgement

I would like to extend my sincere gratitude to my thesis supervisor, Dr. Bibhu Prasad Padhy, without whose valuable guidance, persistent support, and encouragement throughout my Ph.D journey, the thesis would not have been completed. I am deeply grateful for his stronghold on research concepts, crucial advice, and kindness towards me and my family. These have been the key pillars to form the foundation upon which my thesis rests. I profoundly appreciate the administration of the Indian Institute of Technology, Ropar, for offering a great opportunity, conducive research infrastructure, and institute fellowship to smoothly accomplish my Ph.D research program. I wish to express my heartfelt appreciation to my respected teachers as well as Doctoral Committee (DC) members Dr. C.C. Reddy (Chair Person), Dr. Ranjana Sodhi, Dr. Jyotindra Singh Sahambi, and Dr. Rakesh Kumar Maurya for their valuable suggestions and timely support. I deeply acknowledge the continuous support and consistent motivation throughout my journey furnished by Dr. Ancha Satish Kumar, Balakrushna Sahu, Subal Beura, Sourav De, Dr. Baibhay Kumar Gupta, Dr. Mehtab Alam, Amol Ishwarrao Gedam, Aasish Kumar, Nikhil kumar, Surya Kiran, Dr. Vaibhav Shah, Mahesh Pundru, Ritesh Kumar, Manish Kumar, Dr. Samareet singh Dr. Manish Kumar, Dr. Shitikanth dash, and many more. I am grateful to all those who have provided support, both directly and indirectly, throughout this endeavor. I am immensely thankful to my parents Sri Ramnaresh Choudhary and Smt. Baby choudhary, my brother Mr. Nilamber Kumar, sister Mrs. Sweta Sawarn, Sister in law Neha Choudhary, Brother in law Birendra Mohan Choudhary nephews for their selfless support, trust, and prayer. At last, my special thanks go to my sweet and beloved nieces Anika and Aditi, whose infectious smile and unconditional love have been my source of strength and refreshment throughout my Ph.D endeavor.

> Digamber Kumar #210, Electrical Department, JC Bose Block Electrical Engineering Indian Institute of Technology Ropar Rupnagar, Punjab 140001 August, 2024

Certificate

This is to certify that the thesis entitled Assessment and Control of Voltage Stability in Active Distribution Networks, submitted by Digamber kumar (2018EEZ0002) for the award of the degree of Doctor of Philosophy of Indian Institute of Technology Ropar, is a record of bonafide research work carried out under my guidance and supervision. To the best of my knowledge and belief, the work presented in this thesis is original and has not been submitted, either in part or full, for the award of any other degree, diploma, fellowship, associateship or similar title of any university or institution.

In my opinion, the thesis has reached the standard fulfilling the requirements of the regulations relating to the Degree.

Signature of the Supervisor

Dr. Bibhu Prasad Padhy Electrical Engineering

Indian Institute of Technology Ropar

Rupnagar, Punjab 140001

August, 2024

Abstract

As the economy grows, power demand increases accordingly. However, meeting this demand through traditional generation methods is becoming increasingly impractical due to high capital costs, significant transmission expenses and losses, declining fossil fuel reserves, and growing environmental concerns. Renewable-Based Distributed Generation (RBDG) is emerging as the optimal solution. Historically, conventional energy sources accounted for 76% of global power generation, while renewable energy contributed 24%. By 2050, projections indicate a dramatic shift, with RBDGs expected to supply 85% of global power, leaving conventional sources at just 15%. Additionally, the rise of Electric Vehicles (EVs) is driving the expansion of charging infrastructure within distribution networks, boosted by advances in battery energy storage systems. Previously, RBDGs operated at a unity power factor without the capability to control active or reactive power, limiting their ability to manage network voltage profiles. While reinforcing the network with reactive power-compensating devices is a straightforward solution, it is costly. On-Load Tap Changers (OLTC) offer another option, but their limited range and slow response time, along with their inability to handle bidirectional power flow, reduce their effectiveness in active distribution networks. With advancements in power electronic inverter technology, RBDGs can now regulate both active and reactive power, helping maintain network voltage profiles.

Active Power Curtailment (APC) and Reactive Power Compensation (RPC) are common strategies for RBDG inverters to manage voltage issues. However, arbitrarily selecting RBDGs for voltage control is not economically optimal. Thus, evaluating the impact of RBDGs on bus voltage is crucial for developing fast and dynamic voltage control strategies. These strategies are classified into centralized and decentralized control. Decentralized control is preferred over centralized control due to better economic efficiency. In decentralized voltage control, coordination with devices like OLTCs, voltage regulators, and reactive power compensators is necessary. Therefore, a hierarchical voltage control approach is adopted and implemented in multiple stages. In the primary stage, optimal settings for voltage-controlling devices are planned based on the stochastic nature of loads and generation. Subsequently, decentralized control using DGs is carried out.

The increasing integration of RBDGs affects the network's voltage profile and reduces its Hosting Capacity (HC) due to their stochastic characteristics. Battery Energy Storage Systems (BESS) help mitigate these effects through their charging and discharging capabilities. Distribution networks typically include small (residential), medium (community), and large-scale BESS. Larger BESS offer a higher benefit-cost ratio for enhancing the network's HC. However, optimizing the placement of large BESS is challenging due to varying impacts of power fluctuations from RBDGs depending on their size and location. The Sobol sensitivity index is used to identify the most influential RBDGs in the network. Installing BESS with the most dominant RBDG helps improve HC. By optimally managing the BESS charging and discharging profiles and tuning voltage control parameters, the network's HC is further enhanced.

Keywords: Keywords 1;Centralized voltage 2;decentralized voltage control 3;differential entropy 4; renewable based distribted generation 5;state-based probabilistic model 6; probabilistic voltage sensitivity index

Contents

D	eclar	ation		iv
A	ckno	wledge	ement	\mathbf{v}
\mathbf{C}	ertifi	cate		vi
A	bstra	ıct		vii
Li	st of	Figur	res	xiii
Li	st of	Table	es s	xvii
1	Intr	oduct	ion	1
	1.1	Introd	luction	1
		1.1.1	General	1
		1.1.2	Active Distribution Networks	1
		1.1.3	Motivation	1
		1.1.4	Literature Review	4
		1.1.5	Voltage control techniques	5
		1.1.6	Hierarchical voltage control	7
		1.1.7	Hosting capacity of the network	8
		1.1.8	Organization of the Thesis	9
2	Pro	babilis	stic Approach to Investigate the Impact of Distributed Generation o	\mathbf{n}
	Vol	tage D	Deviation in Distribution System	13
	2.1	Introd	luction	13
	2.2	Backg	ground	14
		2.2.1	Traditional method for voltage sensitivity using Monte-Carlo Simulation	
			(MCS)	14
		2.2.2	Analytic method for voltage sensitivity	15
	2.3		ulation of $PVSI$ using PCA	17
	2.4	Case	Study and Discussion	21
		2.4.1	Change in active power at multiple buses	22
		2.4.2	Change in reactive power at multiple buses	26
		2.4.3	Change in active and reactive power both at multiple buses	28
	2.5	Concl	usion	30
3			Selection of Voltage Controlling Parameter in Uncertain Activ	
			ion Network	33
	3.1		luction	33
	3.2		ling of distribution network	34
		3.2.1	Modeling of hourly solar irradiation and power output	34
		3.2.2	Modeling of wind speed and output power	35
		3.2.3	Modeling of Load	36

 ${f x}$

		3.2.4 Modeling of EVs as load	37
		3.2.5 Modeling of BESS at Charging Station	38
	3.3	Problem Formulation	39
		3.3.1 Objective Function	39
	3.4	Jaya algorithm for solving OPF	41
	3.5	Results and Discussion	42
		3.5.1 Enhanced IEEE-33 distribution system	42
		3.5.2 Solar Generation	43
			46
		3.5.4 Mixed Type generation	47
		3.5.5 Unbalanced IEEE-123 distribution system	49
		3.5.6 Discussion	50
	3.6	Conclusion	54
	Б		
4		-Stage Voltage Control For Active Distribution Network With High	E 17
	4.1	etration of Photovoltaic Distributed Generators Using Spectral Clustering Introduction	57
	4.1		59
	4.2		59 59
	4.5	0	59 59
			59 59
	4.4	, 0	59 61
	4.4		62
		v	66
	15	v	
	4.5	v	68
5	Enł	Conclusion	
5	Enł	Conclusion	
5	Enł	Conclusion	68
5	Enh Opt	Conclusion Ancement of Hosting Capacity of Active Distribution Network Utilizing mal Placement of Battery Energy Storage System Introduction	68 69 70
5	Enl Opt	Conclusion Ancement of Hosting Capacity of Active Distribution Network Utilizing mal Placement of Battery Energy Storage System Introduction	68 69
5	Enh Opt	Conclusion Ancement of Hosting Capacity of Active Distribution Network Utilizing mal Placement of Battery Energy Storage System Introduction	68 69 70
5	Enh Opt	Conclusion Ancement of Hosting Capacity of Active Distribution Network Utilizing mal Placement of Battery Energy Storage System Introduction	68 69 70 70 70 70
5	Enh Opt	Conclusion Ancement of Hosting Capacity of Active Distribution Network Utilizing mal Placement of Battery Energy Storage System Introduction	68 69 70 70
5	Enh Opt	Conclusion Ancement of Hosting Capacity of Active Distribution Network Utilizing mal Placement of Battery Energy Storage System Introduction Formulation of load, generation and Battery Energy Storage System (BESS) 5.2.1 Modeling of load, generation and BESS 5.2.2 Modeling of BESS 5.2.3 Charging of BESS 5.2.4 Discharging of BESS Impact of PV-DGs in the active distribution network	68 69 70 70 70 70
5	Enl Opt 5.1 5.2	Conclusion Ancement of Hosting Capacity of Active Distribution Network Utilizing mal Placement of Battery Energy Storage System Introduction Formulation of load, generation and Battery Energy Storage System (BESS) 5.2.1 Modeling of load, generation and BESS 5.2.2 Modeling of BESS 5.2.3 Charging of BESS 5.2.4 Discharging of BESS Impact of PV-DGs in the active distribution network 5.3.1 Sobol sensitivity	68 69 70 70 70 70 70 70 71
5	Enl Opt 5.1 5.2	Conclusion ancement of Hosting Capacity of Active Distribution Network Utilizing mal Placement of Battery Energy Storage System Introduction Formulation of load, generation and Battery Energy Storage System (BESS) 5.2.1 Modeling of load, generation and BESS 5.2.2 Modeling of BESS 5.2.3 Charging of BESS 5.2.4 Discharging of BESS Impact of PV-DGs in the active distribution network 5.3.1 Sobol sensitivity Problem Formulation	68 69 70 70 70 70 70
5	Enl Opt 5.1 5.2	Conclusion Ancement of Hosting Capacity of Active Distribution Network Utilizing mal Placement of Battery Energy Storage System Introduction	68 69 70 70 70 70 70 71 72 74
5	Enlar Opt 5.1 5.2 5.3 5.4	Conclusion Ancement of Hosting Capacity of Active Distribution Network Utilizing mal Placement of Battery Energy Storage System Introduction Formulation of load, generation and Battery Energy Storage System (BESS) 5.2.1 Modeling of load, generation and BESS 5.2.2 Modeling of BESS 5.2.3 Charging of BESS 5.2.4 Discharging of BESS Impact of PV-DGs in the active distribution network 5.3.1 Sobol sensitivity Problem Formulation Results and Discussion 5.5.1 IEEE-33 test system	68 69 70 70 70 70 71 72 74 75
5	Enlar Opt 5.1 5.2 5.3 5.4	Conclusion Ancement of Hosting Capacity of Active Distribution Network Utilizing mal Placement of Battery Energy Storage System Introduction	68 69 70 70 70 70 70 71 72 74 75 76
5	Enlar Opt 5.1 5.2 5.3 5.4	Conclusion Ancement of Hosting Capacity of Active Distribution Network Utilizing mal Placement of Battery Energy Storage System Introduction	68 69 70 70 70 70 71 72 74 75
5	Enlar Opt 5.1 5.2 5.3 5.4 5.5	Conclusion Ancement of Hosting Capacity of Active Distribution Network Utilizing mal Placement of Battery Energy Storage System Introduction Formulation of load, generation and Battery Energy Storage System (BESS) 5.2.1 Modeling of load, generation and BESS 5.2.2 Modeling of BESS 5.2.3 Charging of BESS 5.2.4 Discharging of BESS Impact of PV-DGs in the active distribution network 5.3.1 Sobol sensitivity Problem Formulation Results and Discussion 5.5.1 IEEE-33 test system 5.5.2 IEEE-13 unbalanced test system Conclusion	68 69 70 70 70 70 70 71 72 74 75 76
	Enlar Opt 5.1 5.2 5.3 5.4 5.5	Conclusion Ancement of Hosting Capacity of Active Distribution Network Utilizing mal Placement of Battery Energy Storage System Introduction Formulation of load, generation and Battery Energy Storage System (BESS) 5.2.1 Modeling of load, generation and BESS 5.2.2 Modeling of BESS 5.2.3 Charging of BESS 5.2.4 Discharging of BESS Impact of PV-DGs in the active distribution network 5.3.1 Sobol sensitivity Problem Formulation Results and Discussion 5.5.1 IEEE-33 test system 5.5.2 IEEE-13 unbalanced test system Conclusion Clusion and Future Research	68 69 70 70 70 70 71 72 74 75 76 82
	Enli Opt 5.1 5.2 5.3 5.4 5.5	Conclusion Ancement of Hosting Capacity of Active Distribution Network Utilizing mal Placement of Battery Energy Storage System Introduction Formulation of load, generation and Battery Energy Storage System (BESS) 5.2.1 Modeling of load, generation and BESS 5.2.2 Modeling of BESS 5.2.3 Charging of BESS 5.2.4 Discharging of BESS Impact of PV-DGs in the active distribution network 5.3.1 Sobol sensitivity Problem Formulation Results and Discussion 5.5.1 IEEE-33 test system 5.5.2 IEEE-13 unbalanced test system Conclusion Clusion and Future Research General	68 69 70 70 70 70 71 72 74 75 76 82
	Enlar Opt 5.1 5.2 5.3 5.4 5.5 Cor 6.1	Conclusion Ancement of Hosting Capacity of Active Distribution Network Utilizing mal Placement of Battery Energy Storage System Introduction Formulation of load, generation and Battery Energy Storage System (BESS) 5.2.1 Modeling of load, generation and BESS 5.2.2 Modeling of BESS 5.2.3 Charging of BESS 5.2.4 Discharging of BESS Impact of PV-DGs in the active distribution network 5.3.1 Sobol sensitivity Problem Formulation Results and Discussion 5.5.1 IEEE-33 test system 5.5.2 IEEE-13 unbalanced test system Conclusion Clusion and Future Research General Summary of contribution	68 69 70 70 70 70 71 72 74 75 76 82 83

Contents		xi

\mathbf{A}	Test System Data	97
	A.1 Test Data	97
	A.2 141-Bus System Data	97
В	Appendix List of Publications	103

xii Contents

List of Figures

1.1	(a) Distribution network (b) Active distribution network	3
1.2	(a) Centralized DG control (b) Decentralized DG control	5
1.3	(a) Hosting capacity concept and the effect of its enhancement (b) hosting capacity enhancement technique	10
2.1	Common impedance of the generic distribution system	14
2.2	PDF of change in voltage at bus-27 for 69-bus distribution system (a) Real part of change in voltage ΔV_{27}^r (b) Imaginary part of change in voltage ΔV_{27}^i	17
2.3	Axis transformation of variable data points $(\Delta V_{oa}^r, \Delta V_o^r)$ into new set of orthogonal axis Z_1 and Z_2	18
2.4	69-bus distribution system	22
2.5	The $PVSI$ of active buses for (a) change in voltage at bus 27, (b) change in voltage at bus 141 due to active power perturbation at active buses	24
2.6	The $PVSI$ of active buses for (a) change in voltage at bus 27, (b) change in voltage	
2.7	at bus 141 due to reactive power perturbation at active buses \dots	26
	at bus 141 due to complex power perturbation at active buses	29
3.1	Steps to model PDF	34
3.2	PDF of (a) Solar irradiation of 13h (b) wind speed of 15h (c) load of 13h (d) number of EVs arrival of 13h	36
3.3	Steps to determine optimal setting of voltage controlling parameters	41
3.4	(a) EVs arrival at charging station in hourly time segment for $100 \mathrm{EVs}$, (b) PDF of initial SOC for EV batteries	42
3.5	Enhanced IEEE-33 test system	42
3.6	In case Solar type DGs (a) charging/discharging power with SOC of BESS at bus 22 (b) tap-setting of OLTC (c) network losses for 24 h time period	43
3.7	In case Solar type DGs (a) charging rate of EVs at bus 22 (b) optimal VAR setting	10
	of reactive power compensator	44
3.8	In case Solar type DGs (a) cost Function (b) voltage Levels at all buses with and without optimal setting for 13 h	44
3.9	In case wind type DGs (a) charging/discharging power with SOC of BESS at bus	44
0.5	22 (b) tap-setting of OLTC (c) network losses for 24 h time period	45
3.10	In case wind type DGs (a) charging rate of EVs at bus 22 (b) optimal VAR setting of reactive power compensator	46
3.11	In case wind type DGs (a) cost Function (b) voltage Levels at all buses with and	40
	without optimal setting for 15 h	46
3.12	In case mixed type DGs (a) charging/discharging power with SOC of BESS at bus 22 (b) tap-setting of OLTC (c) network losses for $24h$ time period	47
3.13	In case mixed type DGs (a) charging rate of EVs at bus 22 (b) optimal VAR setting	
	of reactive power compensator for 24 h time period	48

xiv List of Figures

3.14	In case mixed type DGs (a) comparison of cost function by M-Jaya algorithm with
	PSO and GWO algorithm (b) voltage levels at all buses with and without optimal
	setting for 14 h
	IEEE-123 test system
3.16	In case mixed type DGs in IEEE-123 test system (a) charging/discharging power
	with SOC of BESS at bus 35 (b)tap-setting of OLTC (c) charging rate of EVs at
	bus 35
3.17	In case mixed type DGs in IEEE-123 test system (a) optimal VAR setting of reactive power compensator at bus 82-a and 96-b (b) optimal VAR setting of reactive power
	compensator at bus 76-a and 92-b
3.18	In case mixed type DGs (a) Comparison of cost function by M-Jaya algorithm with PSO and GWO algorithm (b) voltage Levels at all buses with and without Optimal
0.10	setting for 14 h
3.19	In case mixed type DGs in IEEE-123 test system for 14 h with and without optimal
	setting (a) voltage level of present buses in phase-a (b) voltage level of present buses
	in phase-b (c) voltage level of present buses in phase-c
4.1	Flowchart of two-stage voltage control
4.2	(a) 37-bus ADN (b) current and future PV-DG installation 62
4.3	In 37-bus system,(a) optimal tap setting of OLTC, (b) optimal charging rate of EVs,
	for 24 h time segment
4.4	Charging/discharging rate of BESS installed at bus 25 with CS in 37-bus system . 63
4.5	In 37-bus system, (a) optimal hourly losses (pu), (b) Quality of Cluster Index (QCI)
	for different number of clusters
4.6	In 37-bus system, voltage profile of all buses with and without two-stage voltage control technique for 13 h
4.7	In 37-bus system, (a) DGs output power in CVC, (b) DGs output power in CBVC 64
4.8	Modified IEEE 123-bus system
4.9	In, IEEE 123-bus system, (a) Quality of Cluster Index (QCI) for different number
	of clusters, (b) rating of DGs with locations
4.10	In modified IEEE 123-bus, voltage profile of all buses with and without two-stage
	voltage control method for 13 h
4.11	In modified IEEE 123-bus system, (a) Optimal tap setting of OLTCs, (b) Optimal
	network losses, for each hourly time segment 6'
5.1	Steps to perform sobol indexing method
5.2	Steps to determine the hosting capacity of the network
5.3	IEEE-33 system
5.4	Charging/discharging profile of BESS for 24 h time period
5.5	In IEEE-33 test system tap-setting of OLTC for 24 h time period
5.6	Voltage profile of the network
5.7	For IEEE-33 test system losses for 24 h time period
5.8	In case of IEEE-13 (a) optimal tap setting of OLTC (b) network losses (c) optimal
0.0	setting of reactive power compensator installed with bus 52 for 24 h time period . 78
5.9	IEEE-13 unbalanced test system
	In case of IEEE 13 test system (a) phase-(a) (b) phase-(b) (c) phase-(c) bus voltage
0	for 13 h

List of Figures xv

5.11	Charging/ discharging profile of BESS installed at (a) phase-(a) of bus 634 and bus	
	671 (b) phase-(b) of bus 634 and bus 671 (c) phase-(c) of bus 634 and bus 671 for	
	24 h time period	81
A.1	141-bus system	97

xvi List of Figures

List of Tables

2.1	Ranking of active bus for change in voltage at observer bus in 69 bus distribution	
	system by traditional MCS, JDE and proposed $PVSI$	24
2.2	Computation time of ranking for ΔP_k	25
2.3	Ranking of active bus for change in voltage at observer bus in 141-bus distribution	
	system by traditional MCS, JDE and proposed $PVSI$	27
2.4	Computation time of ranking for ΔQ_k	28
2.5	Computation time of ranking for ΔS_i	30
3.1	State with their Probability of Input Variables for 13 h in case of Solar type DGs $.$	43
3.2	Combination of States of Input Variable for 13 h in case of Solar type DGs	43
3.3	Comparison of M-Jaya algorithm with PSO and GWO algorithm for 14h on IEEE-33 $$	49
3.4	Bus present in each phases	51
4.1	State with their probability of solar irradiance, number of EVs arrival at CS and	
	load for 13 h	63
4.2	Comparison table on 37-bus system for 13 h	66
4.3	Comparison table on IEEE 123-bus system for 13 h	68
5.1	State with their probability of solar power generation, and load for 13 h $$	74
5.2	Combination of States of Input Variable for 13 h in case of Solar type DGs	74
5.3	Ranking of PV-DGs by Sobol index for IEEE 33 test system	75
5.4	Comparative analysis of different approaches for enhancing hosting capacity	76
5.5	Ranking of PV-DGs by Sobol index for IEEE-13 test system	79
5.6	Comparative analysis of different approaches for enhancing hosting capacity	82
A.1	Branch and Bus Data of 141-Bus System	98
A.2	Branch and Bus Data of 141-Bus System	99
A.3	Branch and Bus Data of 141-Bus System	100
A.4	Branch and Bus Data of 141-Bus System	101
A.5	Branch and Bus Data of 141-Bus System	102

xviii List of Tables

Glossary

Frequently used abbreviations, mathematical variables and symbols are listed below; other used terms are abbreviated in their respective chapters.

Key Abbreviations

AER	All-electric range
APC	Active Power Curtailment
BESS	Battery Energy Storage System
CBVC	Cluster-Based Voltage Control
CM	Column of Matrix
CS	Charging Stations
CVC	Centralized Voltage Control
$\overline{\mathrm{DG}}$	Distributed Generation
DSO	Distribution System Operator
EPS	Electrical Power System
EV	Electric Vehicle
НС	Hosting Capacity
JDE	Joint Differential Entropy
M-Jaya	Modified Jaya algorithm
MCS	Monte-Carlo Simulation
NR	Newton-Raphson
OLTC	On-Load Tap Changer
OPF	Optimal Power Flow
P&O	Perturb and Observe
PCA	Principal Component Analysis
PDF	Probability Density Function
PV-DG	Solar-Based Distributed Generation
PVSI	Probabilistic Voltage Sensitivity Index
PVSI	Probabilistic Voltage Sensitivity Index
QCI	Qulaity of Cluster Index
RBDG	Renewable-Based Distributed Generation
RPC	Reactive Power Compensation
SOC	State of Charge

List of Tables

Chapter 1

Introduction

1.1 Introduction

1.1.1 General

The economic growth of a nation is significantly influenced by the quality of the Electrical Power System (EPS). An EPS is a network that generates, transmits, and distributes electricity from power plants to consumers, ensuring reliable and efficient delivery of electrical energy. Traditionally, power is centrally generated and distributed to consumers, as shown in Fig. 1.1-(a). However, it is not possible to fulfil our increasing power demand through traditional methods due to land, economic, and, most importantly, environmental constraints. Subsequently, Renewable-Based Distributed Generation (RBDG) is used as an alternative. RBDG enhance the availability of green energy to more consumers and reduces network losses in the transmission and distribution networks. However, RBDG exhibits stochastic characteristics that introduce uncertainty into the transmission and distribution network. This uncertainty compromises the stability and reliability of the EPS.

1.1.2 Active Distribution Networks

The distribution network is a key element of EPS, connecting the transmission system directly to the load center. It is classified into primary and secondary distribution networks. The voltage level of primary distribution networks lies between 4 kV to 35 kV, which supplies small-scale industrial customers, and the secondary distribution network supplies residential customers at voltage level of 120/240 V [1], [2]. Nowadays, RBDG is being integrated into primary and secondary distribution networks to meet our power demands due to its economic, operational, and environmental advantages. Traditional distribution networks are inherently passive. However, incorporating RBDG transform them into active distribution systems, allowing them to supply power to local demand [3], [4]. A traditional Active Distribution Network (ADN) is shown in Fig. 1.1-(b).

1.1.3 Motivation

Recently, the expansion of centralized power generation using fossil fuels has been challenged. This is due to high capital costs, significant transmission expenses and losses, decreasing fossil fuel reserves, and rising environmental concerns. Historically, conventional energy sources constituted 76% of global power generation, while renewable energy sources contributed 24%. However, projected trends indicate a substantial transformation by 2050. Renewable energy is expected to dominate, accounting for 85% of worldwide power generation, while conventional energy will represent only 15% [5]. In parallel with the development of battery energy storage devices, Electric Vehicles (EVs) are also increasing in the market [6], [7]. As a consequence, the integration of

charging infrastructure in the distribution network is also increasing. The stochastic nature of RBDG and the number of EVs arriving at charging stations significantly impact the voltage level of the distribution network [8], [9]. Therefore, to ensure the reliable and stable operation of distribution networks, an effective voltage control technique is needed. This technique must consider the unpredictable nature of load, generation and the number of EVs arriving at charging stations.

Previously, RBDG operated at a unity power factor and lacked active and reactive power control capabilities. This limitation prevented RBDG inverters from contributing to power dispatching. In this circumstances, advanced voltage control techniques are essential to address voltage issues. Reinforcing conventional voltage control devices in the active distribution network provides straightforward solutions among the various techniques. However, this approach is expensive. Alternatively, the On-Load Tap Changer (OLTC) can manage voltage deviations. However, it isn't a universal solution for all over and under voltage scenarios due to its limited operating range and slow response time. Additionally, the existing OLTC in the active distribution network is not made for bidirectional power flow. However, with progress in power electronic inverter technology have made it possible to control voltage by regulating the active and reactive power of RBDGs. This provides promising solutions for mitigating voltage issues. Active Power Curtailment (APC) and Reactive Power Compensation (RPC) are commonly used strategies. These strategies enable RBDG inverters to effectively address voltage problems. However, the random selection of RBDGs for maintaining the voltage profile is not seems to be a best solution. Therefore, evaluating the impact of RBDGs on bus voltage is a very crucial factor in formulating fast and dynamic control voltage techniques. In this context, determining the impact of RBDGs on bus voltage, considering their stochastic characteristics by traditional Newton-Raphson (NR), Perturb and Observe (P&O), becomes a computationally burdensome process. It necessitates an analytical approach to minimize computational effort while assessing the effect of RBDGs on network bus voltage.

The voltage control technique, which utilizes APC and RPC of available RBDGs in the network, has been classified into centralized and decentralized control techniques. In the centralized voltage control method, all available RBDGs in the network are used unitedly to maintain the network's voltage profile. However, this approach, involving centralized power curtailment, is not considered economically optimal for the utility grid. Consequently, decentralized voltage control is preferred due to the reduced participation of number of RBDGs. However, such techniques leverages the voltage-controlling capabilities of RBDGs without coordinating available voltage-controlling parameters and thus are not considered to be an effective and optimal solution. For this reason, a hierarchical voltage control techniques are commonly utilized in the literature. In the primary stage, the optimal settings of the available voltage-controlling parameter in the network is planned for the time segment. Furthermore, based on the optimal settings of voltage-controlling parameters, RBDGs are used to address the network's voltage issues. However, estimating the optimal setting of voltage controlling parameters, considering the stochastic characteristics of load and generation by conventional probabilistic load flow (Monte Carlo simulation) method is a computational process. Conversely, in the secondary stage, partitioning of the distribution network is adopted as a part of decentralized control which is inherently a challenging task. The existing literature used voltage sensitivity, electrical distance, and modularity index as an indices to partition the network into different clusters. Further, each cluster's voltage profile is upheld by utilizing the voltage-controlling ability of RBDGs within their respective clusters. However, a significant limitation of the aforementioned indices is their failure to consider the uncertainty of RBDGs. This shortcoming renders conventional two-stage voltage control methods specific to particular scenarios.

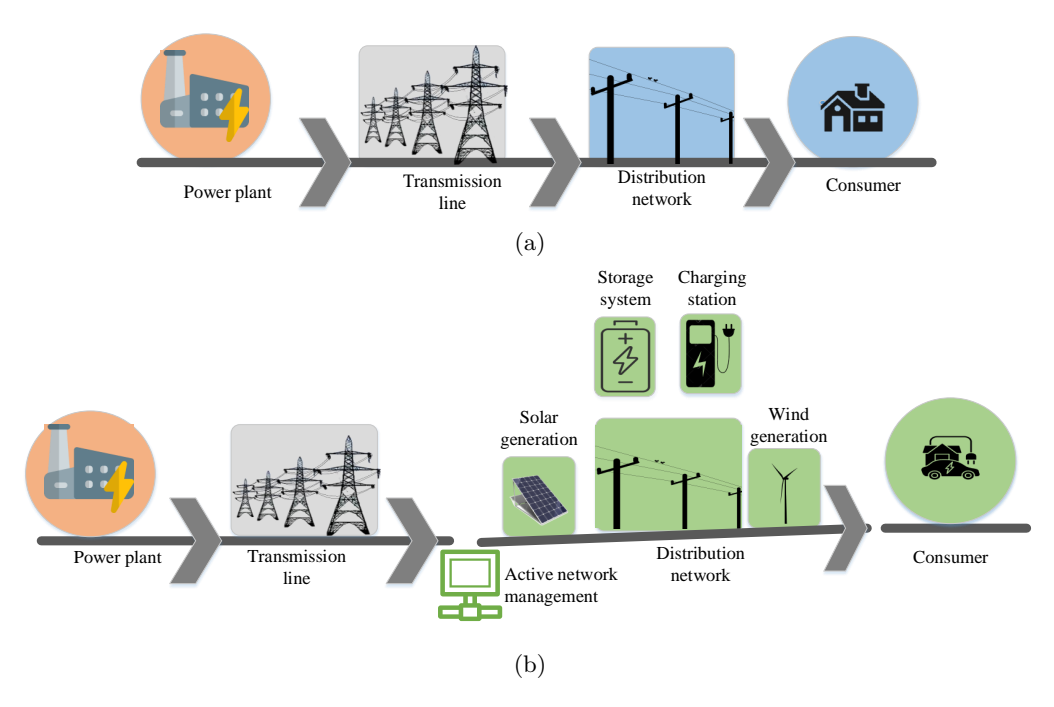


Fig. 1.1: (a) Distribution network (b) Active distribution network

Enhancing the Hosting Capacity (HC) of a distribution network is crucial for incorporating cleaner and more sustainable energy sources while ensuring a stable network voltage profile. HC denotes the maximum capacity of RBDGs that can be added to the distribution system without compromising its performance. Optimal use of voltage-controlling devices, such as OLTCs, reactive power compensators, and Battery Energy Storage Systems (BESS), is seen as a potential solution to increase the HC of the network. BESS enhances the hosting capacity by adjusting the mismatch between load and generation using their charging and discharging properties. Mostly, the distribution network consists of small BESS (residential storage), medium BESS (community storage) and large BESS (serves the entire network). Larger BESS offers a highest benefit-cost ratio for increasing HC in RBDG-integrated distribution systems. Placing BESS to neutralize the impact of RBDG's uncertainty to enhance hosting capacity is a challenging task. After the optimal placement of BESS, the HC of the network can be enhanced by optimally utilizing the BESS's charging and discharging profile along with optimal voltage-controlling parameters.

Objective of the Thesis

The thesis aims to develop fast and dynamic voltage control techniques and hosting capacity enhancement techniques for active distribution networks, which is achieved using the following objectives.

- To investigate the impact of renewable-based generation on bus voltage considering their stochastic characteristics, a probabilistic voltage sensitivity index has been introduced.
- To determine the optimal setting of voltage-controlling parameters in the active distribution network considering the uncertain characteristics of load and generation, the state-based probabilistic method is introduced.
- To maintain the voltage profile of active distribution networks enriched with renewable based generation, a dual-stage voltage control technique has been proposed.

• To enhance the hosting capacity of the active distribution network, a strategic placement of battery energy storage systems is proposed.

1.1.4 Literature Review

A literature review has been meticulously conducted to address the objectives as follows.

1.1.4.1 Impact of Distributed Generation

The distribution network's low X/R ratio makes its voltage profile highly sensitive to power perturbations [10], [11]. The growing presence of Renewable-Based Distributed Generators (RBDGs) leads to voltage perturbation in the distribution network because of their stochastic nature. Sometimes, voltage fluctuation is converted into voltage limit violation at several buses. These voltage limit violations not only damage electrical equipment but also reduce the system's hosting capacity [12], [13]. Therefore, an effective voltage control technique is essential to maintain the voltage levels at all buses within their permissible limits. The traditional method of voltage control, such as OLTC [14], [15], and voltage-regulator [16], have slow response time and are also not made for bidirectional power flow done by integrated DGs. With advancements in inverter technology, the voltage control using active and reactive power of inverter interfaced RBDGs in the network gives a fast and dynamic solution [17], [18]. However, utilizing all available RBDGs or random RBDGs from the distribution system to maintain the voltage profile is not considered as a economically optimal solution for the utility grid. In this context, understanding the effect of power disturbances at RBDG-integrated buses on bus voltage deviations offers valuable insights for keeping the voltage profile within acceptable limits. This is achieved through voltage sensitivity analysis, which measures the influence of DGs on bus voltage.

1.1.4.2 Voltage Sensitivity

Voltage sensitivity directly links power disturbances in available DGs in the nework to changes in bus voltage, as shown in (1.1) [19], [20].

$$\Delta V_i = \sum_i \left(\frac{dV_i}{dP_j} \times \Delta P_j + \frac{dV_i}{dQ_j} \times \Delta Q_j \right)$$
 (1.1)

To obtain ΔV_i , $\frac{dV_i}{dP_j}$, $\frac{dV_i}{dQ_j}$ must be acquired. It is basically evaluated by two methods (a) Traditional methods (b) Analytic Methods.

1.1.4.3 Traditional methods

Traditionally, Newton-Raphson (NR) and Perturbation and Observation (P&O) methods are used to determine $\frac{dV_i}{dP_j}$, $\frac{dV_i}{dQ_j}$ as shown in (1.2)-(1.3).

$$\begin{bmatrix} \Delta \theta_i \\ \Delta V_i \end{bmatrix} = J^{-1} \begin{bmatrix} \Delta P_j \\ \Delta Q_j \end{bmatrix} \tag{1.2}$$

$$\frac{dV_i}{dP_j} \approx \frac{\Delta V_i}{\Delta P_j}, \frac{dV_i}{dQ_j} \approx \frac{\Delta V_i}{\Delta Q_j}$$
(1.3)

Sensitivity analysis is primarily conducted using traditional methods such as NR, while P&O methods are not optimistic for distribution networks because of their radial configuration and low

X/R ratio. Simultaneously, these methods become computationally expensive when considering the stochastic characteristics of load and generation.

1.1.4.4 Analytic methods

In a recent study, several analytic methods of voltage sensitivity have been presented. In [21], a novel voltage sensitivity method is introduced to determine the most appropriate distributed generation for maintaining the network's bus voltage. However, power losses in the network are neglected, which is not a practical solution. In [22], [23], the voltage-controlling capability of RBDGs is utilized to maintain the bus voltage of the network. The analytic sensitivity technique is presented in these literature to find the relationship between voltage variations at any bus with respect to the reference bus. However, these theoretical findings have not been corroborated with simulations. The increasing penetration of RBDGs introduces uncertainty in the network, and it changes the properties of the network. Therefore, the intermittent nature of RBDGs must be incorporated to determine voltage sensitivity. In [24], a probabilistic method is proposed, incorporating smart meter measurements and sensitivity analysis to establish limits for operational indices. In this study, the assumption that real and reactive power consumption by the home are independent is not accurate for real-time scenarios. Similarly, in [25], regression model is employed to estimate voltage sensitivity. Method of calculating voltage sensitivity used in [24], [25] are data dependent. Therefore, the proposed methods are not suitable for large distribution networks. In [26], differential entropy, Kullback-Leibler distance, and Frechet distance index are proposed to identify the primary contributer for voltage deviation at any bus. It gives the effect of power disturbances at DG-integrated buses on bus voltage perturbation. Evaluating this information by these indexes is computationally high process due to the complex analytic formula of change in voltage due to power perturbation at DG-integrated bus has been used to formulate these logarithmic indexes. Previously, DG operated with a unity power factor. However, with advancements in power electronics converters, voltage control is now achieved through the management of both active and reactive power [27], [28]. Further, on the basis of impact of DGs, fast and dynamic voltage control techniques can be formulated, which is described in next sections.

1.1.5 Voltage control techniques

Active Power Curtailment (APC) and Reactive Power Compensation (RPC) are two methods that are used by inverter-interfaced DGs to tackle voltage issues in the distribution network. Broadly,

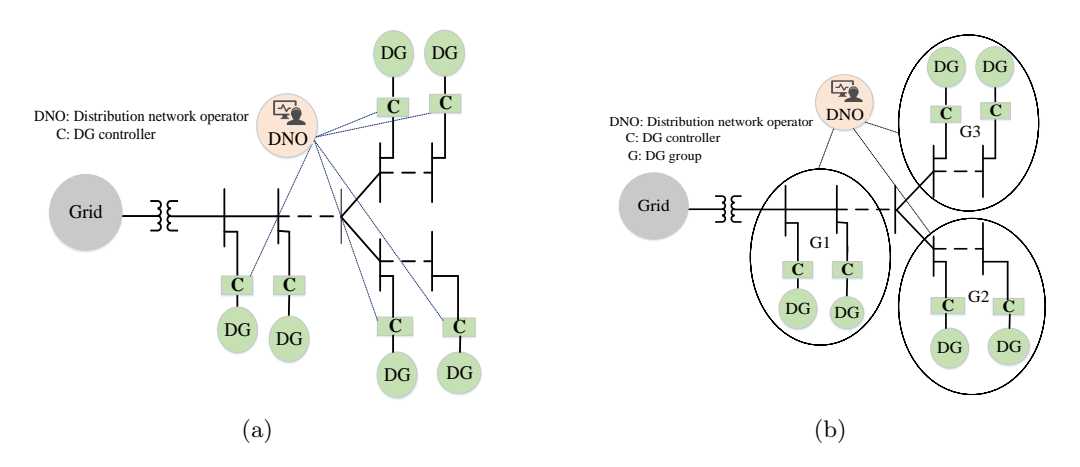


Fig. 1.2: (a) Centralized DG control (b) Decentralized DG control

voltage control using the voltage-regulating capabilities of DGs is divided into centralized and decentralized voltage control.

1.1.5.1 Centralized voltage control

APC and RPC are the techniques used by inverter-interfaced DGs to tackle voltage issues in the distribution network. Voltage control leveraging the voltage-regulating capabilities of DGs is typically categorized into centralized and decentralized techniques. In [29], utilizing droop characteristics of available DGs in the network, uniform and nonuniform centralized active power curtailment have been done to sustain the network's voltage profile. To preserve the voltage profile of the network, a multi-agent distributed voltage control technique is presented in [30]. In [31], a new real power adaptive capping approach has been suggested for preserving the bus voltage in the ADN. While preserving the voltage profile, real-power curtailments have been done from all the available DGs in the network. Due to adaptive capping, all the available DGs have an equal opportunity to share the duty of voltage stabilization. Further, the efficiency and feasibility of reactive power compensation have been shown in [32], [33]. However, DGs have restricted reactive power-controlling capabilities due to economic concerns. Therefore, the optimal utilization of active and reactive power of DGs for voltage control is considered as the optimistic solution for voltage control. In [33], both active and reactive power of DGs have been utilized to maintain the voltage control of the network. However, centralized voltage controls all the available DGs that are utilized together, so it is not an economically optimal solution for utility grids. Simultaneously, centralized voltage control takes relatively high computation to determine the optimal operating point of available DGs due to the large size of the distribution network. Therefore, decentralized voltage control is preferred.

1.1.5.2 Decentralized voltage control

In the decentralized voltage control technique, the distribution network is divided into multiple subgroups, and the DGs available in that subgroup are utilized to maintain their respective voltage profile [34]. In [35], ϵ decomposition has been carried out to separate the distribution network into a subnetwork. Further, optimal use of active and reactive power of available DGs in the subgroup has been used for maintaining the voltage profile. Similarly, based on an improved modularity index, a network is segregated into different sub-community [36]. Moreover, to mitigate the overvoltage issues in the network, a multi-objective optimization problem is solved by Particle Swarm Optimization (PSO) for curtailing the minimum active power from the available DGs in the sub-community. A network partitioning technique utilizing the k-means algorithm has been introduced in [37] to support ancillary services within distribution networks that incorporate DGs. It is implemented for observing the steady state voltage control in 20kV distribution system. In [38], an innovative method for forming microgrids by partitioning a distribution network in the aftermath of a natural disaster. This approach is designed to restore electricity to critical loads by creating targeted microgrids within the system. In [39], the decentralized optimal inverter dispatch (DOID) framework was introduced to improve inverter control flexibility. The method divides the distribution network into clusters, each managed by an energy manager and containing multiple PV inverters. Clusters are optimized independently with minimal voltage information exchange, ensuring system-wide voltage coordination. In [40] proposes organizing DGs into clusters within a typical microgrid to improve their coordinated management.

In the aforementioned work, the coordination of DGs with existing voltage control devices, such as OLTCs, voltage regulators, and reactive power compensators, have not been addressed to mitigate

network voltage issues. These devices, however, significantly impact the voltage profile of the network. Therefore, Hierarchical voltage control is opted for maintain the voltage profile of the network.

1.1.6 Hierarchical voltage control

Hierarchical voltage control techniques give the autonomy to utilize the available voltage-controlling parameters in the network with decentralized voltage control by DGs. It is implemented into multiple layers, and each layer output is implemented into multiple time scales [41].

1.1.6.1 Primary stage voltage control

In the primary stage, the optimal settings for voltage-regulating devices like OLTC, reactive power compensators, and BESS charging-discharging rates are determined for a defined time interval. On the basis of that optimal setting, the secondary voltage control technique performed [42], [43]. In [44], [45], several works have been done to evaluate the optimal settings of voltage regulating parameters for a specific interval. The voltage control method using optimal coordination among the voltage-controlling capability of DG, OLTC and BESS is proposed in [44], [46]. In this regard, the optimal operating point for available voltage-controlling components is determined by solving the centralized optimal power flow. The objective functions include loss minimization, voltage deviation minimization, and reactive power absorption minimization [47]. The conventional method of solving OPF is a gradient-based optimization algorithm that uses linear programming, quadratic programming, the Newton-Raphson method, and the interior point method. The OPF is a multimodal, non-linear or non-convex problem [47]. Therefore, heuristic optimization techniques are now prioritized over traditional methods in solving OPF due to their ability to potentially find global solutions. In [47], [48], a comprehensive literature survey of heuristic optimization techniques for solving OPF for various objective functions has been presented. The stochastic characteristics of load and generation severely impact the voltage stability of the network. Therefore, it is essential to consider their intermittent nature while determining the optimal setting of voltage-controlling parameters. In [49], the influence of uncertainty in DGs output power on voltage profile has been evaluated on bus voltage by probabilistic load flow using P-V and Q-V curves. However, the stochastic characteristics of the load have not been included. To determine the impact uncertainty on load, generation and network configuration using probabilistic load flow has been proposed in [45]. In both literature, the effect of load and generation intermittency on the voltage profile is assessed using probabilistic load flow. This method is challenging to implement when determining the optimal settings for voltage-controlling parameters. In [50], the optimal placement of distributed generation is determined with the objective of minimization of network losses. Further, to consider the intermitent nature of load and generation, a state-based probabilistic method is used. The state-based probabilistic model estimates all the probable output of any input variables from their probabilistic model. In the primary stage, centralized OPF is solved to determine the optimal settings for voltage-controlling parameters. Process is time-consuming and requires significant computational effort. Increasing penetration of renewable based DGs required fast dynamic solution due to their intermittent nature. Therefore, in secondary stage decentralized voltage control is utilized to maintain the voltage profile of the network using voltage control ability of installed DGs.

1.1.6.2 Secondary stage voltage control

In this stage, a group of DGs among all the available DGs are utilized to maintain the voltage profile of the network. Regarding this, portioning the distribution network on the basis of the impact of DGs on bus voltage is a challenging task. Conventionally, it is done on the basis of the territorial area or local administration, which is relevant for traditional radial structured distribution networks. The integration of DGs in the distribution system, the passive distribution network becomes active. Therefore, an advanced partitioning technique is needed to accommodate the behaviour of the distribution network with the incorporation of DGs. In this regard, electrical distance [51], modularity index [52], and sensitivity index [53], [54] are derived as clustering indices, which establish the relationship between the impact of DGs on bus voltage. Further, based on these indices, clustering such as K-mean, fuzzy C-mean are performed [54]. Following clustering, diverse voltage control techniques are employed to sustain the network's voltage profile. In [52], [51], the primary level is used to determine the hourly setting of the OLTC setting and charging-discharging profile of BESS for 24 h planning horizon. Furthermore, the secondary level, a grouped DG, is utilized for the better voltage level of the network. In [52], the modularity index is utilized to partition the network, whereas, in [51], the voltage sensitivity index coupled with spectral clustering is employed for network partitioning. In [55], introduces a structured method that divides distribution networks into multiple distinct control areas. This segmentation ensures prompt management of the voltage level in each area, which is essential for real-time execution. Further, utilizing the reactive power controlling ability of DGs available in each segment, their voltage level is managed. In [56], proposes a systematic method for dividing smart distribution networks into microgrids that are self-sufficient. This process uses an objective function that incorporates multiple performance indices, such as voltage profile and energy loss. Furthermore, to enhance the benefits and integration of DGs, two control strategies are assessed: OLTC and adaptive power factor control. A Distributed Adaptive Robust Voltage-Var Control (DAR-VVC) method for active distribution networks is presented in [57]. The DAR-VVC system uses a distributed algorithm to coordinate OLTCs, capacitor banks, and PV inverters across various operational stages, aiming to minimize network power loss. A clustering technique is implemented to minimize data exchange between neighbouring partitions, thereby improving the algorithm's overall efficiency. In [58], a two-stage, zone-based approach for optimizing VOLT-VAR control in ADN is introduced. This method segments the system into distinct zones according to customer types, such as residential, commercial, and industrial. The optimal VAR settings for each zone are derived using a hierarchical distributed algorithm that leverages cordal relaxation and Semi-Definite Programming (SDP). Increasing penetration of DGs into the network fulfils power demands but also pushes the network beyond normal operational conditions. Hence, enhancing the hosting capacity of the network while preserving its voltage profile poses a significant challenge.

Increasing ratio of DG into the network fulfils power demands but also pushes the network beyond normal operational conditions. Hence, enhancing the hosting capacity of the network while preserving its voltage profile poses a significant challenge.

1.1.7 Hosting capacity of the network

The Hosting Capacity (HC) is defined as the maximum number of DGs units that can be integrated into the power distribution network without compromising system performance. Beyond this level of penetration, the distribution network becomes unacceptable [59]. Fig. 1.3-(a) illustrates the concept of HC, clearly demonstrating that increasing the system's HC permits the incorporation of more DG units without surpassing performance limits. Broadly, the method of calculating HC

is classified as follows: (a) Analytic method, (b) Stochastic method, (c) Streamlined method [60], [61]. Analytic and stochastic methods to evaluate the HC is the computational process because both methods utilize multiple times of load flows. However, the streamlined method is based on detailed results from the HC study. Therefore, it provides a faster solution compared to analytic and stochastic methods, but at the cost of reduced accuracy [62]. Assessing HC is a planning issue where accuracy is more crucial than computation time. Hence, estimating the HC by considering the uncertain characteristics of generation and load is a challenging task. The traditional approach of calculating hosting capacity considering stochastic characteristics is presented in [63], [64]. In [65], HC analysis has been done on three Swedish distribution networks. It is concluded that over-voltage is the primary performance constraint in HC calculations. Simultaneously, it is observed that reactive power control and transformer tap changer adjustments are effective techniques for increasing HC and mitigating over-voltage issues. Numerous studies have been conducted in the literature to improve the network's HC by maintaining the voltage profile of the network. The methods utilized for enhancing the HC are as follows: optimal utilization OLTC [66], distribution network management [67], [68], [69], load balancing [70], optimal DG placement and sizing [71], [72], [73], reactive power compensator [74] and BESS [75]. The optimal coordination among all the available voltage-controlling devices in the network with the objective of enhancing the hosting capacity of the network is determined by solving the OPF problem [76], [77], [78]. The volt/VAR control problem aimed at maximizing hosting capacity is formulated as a single-objective optimization problem [79], [80]. This model is further developed into a multiobjective optimization problem in [81], utilizing a cuckoo search method to enhance voltage profiles and minimize losses by optimizing the allocation of Distributed Generation (DG). The method proposed for enhancing the hosting capacity from [65]-[81] is not considered the stochastic characteristics of load and generation. Monte Carlo Simulation (MCS) is a commonly applied technique in probabilistic power flow (PPF) analysis to enhance the hosting capacity (HC). Although MCS provides high accuracy, it can be time-intensive because it requires a large amount of input data, such as load demand, distributed generation (DG) output, and network configuration [82], [83], [84]. To avoid the computational burden in [85], a probability density function-based method has been proposed to enhance the hosting capacity of the network. The intermittent nature of load and generation hinders the enhancement of the hosting capacity of the network due to fast voltage regulation. BESS can address voltage issues in the network through optimal charging and discharging of their energy, thereby increasing the network's HC. Despite the high cost of BESS, it offers unique benefits that other solutions cannot provide. To enhance the network's HC, optimal sizing of BESS has been explored in [86]. In [75], [87], the BESS of EVs is utilized by its optimal charging and discharging. BESS is employed to alleviate voltage regulation issues and reduce network losses by tackling the multiobjective optimal power flow problem in [88]. It is validated on the MV and LV distribution network of Western Australia. It is observed that the advantage of BESS depends on the generation, load profile and network configuration.

1.1.8 Organization of the Thesis

The entire thesis work is organized into six chapters. A brief summary of each chapter is given as follows.

Chapter 1: Introduction

This chapter provides an overview of active distribution networks, emphasizing the various challenges in maintaining their voltage profiles and hosting capacity. Furthermore, it explores

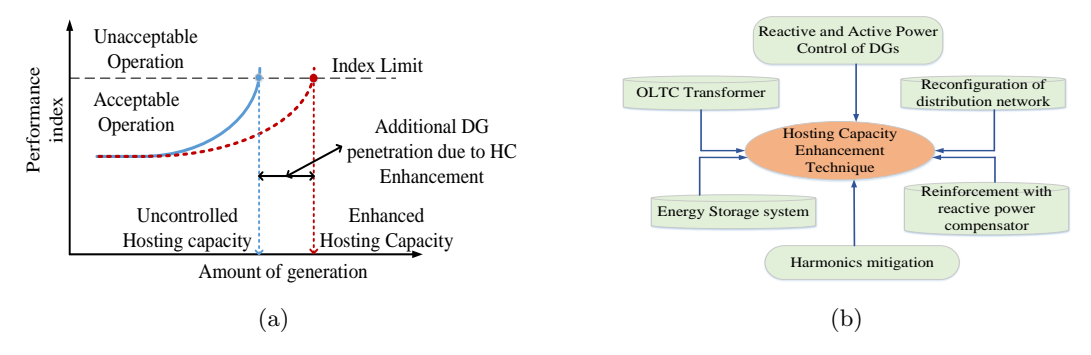


Fig. 1.3: (a) Hosting capacity concept and the effect of its enhancement (b) hosting capacity enhancement technique

existing solutions to achieve specific objectives while recognizing their limitations. Finally, the chapter outlines the research motivation behind this thesis.

Chapter 2: Probabilistic Approach to Investigate the Impact of Distributed Generation on Voltage Deviation in Distribution System

In this chapter, an analytical technique for evaluating the effects of power fluctuations on voltage deviations at any bus within a distribution network integrated with RBSGs is presented. The growing adoption of RBDGs in distribution networks introduces uncertainty in bus voltages because of their inherent intermittent nature. This uncertainty can occasionally result in voltage limit breaches at various buses. Conventional voltage control techniques often fail to manage these issues due to their delayed response time. Voltage-controlling strategies utilizing the voltage-regulation feature of present RBDGs in the network give fast and adaptive control solution. In this context, analyzing the implication of power disturbances at DG-integrated buses on bus voltages is critically important. Assessing this information with the conventional probabilistic load flow method is inefficient for real-time applications due to prolonged computational time. To address this, a novel Probabilistic Voltage Sensitivity Index (PVSI) based on Principal Component Analysis (PCA) is proposed. This index ranks DG-integrated buses by assessing the repercussions of power perturbations at these buses on voltage variations throughout the network. The PVSI is analytically derived to speed up the ranking process by decreasing computation time. Additionally, the efficiency of proposed PVSI is corroborated on the 69-bus and 141-bus distribution networks by assessing its performance relative to traditional Monte Carlo Simulation (MCS) and Joint Differential Entropy (JDE) in terms of accuracy and computation time.

Chapter 3: Optimal Selection of Voltage Controlling Parameter in Uncertain Active Distribution Network

In this chapter, the optimal setting of the voltage-controlling parameter is determined for the ADN. The share of Converter-Based Generation (CBG) and charging infrastructure in the distribution network is growing rapidly. Therefore, sustaining a stable voltage profile in the distribution network is a challenging task. This difficulty arises due to the unpredictable nature of CBG, the number of EVs arrival at Charging Stations (CS), and power demands. The voltage profile can be improved by selecting the optimal voltage-controlling parameters available in the network. This is achieved by addressing multiobjective OPF problems in a distribution system that includes the uncertainty of load, CBG like solar and wind and the number of EVs arriving at charging stations. The Modified Jaya (M-Jaya) algorithm is employed to solve the optimization problem by integrating multiple objectives such as minimizing line losses, voltage deviation, and maximizing CBG output power.

The state-based probabilistic modelling is proposed to incorporate the stochastic characteristics of output from CBG, the number of EVs arriving at the CS and power demand by the load in the OPF.

Chapter 4: Dual-Stage Voltage Control for Active Distribution Network with High Penetration of Photovoltaic Distributed Generators using Spectral Clustering

In this chapter, dual-stage voltage control for active distribution networks with high penetration of Photovoltaic Distributed Generators (PV-DGs) is presented using spectral clustering. It is executed in two stages. In the primary stage, utilizing the hourly state-based probabilistic modelling of the output power from PV-DGs, load power demand and available EVs in the charging station, optimal tap-setting of OLTC, charging-discharging of BESS and optimal charging of EVs is determined for 24 hour (h) time segment. It is done by solving the OPF problem for the minimization of voltage deviation and network losses. When the optimal hourly settings of the available voltage-controlling devices fail to maintain the voltage profile due to a high generation-to-load ratio, the voltage profile is affected. To restore it, CBVC is implemented in the secondary stage. In CBVC, the voltage-controlling capability of PV-DGs is utilized to mitigate overvoltage issues within the cluster. The optimal operating power of PV-DGs is determined by solving OPF for each cluster independently with the objective of reducing the active power curtailment and reactive power absorption by the available PV-DGs in the cluster. Additionally, the effectiveness of the proposed method is evaluated by comparing it with the Centralized Voltage Control (CVC) method. The comparison includes several factors: voltage profile, cumulative active power curtailment, reactive power absorption by PV-DGs, network losses, and computation time.

Chapter 5: Enhancement of hosting capacity of active distribution network utilizing optimal placement of battery energy storage system

In this chapter, the hosting capacity of the distribution network is enhanced by placing the BESS with dominant distributed generation of the network. Increasing power demand requires enhancement of the HC of a distribution network. Incorporating PV-DGs into the network fulfils power demands but also pushes the network beyond its normal operational conditions. Hence, enhancing the hosting capacity of the network while preserving its voltage profile poses a significant challenge, primarily due to the uncertain nature of PV-DGs. The BESS possesses the capability to compensate the uncertain characteristics of PV-DG in the network through its charging and discharging capabilities. In this work, the HC of the distribution network is improved by installing the BESS with the most dominant PV-DG. The Sobol voltage sensitivity index is used to determine the dominant PV-DG in the distribution network. Further, through the optimal utilization of the charging and discharging profile of the BESS with optimal voltage-controlling parameters, the HC of the network is enhanced.

Chapter 6: Conclusion and future scope

Finally, summarizes the key findings of the research presented in this thesis and for future research directions.

Chapter 2

Probabilistic Approach to Investigate the Impact of Distributed Generation on Voltage Deviation in Distribution System

2.1 Introduction

The growing integration of renewable energy sources into the distribution network introduces a significant degree of variability to the bus voltage, primarily due to the unpredictable nature of renewable generation. This variability leads to frequent deviations in voltage levels, resulting in multiple instances where the voltage exceeds the acceptable limits across various buses within the network. Such voltage limit violations can have detrimental effects, including potential damage to electrical equipment and a decrease in the network's ability to accommodate additional renewable generation. Therefore, it is imperative to implement an effective voltage control strategy to maintain the voltage levels at all buses within their permissible range, ensuring the stability and reliability of the distribution network.

As discussed in Chapter 1, the traditional methods of voltage control, such as On Load Tap Changing Transformers (OLTC) and voltage regulators, have slow response times and are also not made for bidirectional power flow done by integrated Distributed Generations (DGs). With advancements in inverter technology, voltage control using active and reactive power of inverter-interfaced DGs in the network provides a fast and dynamic solution. However, utilizing all available DGs or random DGs from the distribution system to maintain the voltage profile is not considered as an economical solution for the utility grid. In this context, an analytical technique for evaluating the effects of power fluctuations on voltage deviations at any bus within a distribution network integrated with renewable-based generation is presented. The increasing adoption of renewable energy sources in distribution networks introduces uncertainty in bus voltages because of their inherent intermittent nature. This uncertainty can occasionally result in voltage limit breaches at various buses. Conventional voltage control techniques often fail to manage these issues due to their sluggish response time. Voltage control strategies utilizing the voltage-regulation feature of present DGs in the network give fast and adaptive control methods. To formulate such voltage control technique, determining the implication of power disturbances at DG-integrated buses on bus voltages is critically important. Assessing this information with the conventional probabilistic load flow method is inefficient for real-time applications due to prolonged computational time. To tackle this problem, a novel Probabilistic Voltage Sensitivity Index (PVSI) based on Principal Component Analysis (PCA) is proposed. This index ranks DG-integrated buses by determining the repercussions of power perturbations at these buses on voltage variations

throughout the network. The PVSI is analytically derived to speed up the ranking process by decreasing computation time. Additionally, the efficiency of the proposed PVSI is corroborated on the 69-bus and 141-bus distribution networks by assessing its performance relative to traditional Monte Carlo Simulation (MCS) and Joint Differential Entropy (JDE) in terms of accuracy and computation time.

This Chapter is organized as follows. In section 2.2, the traditional method for determining the impact of power perturbation at DG integrated bus on voltage deviation is discussed. A brief explanation of the analytic method for calculating the upper bound of voltage deviation is detailed in section 2.3. The formulation of the PVSI using PCA is presented in Section 2.4. The validation of PVSI on 69-bus and 141-bus distribution systems is discussed in section 2.5. This work is concluded in Section 2.6.

2.2 Background

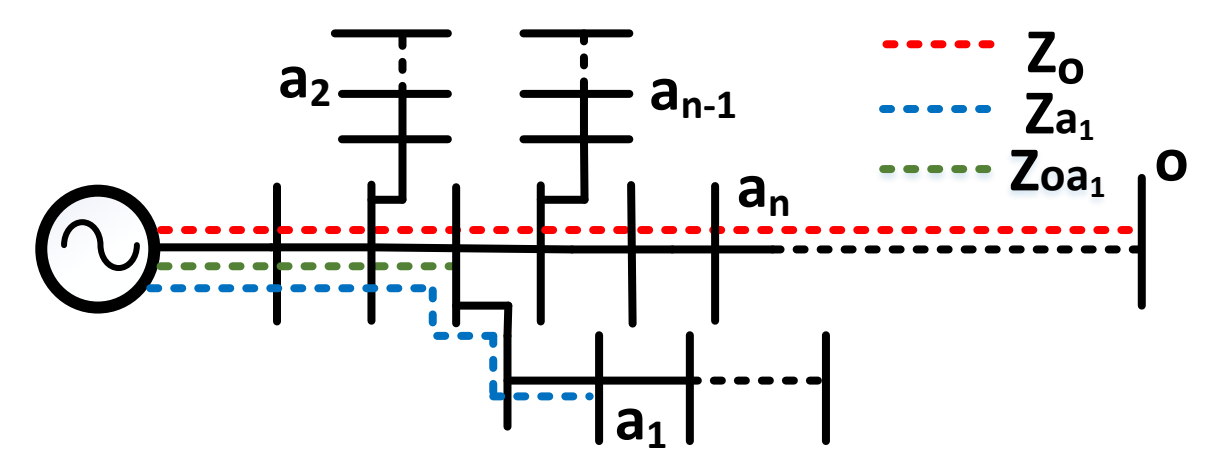


Fig. 2.1: Common impedance of the generic distribution system

Fig. 2.1 shows a schematic of a generic active distribution system coupled with the main AC grid. $a \in \{a_1, a_2...a_n\}$ symbolize the active bus and O symbolize the observer bus. The bus with distributed generations is taken as an active bus. Similarly, the bus which is selected for observing the impact of power perturbation at DG-integrated buses is termed an observer bus. If, the complex power changes at active bus changes S_{a_1} to $S_{a_1} + \Delta S_{a_1}$ then voltage at observer bus becomes V_o to $V_o + \Delta V_o$. A brief description of evaluating voltage sensitivity (ΔV_o) by traditional method using MCS and analytic methods is explained in subsections (A) and (B).

2.2.1 Traditional method for voltage sensitivity using Monte-Carlo Simulation (MCS)

The voltage sensitivity gives a direct relationship between power perturbation at DG-integrated buses with the change in bus voltage, as in (2.1) [19].

$$\Delta V_i = \sum_i \left(\frac{dV_i}{dP_j} \times \Delta P_j + \frac{dV_i}{dQ_j} \times \Delta Q_j \right)$$
 (2.1)

To obtain ΔV_i , $\frac{dV_i}{dP_j}$, $\frac{dV_i}{dQ_j}$ must be acquired. Traditionally, Newton-Raphson (NR) and Perturbation and Observation (P&O) methods are used to determine $\frac{dV_i}{dP_j}$, $\frac{dV_i}{dQ_j}$.

$$\begin{bmatrix} \Delta \theta_i \\ \Delta V_i \end{bmatrix} = J^{-1} \begin{bmatrix} \Delta P_j \\ \Delta Q_j \end{bmatrix} \tag{2.2}$$

$$\frac{dV_i}{dP_i} \approx \frac{\Delta V_i}{\Delta P_i}, \frac{dV_i}{dQ_j} \approx \frac{\Delta V_i}{\Delta Q_j}$$
(2.3)

In NR method, $\frac{dV_i}{dP_j}$, $\frac{dV_i}{dQ_j}$ is determined by Jacobian matrix as in (2.2). When the Jacobian matrix is not accessible, then the P&O method can be used. $\frac{dV_i}{dP_j}$, $\frac{dV_i}{dP_j}$ is obtained through the multi-run simulation by means of perturb the power at j^{th} active bus and observe the change in voltage at i^{th} observer bus, then formulate it as shown in (2.3).

For considering the stochastic nature of load and generation, these two methods are applied with MCS to determine the uncertainty in the voltage deviation. It is computationally expensive; hence it lacks practical implementation. In this work, it is used to measure the accuracy of the proposed PVSI. Further, the accuracy study is measured in terms of a ranking index. The steps involved in ranking the impact of power perturbation at the active bus on the change in voltage at the observer bus with the MCS method are as follows:

- Determine the variance of change in voltage at the observer bus due to power perturbation at active buses using the NR method with MCS.
- Consider zero power perturbation for the active bus, whose effect has to be calculated on change in voltage at the observer bus. Repeat step one.
- The Active bus, which reduces more in the variance of change in voltage at the observer bus, is considered as the most impactful bus for the observer bus.

2.2.2 Analytic method for voltage sensitivity

The analytic method gives an upper bound of voltage deviation due to power change at active bus [89]. The upper bound of voltage deviation (ΔV_o) at observer has been shown in (2.4).

$$\Delta V_o \le -\frac{\Delta S_{oa_1} Z_{oa_1}}{\Delta V_{a_1}^*} \tag{2.4}$$

$$Z_{bus} = \begin{bmatrix} Z_{11} & \dots & Z_{1O} & \dots & Z_{1n} \\ \dots & \ddots & \vdots & \dots & \vdots \\ Z_{O1} & \vdots & Z_{OO} & \dots & Z_{On} \\ \vdots & \vdots & \vdots & \ddots & \vdots \\ Z_{n1} & \vdots & Z_{On} & \dots & Z_{nn} \end{bmatrix}$$
(2.5)

where Z_{oa_1} is the common impedance shared between active bus a_1 and observer bus O. In Fig. 2.1, it is represented by the green line. It is determined from the impedance matrix (Z_{bus}) , which is shown in (2.5). The off-diagonal element of (Z_{bus}) is considered as common impedance. To formulate the (Z_{bus}) , impedance building algorithm is used [90]. $\Delta V_{a_1}^*$ is a complex conjugate of pre-perturb voltage at the active bus a_1 . If complex power changes at multiple buses, then voltage deviation is calculated at the observation bus by superposition theorem [89]. Expression

for voltage deviation is shown in (2.6).

$$\Delta V_o = -\sum_{a_n} \left(\frac{\Delta S_{a_n} Z_{oa_n}}{\Delta V_{a_n}^*} \right) = \sum_{a_n} (\Delta V_{oa_n})$$
 (2.6)

$$\Delta V_o = \sum_{a_n} \left(\Delta V_{oa_n}^r \right) + i \sum_{a_n} \left(\Delta V_{oa_n}^i \right) \tag{2.7}$$

after simplifying (2.4)

$$\Delta V_{oa_n}^r = -\frac{1}{|V_{a_n}|} (\Delta P_{a_n} (R_{oa_n} \cos \theta_{a_n} - X_{oa_n} \sin \theta_{a_n})$$

$$-\Delta Q_{a_n} (R_{oa_n} \sin \theta_{a_n} + X_{oa_n} \cos \theta_{a_n}))$$

$$(2.8)$$

$$\Delta V_{oa_n}^i = -\frac{1}{|V_{a_n}|} (\Delta Q_{a_n} (R_{oa_n} \cos \theta_{a_n} - X_{oa_n} \sin \theta_{a_n})$$

$$+\Delta P_{a_n} (R_{oa_n} \sin \theta_{a_n} + X_{oa_n} \cos \theta_{a_n}))$$

$$(2.9)$$

where $\Delta V_{oa_n}^r$, $\Delta V_{oa_n}^i$ are real and imaginary part of change in voltage at observer bus O due to power perturbation at active bus a_n . ΔP_{a_n} and ΔQ_{a_n} are active and reactive power perturbation at n^{th} active bus. ΔV_{a_n} , θ_{a_n} is pre-perturb voltage magnitude and angle of n^{th} active bus. R_{oa_n} , X_{oa_n} is common resistance and reactance between observer bus and n^{th} active bus. It is real and imaginary part of the common impedance Z_{oa_n} . Using (2.8) and (2.9), the real and imaginary part of the change in voltage due to power perturbation at any buses can be calculated. In general, the pre-perturb voltage at the active bus of the distribution system always remains within the permissible limit [91]. Therefore, $|V_{a_n}| \angle \theta_{a_n} = 1 \angle 0$ then, (2.8) and (2.9) becomes

$$\Delta V_{oa_n}^r = -\left(\Delta P_{a_n} R_{oa_n} - \Delta Q_{a_n} X_{oa_n}\right) \tag{2.10}$$

$$\Delta V_{oa_n}^i = -\left(\Delta Q_{a_n} R_{oa_n} + \Delta P_{a_n} X_{oa_n}\right) \tag{2.11}$$

$$\Delta S_k = \sim \mathcal{N}\left(\begin{bmatrix} 0\\0 \end{bmatrix}, \begin{bmatrix} 1 & -.04472\\ -.04472 & 0.2 \end{bmatrix}\right), k \in \{2, 8..\}$$
 (2.12)

$$Mean(\Delta V_o^r) = \sum_{k=1}^n E(\Delta V_{oak}^r)$$

$$= -R_{oak} \sum_{k=1}^n E(\Delta P_{oak}) + X_{oak} \sum_{k=1}^n E(\Delta Q_{oak})$$
(2.13)

$$Mean(\Delta V_o^i) = \sum_{k=1}^n E(\Delta V_{oak}^i)$$

$$= -R_{oak} \sum_{i=1}^n E(\Delta Q_{oak}) - X_{oak} \sum_{i=1}^n E(\Delta P_{oak})$$
(2.14)

$$var(\Delta V_o^r) = \sum_{k=1}^n var(\Delta V_{oak}^r)$$

$$= \sum_{k=1}^n var(\Delta V_{oak}^r) + \sum_{\substack{j=1\\k \neq j}}^n (\Delta V_{oak}^r \Delta V_{oaj}^r)$$
(2.15)

$$var(\Delta V_o^i) = \sum_{k=1}^n var(\Delta V_{oak}^i)$$

$$= \sum_{k=1}^n var(\Delta V_{oak}^i) + \sum_{\substack{j=1 \ j, j \neq i}}^n (\Delta V_{oak}^i \Delta V_{oaj}^i)$$
(2.16)

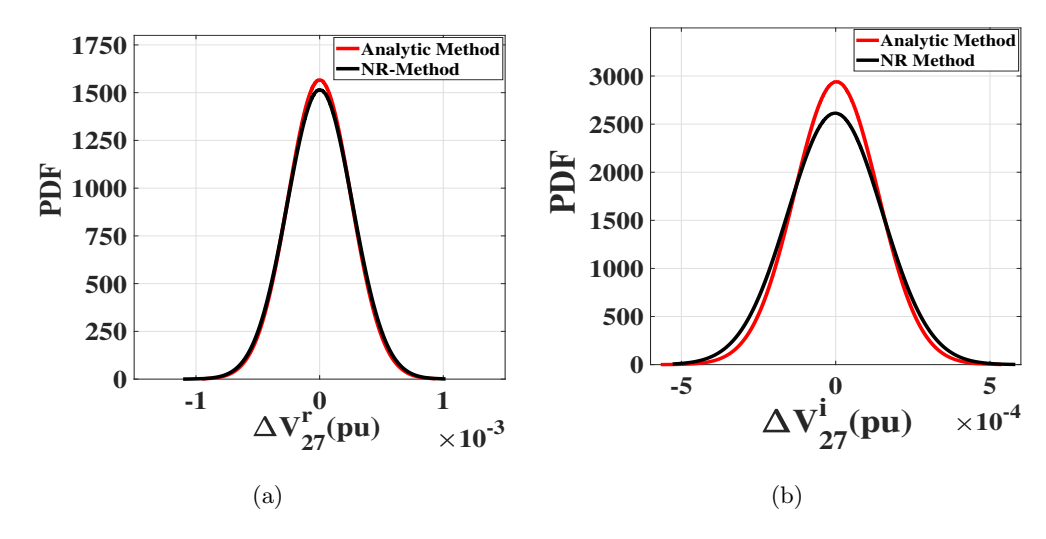


Fig. 2.2: PDF of change in voltage at bus-27 for 69-bus distribution system (a) Real part of change in voltage ΔV_{27}^r (b) Imaginary part of change in voltage ΔV_{27}^i

Equation (2.10) and (2.11) give a straightforward relationship between the active and reactive power perturbation with voltage deviation.

Due to the stochastic nature of injected complex power by the renewable-based generation, it is highly important to define voltage deviation in a stochastic sense. Therefore, the mean, variance, and Probability Density Function (PDF) of voltage deviation are the essential components to be obtained. For validating the stochastic properties of analytic formulation of change in voltage as shown in (2.10) and (2.11), 69-bus distribution system is considered.

Complex power perturbation is considered at twelve buses, from bus 2 to bus 69, in the interval of six buses. It is modeled by normal random vector $N(0, \bar{\sigma}^2)$, as shown in (2.12). In the (2.12), the first and fourth elements of covariance matrix $(\bar{\sigma}^2)$ represents the variance of active (σ_p^2) and reactive (σ_q^2) power, respectively. The third and fourth element represents covariance between active and reactive power $(\rho_{pq}\sqrt{\sigma_p^2\sigma_q^2})$. DGs provide reactive power by curtailing active power. Hence, the active-reactive power correlation coefficient (ρ_{pq}) is taken as -0.1. The change in voltage at bus 27 is calculated using the analytic method. The mean, variance, and PDF of voltage deviation are determined using (2.13) to (2.16). For evaluating the accuracy of the analytic method, PDF of the change in voltage at bus 27 is also determined by the NR method using MCS for 10,000 scenarios. In this case, mean and variance are estimated using the normal distribution mean, and variance formula [92]. After comparing both the PDF of ΔV_{27}^r and ΔV_{27}^i , it is observed that both methods give a similar PDF for change in voltage at bus 27, as shown in Fig.2.2. But the analytic method reduces huge computation time. In this work analytic method of calculating the change in voltage at the observer bus, as shown in (2.10) and (2.11), are used to formulate PVSI for ranking the impact of power perturbation at the active bus on change in voltage at observer bus.

2.3 Formulation of PVSI using PCA

The traditional method of finding out the impact of power perturbation at active buses on observer buses is computationally inefficient. Thus, in this work, novel PVSI is proposed. The proposed method is based on Principal Component Analysis (PCA). PCA gives the variance of linearly correlated variable data points by reducing their dimensionality [93]. Linear correlation between

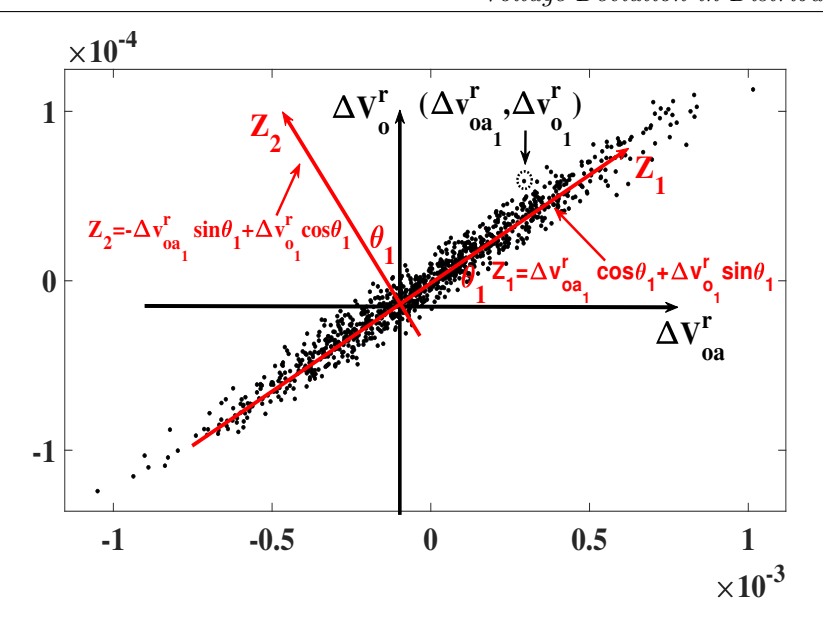


Fig. 2.3: Axis transformation of variable data points $(\Delta V_{oa}^r, \Delta V_o^r)$ into new set of orthogonal axis Z_1 and Z_2

the data points is determined by the correlation coefficient as shown in (2.17).

$$\rho_{(\Delta V_{oa}^r \Delta V_o^r)} = \frac{cov(\Delta V_{oa}^r, \Delta V_o^r)}{\sigma_{\Delta V_{oa}^r} \sigma_{\Delta V_o^r}}, \rho_{(\Delta V_{oa}^r \Delta V_o^r)} \in (-1, 1)$$

$$(2.17)$$

The maximum eigenvalue along the principal component axis of the covariance matrix for linearly correlated variable data points is considered as their variance. Considering this point, in this work, PCA is used for calculating the variance of correlated data point $(\Delta V_{oa}^r, \Delta V_o^r)$, $(\Delta V_{oa}^i, \Delta V_o^i)$ and $(\Delta V_{oa}, \Delta V_o)$ along the principal component axis. Here, ΔV_{oa}^r , ΔV_{oa}^r and ΔV_{oa} are the real part of the change in voltage, the imaginary part of the change in voltage and the absolute change in voltage at observer bus O due to power perturbation at k^{th} active buses and ΔV_o^r , ΔV_o^i and ΔV_o are the cumulative real part of the change in voltage, the imaginary part of change in voltage and absolute change in voltage at the observer bus O due to power perturbation at the active bus together. The methods to determine the variance of correlated data points $(\Delta V_{oa}^r, \Delta V_o^r)$ along the principal component axis is explained below. Similarly, variance of correlated data points $(\Delta V_{oa}^i, \Delta V_o^i)$ and $(\Delta V_{oa}, \Delta V_o)$ along the principal component axis is determined. For evaluating the variance of correlated data points $(\Delta V_{oa}^r, \Delta V_o^r)$ along the principal component axis, first of all variable data point $(\Delta V_{oa}^r, \Delta V_o^r)$ is transformed into new set of orthogonal axis Z_1 and Z_2 as illustrated in Fig. 2.3. After that, variance of variable data points $(\Delta V_{oa}^r, \Delta V_o^r)$ along Z_1 and Z_2 is calculated, as shown in (2.18) to (2.41). In Fig. 2.3, transformation of data point $(\Delta v_{oa_1}^r, \Delta v_{o_1}^r)$ along Z_1 and Z_2 is shown. Similarly, all the data points present on axis ΔV_{oa}^r and ΔV_{o}^r are transformed onto the new axis Z_1 and Z_2 and it is expressed in matrix form as following:

$$Z = A^{T}X$$

$$\text{where } Z_{n \times 1} = \begin{bmatrix} Z_{1} \\ Z_{2} \end{bmatrix}, X_{m \times 2} = \begin{bmatrix} v_{oa_{1}}^{r} & \dots & v_{oa_{m}}^{r} & v_{o_{1}}^{r} & \dots v_{om}^{r} \end{bmatrix}^{T}$$

$$A^{T} = \begin{bmatrix} \cos \theta_{1} & \dots & \cos \theta_{m} & \sin \theta_{1} & \dots & \sin \theta_{m} \\ -\sin \theta_{1} & \dots & -\sin \theta_{m} & \cos \theta_{1} & \dots & \cos \theta_{m} \end{bmatrix} = \begin{bmatrix} a_{1} \\ a_{2} \end{bmatrix}$$

The Z_1 and Z_2 are orthogonal to each other. Therefore it can be written as:

$$a_n^T a_n = 1 \quad n \in \{1, 2\} \tag{2.19}$$

where A is transformation matrix. Now, variance of data point along the Z_n is calculated as using (2.18) and (2.19):

$$var(Z_n) = var(a_n^T X) = var(a_n^T X a_n^T a_n) = a_n^T var(Z_n) a_n, n \in \{1, 2\}$$
(2.20)

$$a_n^T var(Z_n) a_n = a_n^T \sum_{(\Delta V_{og}^r, \Delta V_o^r)} a_n, \tag{2.21}$$

$$\Sigma_{(\Delta V_{oa}^r, \Delta V_o^r)} = \begin{bmatrix} var(\Delta V_{oa}^r) & cov(\Delta V_{oa}^r, \Delta V_o^r) \\ cov(\Delta V_{oa}^r, \Delta V_o^r) & var(\Delta V_o^r) \end{bmatrix}$$
(2.22)

$$\Sigma_{(\Delta V_{oa}^r, \Delta V_o^r)} = \begin{bmatrix} \sigma_{11} & \sigma_{12} \\ \sigma_{21} & \sigma_{22} \end{bmatrix}$$

$$(2.23)$$

In (2.21) and (2.22), $\Sigma_{(\Delta V_{oa}^r, \Delta V_{o}^r)}$ is covariance matrix for calculating the impact on real part of change in voltage at observer bus due to power perturbation at active bus. Its diagonal element represents variance and off-diagonal element represents covariance of variable ΔV_{oa}^r and ΔV_{o}^r , respectively.

$$\Sigma_{(\Delta V_{oak}, \Delta V_o)} = \begin{bmatrix} var(\Delta V_{oak}^r) & cov(\Delta V_{oak}^i, \Delta V_{oak}^r) & cov(\Delta V_{oak}^r, \Delta V_o^i) & cov(\Delta V_{oak}^r, \Delta V_o^r) \\ cov(\Delta V_{oak}^i, \Delta V_{oak}^r) & var(\Delta V_{oak}^i) & cov(\Delta V_{oak}^i, \Delta V_o^r) & cov(\Delta V_{oak}^i, \Delta V_o^i) \\ cov(\Delta V_o^r, \Delta V_{oak}^r) & cov(\Delta V_{oak}^i, \Delta V_o^r) & var(\Delta V_o^r) & cov(\Delta V_o^i, \Delta V_o^r) \\ cov(\Delta V_{oak}^r, \Delta V_o^r) & cov(\Delta V_{oak}^i, \Delta V_o^i) & cov(\Delta V_o^i, \Delta V_o^r) & var(\Delta V_o^i) \end{bmatrix}$$
 (2.24)

$$\Sigma_{(\Delta V_{oak}^i, \Delta V_o^i)} = \begin{bmatrix} var(\Delta V_{oak}^i) & cov(\Delta V_{oak}^i, \Delta V_o^r) \\ cov(\Delta V_{oak}^i, \Delta V_o^r) & var(\Delta V_o^i) \end{bmatrix}$$
(2.25)

$$cov(\Delta V_{oak}^r, \Delta V_o^r) = E(\Delta V_{oak}^r, \Delta V_o^r) = E(\Delta V_{oak}^r \sum_{j=1}^n \Delta V_{oaj}^r)$$

$$= E(\Delta V_{oak}^r \Delta V_{oak}^r) + E(\sum_{i=1}^n \Delta V_{oak}^r \Delta V_{oaj}^r)$$
(2.26)

$$= E(\Delta V_{oak}^r \Delta V_{oak}^r) + E(\sum_{\substack{j=1\\k\neq j}}^n \Delta V_{oak}^r \Delta V_{oaj}^r)$$

$$= var(\Delta V_{oak}^r) + \sum_{\substack{j=1\\k\neq j}}^n E(\Delta V_{oak}^r \Delta V_{oaj}^r)$$
(2.27)

$$cov(\Delta V_{oak}^i, \Delta V_o^i) = E(\Delta V_{oak}^i, \Delta V_o^i) = E(\Delta V_{oak}^i, \sum_{i=1}^n \Delta V_{oaj}^i)$$

$$= var(\Delta V_{oak}^i) + \sum_{\substack{j=1\\k \neq j}}^n E(\Delta V_{oak}^i \Delta V_{oaj}^i)$$
(2.28)

From (2.10)

$$var(\Delta V_{oak}^r) = var(\Delta Q_{ak} X_{oak} - \Delta P_{ak} R_{oak})$$
(2.29)

$$= X_{oak}^2 var(\Delta Q_{ak}) + R_{oak}^2 var(\Delta P_{ak})$$

$$-2R_{oak} X_{oak} cov(\Delta P_{ak} \Delta Q_{ak})$$

$$(2.30)$$

$$E(\Delta V_{oak}^r, \Delta V_{oaj}^r) = E((\Delta Q_{ak} X_{oak} - \Delta P_{ak} R_{oak})$$

$$(\Delta Q_{aj} X_{oaj} - \Delta P_{aj} R_{oaj}))$$
(2.31)

$$= E(\Delta Q_{aj} \Delta Q_{ak} X_{oak} X_{oaj}) - E(\Delta Q_{aj} \Delta P_{ak} R_{oak} X_{oaj})$$

$$-E(\Delta Q_{ak} \Delta P_{aj} R_{oaj} X_{oak}) + E(\Delta P_{aj} \Delta P_{ak} R_{oak} X_{oak})$$

$$= X_{oak} X_{oaj} E(\Delta Q_{aj} \Delta Q_{ak}) - R_{oak} X_{oaj} E(\Delta Q_{aj} \Delta P_{ak})$$

$$-R_{oaj} X_{oai} E(\Delta Q_{ak} \Delta P_{aj}) + R_{oai} X_{oak} E(\Delta P_{aj} \Delta P_{ak})$$

$$= X_{oak} X_{oaj} cov(\Delta Q_{aj} \Delta Q_{ak}) - R_{oak} X_{oaj} cov(\Delta Q_{aj} \Delta P_{ak})$$

$$-R_{oaj} X_{oai} cov(\Delta Q_{ak} \Delta P_{aj}) + R_{oai} X_{oak} cov(\Delta P_{aj} \Delta P_{ak})$$

$$(2.32)$$

From (2.11)

$$var(\Delta V_{oak}^i) = var(-\Delta Q_{ak} R_{oak} - \Delta P_{ak} X_{oak})$$
(2.33)

$$= R_{oak}var(\Delta Q_{ak}) + X_{oak}var(\Delta P_{ak})$$

$$+2X_{oak}R_{oak}cov(\Delta Q_{ak}\Delta P_{ak})$$
(2.34)

$$E(\Delta V_{oak}^{i}, \Delta V_{oaj}^{i}) = E((-\Delta Q_{ak} R_{oak} - \Delta P_{ak} X_{oak})$$

$$(-\Delta Q_{aj} R_{oaj} - \Delta P_{aj} X_{oaj}))$$

$$(2.35)$$

$$R_{oai}R_{oaj}cov(\Delta Q_{ak}\Delta Q_{aj}) + R_{oaj}X_{oak}cov(\Delta P_{ak}\Delta Q_{aj})$$

$$X_{oaj}R_{oak}cov(\Delta P_{aj}\Delta Q_{ak}) + X_{oaj}X_{oak}cov(\Delta P_{ak}\Delta P_{aj})$$
(2.36)

$$E(\Delta V_{oak}^r, \Delta V_o^i) = E((\Delta Q_{ak} R_{oak} - \Delta P_{ak} X_{oak})$$

$$(-\Delta Q_{aj} R_{oaj} - \Delta P_{aj} X_{oaj}))$$
(2.37)

$$-X_{oak}R_{oaj}cov(\Delta Q_{ak}\Delta Q_{aj}) + R_{oaj}R_{oak}cov(\Delta P_{ak}\Delta Q_{aj})$$
$$-X_{oak}X_{oak}cov(\Delta P_{aj}\Delta Q_{ak}) + X_{oak}R_{oaj}cov(\Delta P_{ak}\Delta P_{aj})$$

$$E(\Delta V_{oak}^{i}, \Delta V_{o}^{r}) = -X_{oaj}R_{oak}cov(\Delta Q_{ak}\Delta Q_{aj})$$

$$+ R_{oaj}R_{oak}cov(\Delta P_{aj}\Delta Q_{ak} + X_{oak}R_{oaj}cov(\Delta P_{ak}\Delta P_{aj})$$

$$- X_{oak}X_{oaj}cov(\Delta P_{ak}\Delta Q_{aj})$$
(2.38)

Similarly, covariance matrices $\Sigma_{(\Delta V_{oa}^i, \Delta V_o^i)}$ and $\Sigma_{(\Delta V_{oa}, \Delta V_o)}$ are formulated to determine the impact of power perturbation at active bus on imaginary and absolute part of change in voltage at observer bus. Elements of covariance matrices $\Sigma_{(\Delta V_{oa}^r, \Delta V_o^r)}$, $\Sigma_{(\Delta V_{oa}^i, \Delta V_o^i)}$ and $\Sigma_{(\Delta V_{oa}, \Delta V_o)}$ is analytically derived using (2.13)-(2.16) and (2.27)-(2.38). Orthogonality of Z_1 and Z_2 is show in (2.19). Using (2.19) and (2.20), Lagrange-multiplier is formulated for determining the maximum variance of variable data points $(\Delta V_{oa}^r, \Delta V_o^r)$ along the new axis Z_n , as shown in (2.39).

$$L = a_n^T \Sigma_{(\Delta V_{oa}^T, \Delta V_o^T)} a_n - \lambda (a_n^T a_n - 1)$$
(2.39)

$$\frac{dL}{da_n} = \left(\sum_{(\Delta V_{oa}^r, \Delta V_o^r)} - \lambda I\right) a_n = 0 \tag{2.40}$$

For determining the maximum variance of variable data points along the new axis Z_n , Lagrange-multiplier is differentiated in term n^{th} row element (a_n) of transformation matrix A because the position of variable data points on new transformed axis is decided by (a_n) . After simplifying (2.39), it is found that, (2.40) represents characteristic of covariance matrix $\Sigma_{(\Delta V_{oa}^r, \Delta V_o^r)}$; where λ represents the eigenvalue of $\Sigma_{(\Delta V_{oa}^r, \Delta V_o^r)}$. From (17) and (20), it is seen that the trace of the co-variance matrix and summation of their eigenvalues are equal due to Z_1 and

 Z_2 , as shown in (2.41).

$$\sum_{h=1}^{m} \sigma_{hh} = trace\left(\Lambda\right) = \sum_{h=1}^{p} (\lambda_h)$$
(2.41)

From (2.41), it is concluded that the maximum variance of data point along the principal component axis is the eigenvalue of the co-variance matrix. Now a selection of principal component axis for determining the PVSI is done on the basis η_h as given in (2.42). η_h gives a fraction of the total variance shared by the principal component axis. The higher value of η_h means that higher value data point lies along that axis. On the basis of variance along that axis, the variance of variable data point can be estimated. In this work, the axis which has the highest value of η_h that principal component axis is considered for evaluating PVSI.

$$\eta_h = \frac{\lambda_h}{\sum_{h=1}^{M} \lambda_h}, h \in \{1, 2, 3, \dots M\}$$
 (2.42)

$$PVSI_{k_r} = max\{\lambda_{\Sigma_{(\Delta V_{oak}^r, \Delta V_o^r)}}\}$$
 (2.43)

where k represents active bus number i.e, $k \in \{2, 4, 6, \dots\}$

To evaluate the impact of power perturbation on the real part of the change in voltage $PVSI_{k_r}$ is formulated as shown in (2.43). Similarly, $PVSI_{k_i}$ and $PVSI_k$ are formulated to determine the impact of power perturbation on imaginary and absolute parts of change in voltage, respectively. Algorithm 1 gives the steps to calculate the $PVSI_{k_r}$, $PVSI_{k_i}$ and $PVSI_k$ for ranking the impact of power perturbation at active buses on ΔV_o^r , ΔV_o^i and ΔV_o , respectively.

Algorithm 1 calculation of PVSI

- 1: Construct the impedance matrix (Z_{bus}) to determine common impedance (Z_{oa_k}) , reactance (X_{oa_k}) , and resistance (R_{oa_k}) between the active bus k and observer bus k. The off-diagonal element of Z_{bus} is the common impedance, and their real and imaginary parts are common resistance and reactance, respectively; where $k \in \{2, 4, 6, \ldots\}$
- 2: Estimate the power perturbation at all active buses using a zero mean normal probability density function.
- 3: Calculate covariance matrices $cov(\Delta V_{oak}^r, \Delta V_o^r)$, $cov(\Delta V_{oak}^i, \Delta V_o^i)$ and $cov(\Delta V_{oak}, \Delta V_o)$. The elements of covariance matrix are analytically determined as given in (2.24)-(2.38).
- 4: Evaluate the eigenvalues of covariance matrices $cov(\Delta V_{oak}^r, \Delta V_o^r), \ cov(\Delta V_{oak}^i, \Delta V_o^i), \ cov(\Delta V_{oak}, \Delta V_o).$
- 5: Calculate $PVSI_{k_r},\ PVSI_{k_i},\ PVSI_k$ as following:
 - [a] The impact of power perturbation at the active bus on the real part of the change in voltage at the observer bus (ΔV_o^r) is determined on the basis of $PVSI_{k_r}$. $PVSI_{k_r} = max(\lambda_{(\Delta V_{och}^r \Delta V_o^r)})$
 - [b] The impact of power perturbation at active bus on imaginary part of change in voltage at observer bus (ΔV_o^i) is determined on the basis of $PVSI_{k_i}$; $PVSI_{k_i} = max(\lambda_{(\Delta V_{oak}^i, \Delta V_o^i)})$
 - [c] The impact of power perturbation at active bus on absolute change in voltage at observer (ΔV_o) is determined on the basis of $PVSI_k PVSI_k = max(\lambda_{(\Delta V_{oak}, \Delta V_o)})$
- 6: Rank the active buses on the basis of *PVSI*. The bus which has highest value of *PVSI* is considered as most impactful bus for change in voltage at observer bus.

2.4 Case Study and Discussion

To verify PVSI for ranking the impact of power perturbation at active buses on change in voltage at observer buses 69-bus and 141-bus distribution system is taken into account. The system data are given in [94, 95]. The structure, branch data and bus data of 141-bus system is presented in Chapter-A. The test system's nominal voltage and power ratings are taken as 12.47 kV and 100 MVA, respectively. The PVSI is capable of determining the impact of power perturbation at the active bus on voltage deviation at the observer bus with the arbitrary number of DGs at a

random position. However, for simplicity, in both the test system, the even number bus is selected as the active bus, and the far-end odd number bus from the grid has been selected as the observer bus. For finding out PVSI, Algorithm 1 is implemented in MATLAB R2019b with the system configuration of Intel-Core i7-8700, CPU @ 3.20 GHz. It is verified in three scenarios on 69-bus and 141-bus distribution systems by comparing the results with the traditional MCS method as explained in section II-A and JDE method [26].

2.4.1 Change in active power at multiple buses

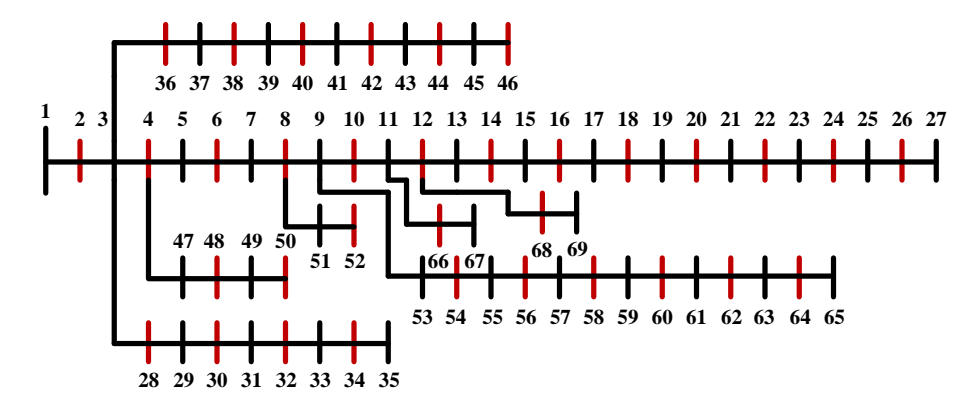


Fig. 2.4: 69-bus distribution system

The output power from (DGs) depends on weather conditions, due to which it is very important to gather information about the impact of active power perturbation on voltage deviation for the optimal and dynamic solution of voltage control. The variance of power perturbation at any active bus depends on the size of DG at that bus. In this case, three different sizes of normal random variables is taken to model the active power perturbation at multiple locations in distribution systems, as shown in the (2.44), (2.45) and (2.46).

The power perturbation on available DGs in the distribution system is correlated. The correlation exists among them due to several factors, such as environmental factors like solar irradiance, wind speed or change in the price of electricity. For incorporating the correlation among the DGs for active power perturbation, The correlation coefficient (ρ_p) for active power perturbation has been taken as 0.2 [89].

$$\Delta P_k = N(0, 1\sqrt{2}), k \in \{2, 8, \dots\}$$
 (2.44)

$$\Delta P_k = N(0, 2\sqrt{2}), k \in \{4, 10, \dots\}$$
 (2.45)

$$\Delta P_k = N(0, 3\sqrt{2}), k \in \{6, 12, \dots\}$$
(2.46)

2.4.1.1 69-bus distribution system

Active power perturbation (ΔP_k) is considered on thirty-four active buses as given in (2.44), (2.45) and (2.46); where k represents the active buses $k \in \{2, 4, 6, ..., 68\}$, and it is shown in Fig.2.4. Observing their effect on change in voltage, bus 27, bus 45 and bus 51 are selected as observer buses.

2.4.1.2 141-bus distribution system

Active power perturbation (ΔP_k) is considered on seventy active buses as shown in (2.44), (2.45) and (2.46); where $k \in \{2, 4, 6, \dots, 140\}$ and for observing their effect on change in voltage, bus 59,

bus 129 and bus 141 are selected as observer buses.

2.4.1.3 Calculation of PVSI in 69-bus distribution system for active bus 68

1. For finding out the impact of active power perturbation at bus 68 on real, imaginary and absolute part of change in voltage at observer bus 27, firstly covariance matrices $\Sigma_{(\Delta V_{27.68}^r, \Delta V_{27}^r)}$, $\Sigma_{(\Delta V_{27.68}^i, \Delta V_{27}^i)}$ and $\Sigma_{(\Delta V_{27.68}, \Delta V_{27}^i)}$ are calculated as given below:

$$\Sigma_{(\Delta V_{68,27}^r, \Delta V_{27}^r)} = 10^- 6 \begin{bmatrix} 0.2804 & 0.0048 \\ 0.0048 & 0.0047 \end{bmatrix}$$

$$\Sigma_{(\Delta V_{27,68}^i, \Delta V_{27}^i)} = 10^- 7 \begin{bmatrix} 0.7965 & 0.0160 \\ 0.0160 & 0.0152 \end{bmatrix}$$

$$\Sigma_{(\Delta V_{27,68}, \Delta V_{27})} = 10^- 6 \begin{bmatrix} 0.0047 & 0.0014 & 0.0048 & 0.0013 \\ 0.0014 & 0.0015 & 0.0014 & 0 \\ 0.0048 & 0.0014 & 0.2804 & 0.0664 \\ 0.0013 & 0 & 0.0664 & 0.0796 \end{bmatrix}$$

2. After that, eigenvalues of covariance matrices $\Sigma_{(\Delta V_{27,68}^r, \Delta V_{27}^r)}$, $\Sigma_{(\Delta V_{27,68}^i, \Delta V_{68}^i)}$ and $\Sigma_{(\Delta V_{27,68}, \Delta V_{68})}$ are evaluated as given below:

$$PVSI_{68_r} = max(0.0460 \times 10^-7, 0.2804 \times 10^-6)$$

$$PVSI_{68_i} = max(0.0149 \times 10^-7, 0.7968 \times 10^-7)$$

$$PVSI_{68} = max(-0.0010 \times 10^-6, 0.0051 \times 10^-6, 0.0596 \times 10^-6, 0.3005 \times 10^-6)$$

3. The eigenvalues which have the highest value of the corresponding covariance matrix are selected for $PVSI_{68_r}$, $PVSI_{68_i}$ and $PVSI_{68}$ to evaluate the impact of active power perturbation on real, imaginary and absolute part of the change in voltage at observer bus 27 as shown below:

$$PVSI_{68_r} = 0.2804 \times 10^-6$$

 $PVSI_{68_i} = 0.7968 \times 10^-7$
 $PVSI_{68} = 0.3005 \times 10^-6$

Similarly, $PVSI_{k_r}$, $PVSI_{k_i}$ and $PVSI_k$ are evaluated for thirty-four active buses in 69-bus distribution system and for seventy active in 141-bus distribution test systems. On the basis of PVSI, the impact of power perturbation at active buses on the change in voltage at observer bus are ranked.

2.4.1.4 Discussion

Ranking of active buses for perturbation in active power are done using proposed PVSI, JDE and the traditional MCS methods, as explained in section II-A for 10,000 scenarios. For measuring the accuracy of PVSI, JDE and the traditional MCS method are used. In Table 2.1, the ranking of an active bus for the 69-bus distribution system is presented. Similarly, the ranking of active buses for the 141-bus distribution system is presented in Table 5.5. In Table 2.1 and Table 5.5,

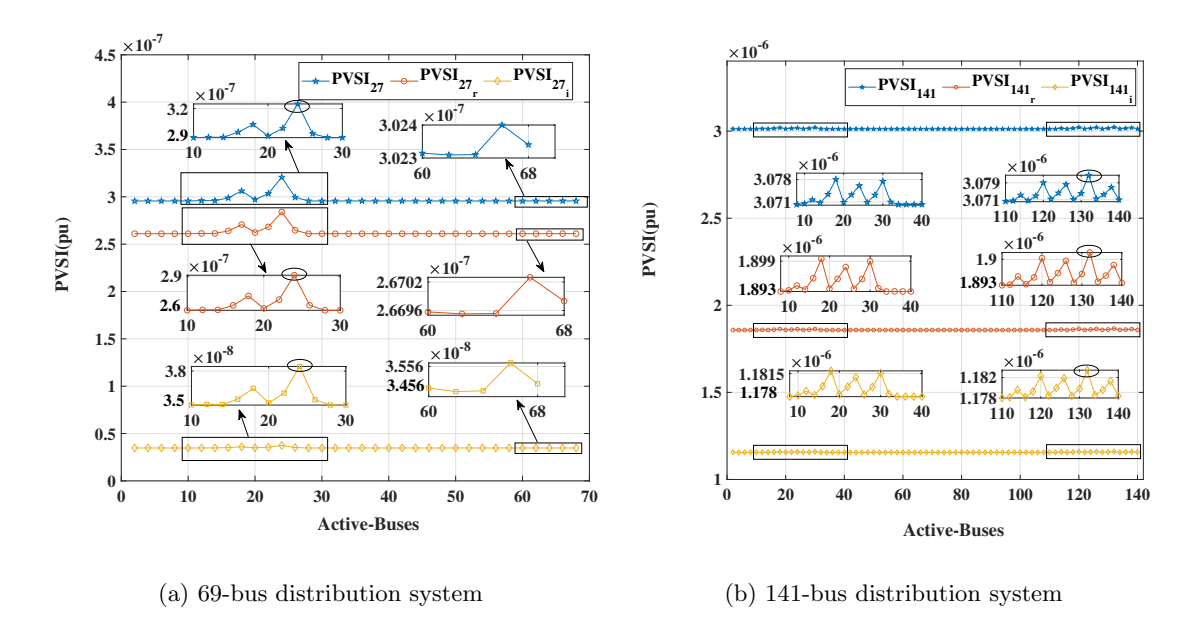


Fig. 2.5: The PVSI of active buses for (a) change in voltage at bus 27, (b) change in voltage at bus 141 due to active power perturbation at active buses

Table 2.1: Ranking of active bus for change in voltage at observer bus in 69 bus distribution system by traditional MCS, JDE and proposed PVSI

Ranking	$MCS_{\Delta V_{27}}$	$JDE_{\Delta V_{27}}$	$PVSI_{\Delta V_{27}}$
1	24	18	24
2	18	22	18
3	22	24	22
4	16	26	16
5	26	16	26
6	20	20	20
7	12	14	14
8	14	12	12
9	66	66	66
10	68	68	68

Ranking	$MCS_{\Delta V_{45}}$	$JDE_{\Delta V_{45}}$	$PVSI_{\Delta V_{45}}$
1	66	66	66
2	60	60	60
3	54	54	54
4	68	68	68
5	58	58	58
6	64	64	64
7	52	52	52
8	36	48	48
9	42	36	36
10	30	42	42

(a) For change in voltage at bus 27

(b) For change in voltage at bus 45

Ranking	$MCS_{\Delta V_{51}}$	$JDE_{\Delta V_{51}}$	$PVSI_{\Delta V_{51}}$
1	66	60	66
2	54	24	54
3	60	12	60
4	24	54	18
5	18	18	24
6	12	66	12
7	64	52	52
8	52	64	64
9	58	58	58
10	22	22	22

(c) For change in voltage at bus 51

the top ten active buses are arranged in descending order on the basis of their effect on the change in voltage at the observer bus. In the first column, ranking by the traditional MCS method; in the second column, ranking by the JDE method; and in the third column, ranking by PVSI have been presented. The computation time for all three methods of ranking is given in Table

Distribution System	Method	Computation time
		*
69-bus	Traditional MCS	3250.8 sec
69-bus	JDE	0.7672ec
69-bus	PVSI	0.1091 sec
141-bus	Traditional MCS	10430 sec
141-bus	JDE	0.8484 sec
141-bus	PVSI	0.120 sec

Table 2.2: Computation time of ranking for ΔP_k

5.5. The traditional MCS method runs $(k+1) \times 10,000$ times load flow for considering 10,000 scenarios of power perturbation at active buses to rank the active buses on the basis of their impacts on the observer bus voltage. Here, k is the number of active buses. Therefore, it takes a very high computation time for ranking, which makes this method inefficient to use in a real-time scenario. The JDE takes relatively very less computation time than traditional MCS because it is analytically derived. However, the analytic formulation of change in voltage at the observer bus due to power perturbation at active buses used to formulate JDE requires an initial condition voltage profile at the active buses. And it is determined by load flow which increases the computation time. To formulate the PVSI, the analytic formula of change in voltage at the observer bus due to power perturbation at active buses does not require the initial condition of voltage profile at active buses. Therefore, it takes less computation time than the traditional MCS and JDE. After comparing PVSI with JDE and traditional MCS methods in terms of accuracy and computation time, it is observed that PVSI gives a similar ranking as the traditional MCS method in less computation time than JDE, as shown in Tables 2.1, 5.5 and 2.2. Therefore, it can be applied in a real-time scenario to determine the impact of active power perturbation on voltage deviation at any bus.

In this case, PVSI is the maximum variance of a two-dimensional data point $(\Delta V_{oak}^r, \Delta V_o^r)$, $(\Delta V_{oak}^i, \Delta V_o^i)$ and $(\Delta V_{oak}, \Delta V_o)$ along the principal component axis due to perturbation in active power at active buses. Here, $\Delta V_{oak}^r, \Delta V_{oak}^i$ and ΔV_{oak} are real part of change in voltage, imaginary part of change in voltage and absolute change in voltage at observer bus O due to active power perturbation at k^{th} active bus. $\Delta V_o^r, \Delta V_o^i$ and ΔV_o are the cumulative real part of change in voltage, imaginary part of change in voltage and absolute change in voltage at the observer bus O due to active power perturbation at the active bus together.

Fig. 2.5 shows PVSI values for all the active buses due to active power perturbation at active buses. Considering bus 27 as the observer bus of the 69 bus system, PVSI values are shown in Fig. 2.5-(a) and considering bus 141 as the observer bus of the 141 bus system, the PVSI value are shown in Fig. 2.5-(b). In Fig. 2.5, at the Y-axis PVSI value of all the active buses and at the X-axis, active-buses k=2,3,6... are represented. The brown line represents the value of $PVSI_{k_r}$ for all the active buses, and it shows the impact of active power perturbation on the real part of the change in voltage. The yellow colour represents the value of $PVSI_{k_i}$ for all active buses, and it shows the impact of active power perturbation on the imaginary part of the change in voltage, and the blue line represents the value of $PVSI_k$ and it shows the impact of active power perturbation on the absolute change in voltage.

In Fig. 2.5, the highest value of $PVSI_k$ is observed at active bus 24. Therefore, in the 69-bus distribution system, bus 24 is selected as the most impactful bus for change in voltage at bus 27. From all the active buses, bus 24 has the highest impact on the voltage profile of bus 27 due to active power perturbation at active buses. Similarly, for the observer bus 45 and 51, the highest value of $PVSI_k$ is observed. Thus, bus 66 is selected as the most impactful bus for change in

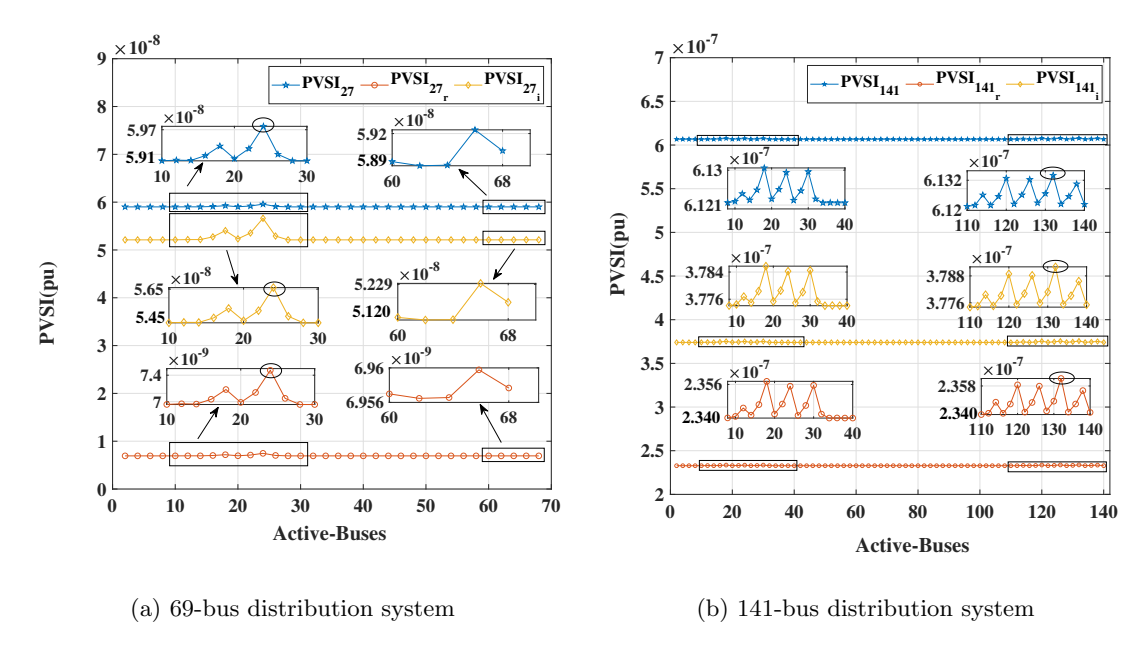


Fig. 2.6: The PVSI of active buses for (a) change in voltage at bus 27, (b) change in voltage at bus 141 due to reactive power perturbation at active buses

voltage at both the observer bus 45 and 51. From all the active buses, 66 has the highest impact on the voltage profile of both the observer buses 25 and 51 due to active power perturbation at active buses. In Fig. 2.5, the highest value of $PVSI_k$ is observed at bus 138. Thus, in the 141-bus distribution system, bus 138 is selected as the most impactful bus for change in voltage at bus 141. Similarly, for 59 and 129 the highest value of $PVSI_k$ observed at buses 54 and 126. Hence, buses 54 and 126 have the highest impact on change in voltage at observer buses 59 and 129 due to active power perturbation at active buses. $PVSI_{k_r}$ gives the impact of power perturbation on the real part of the change in voltage while $PVSI_{k_i}$ gives the impact of power perturbation on the imaginary part of the change in voltage. In Fig 5, it is seen that the value of $PVSI_{k_i}$ is more than $PVSI_{k_i}$ for all active buses. Therefore, it is concluded that perturbation in active power has more influence on $PVSI_{k_r}$ than $PVSI_{k_i}$ at the observer bus.

2.4.2 Change in reactive power at multiple buses

With the development of electronic power inverters, inverter interfaced DG itself offers reactive power compensation for maintaining the voltage profile. Study the impact of reactive power perturbation on voltage deviation; reactive power perturbation is considered at multiple buses. Their effect on change in voltage at the observer bus is determined based on the basis PVSI, JDE and the traditional MCS method. Perturbation in reactive power are modeled by a zero-mean normal random variable and as given in (2.47), (2.48) and (2.49). For considering the correlation among reactive power perturbation among the available DGs, the reactive power correlation coefficient (ρ_q) is taken as 0.2.

$$\Delta Q_k = N(0, \sqrt{2}), k \in \{2, 8, \dots\}$$
 (2.47)

$$\Delta Q_k = N(0, 2\sqrt{2}), k \in \{4, 10....\}$$
(2.48)

$$\Delta Q_k = N(0, 3\sqrt{2}), k \in \{6, 12....\}$$
(2.49)

2.4.2.1 69-bus distribution system

Reactive power perturbation (ΔQ_k) are considered on thirty-four active buses as given in (2.47), (2.48) and (2.49); where $k \in \{2, 4, 6,68\}$ and for observing their effect on change in voltage, bus 27, bus 45 and bus 51 are selected as observer buses.

2.4.2.2 141-bus distribution system

Reactive power perturbation (ΔQ_k) is considered on seventy active buses as shown in (2.47), (2.48) and (2.49); where $k \in \{2, 4, 6, ..., 140\}$ and for observing their effect on change in voltage, bus 59, bus 129 and bus 141 are selected as observer buses.

Table 2.3: Ranking of active bus for change in voltage at observer bus in 141-bus distribution system by traditional MCS, JDE and proposed PVSI

Ranking	$MCS_{\Delta V_{59}}$	$JDE_{\Delta V_{59}}$	$PVSI_{\Delta V_{59}}$
1	54	72	54
2	60	60	60
3	48	54	48
4	66	66	66
5	72	44	72
6	84	78	78
7	78	84	84
8	42	48	42
9	56	64	52
10	48	58	48

Ranking	$MCS_{\Delta V_{129}}$	$JDE_{\Delta V_{129}}$	$PVSI_{\Delta V_{129}}$
1	126	126	126
2	120	120	120
3	132	132	132
4	138	30	138
5	30	138	30
6	18	18	18
7	124	24	124
8	130	124	130
9	24	130	118
10	118	118	24

⁽b) For change in voltage at bus 129

Ranking	$MCS_{\Delta V_{141}}$	$JDE_{\Delta V_{141}}$	$PVSI_{\Delta V_{141}}$
1	138	138	138
2	120	120	120
3	126	126	126
4	24	24	24
5	18	18	18
6	138	138	138
7	30	130	30
8	124	124	124
9	130	118	130
10	114	124	114

⁽c) For change in voltage at bus 141

2.4.2.3 Discussion

Ranking of active buses for perturbation in reactive power at active buses is done using the proposed PVSI, JDE [26] and traditional MCS methods for 10,000 scenarios. After comparing PVSI with JDE and traditional MCS methods, it is observed that the ranking due to perturbation in reactive power at active buses gives a similar ranking as active power perturbation at active buses, as shown in Table 2.1 and Table 5.5. Their computation time is given in Table 2.4. After comparing the ranking method PVSI with JDE and the traditional method, it is observed that PVSI gives a similar ranking as traditional MCS in less computation time than the JDE due to their simplistic analytic formulation.

⁽a) For change in voltage at bus 59

In this case, PVSI is the maximum variance of a two-dimensional data point $(\Delta V_{oak}^r, \Delta V_o^r)$, $(\Delta V_{oak}^i, \Delta V_o^i)$ and $(\Delta V_{oak}, \Delta V_o)$ along the principal component axis due to perturbation in reactive power at active buses. Here, ΔV_{oak}^r , ΔV_{oak}^r and ΔV_{oak} are the real part of change in voltage, imaginary part of change in voltage and absolute change in voltage at observer bus O due to reactive power perturbation at k^{th} active buses and ΔV_o^r , ΔV_o^i and ΔV_o are the cumulative real part of change in voltage, imaginary part of change in voltage and absolute change in voltage at the observer bus O due to reactive power perturbation at the active bus together.

Fig. 2.6 shows PVSI values for all the active buses due to reactive power perturbation at active buses. Considering bus 27 as the observer bus of the 69 bus system, PVSI values are shown in Fig. 2.6-(a) and considering bus 141 as the observer bus of the 141 bus system, the PVSI value are depicted in Fig. 2.6-(b).

In Fig. 2.6-(a), the highest value of PVSI is observed at bus 24. Therefore, in the case of the 69-bus distribution system, reactive power perturbation at bus 24 is selected as the most impactful bus for change in voltage at bus 27 due to reactive power perturbation at active buses. Similarly, the highest value of PVSI is observed at bus 66 for observer buses 45 and 51. Therefore, active buse 66 is selected as the most impactful bus for observer buses 45 and 51 due to reactive power perturbation at active buses.

In Fig. 2.6-(b), the maximum value PVSI is observed at bus 132. Therefore, in the case of the 141-bus distribution system, bus 132 is considered as the most impactful bus for change in voltage at bus 141 due to reactive power perturbation at active buses. Similarly, for the observer bus 59 and 129, the higher value of PVSI is observed at 54 and 126, respectively. Therefore, active bus 54 and 126 is selected as the most impactful bus for observer buses 59 and 129 due to reactive power perturbation at active buses. In Fig 2.6, it is seen that the value of $PVSI_{k_i}$ is more than $PVSI_{k_i}$ for all active buses. Therefore, it is concluded that perturbation in reactive power has more influence on ΔV_o^i than ΔV_o^r at the observer bus.

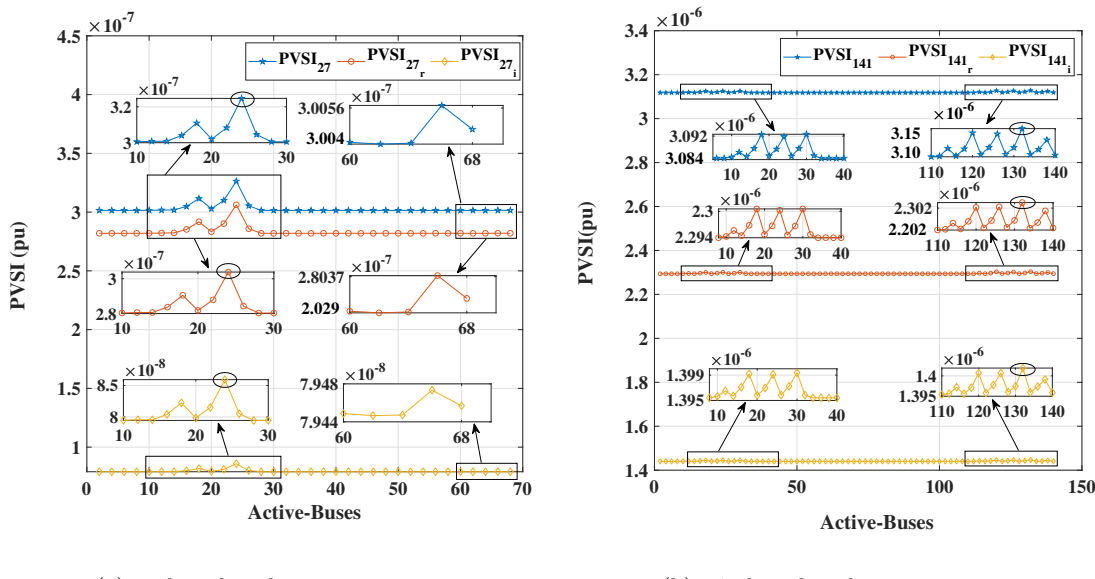
Distribution System	Method	Computation time	
69-bus	Traditional MCS	3310.8 sec	
69-bus	JDE	0.7723 sec	
69-bus	PVSI	0.1100 sec	
141-bus	Traditional MCS	10694sec	
141-bus	JDE	$0.8658 \mathrm{sec}$	
141-bus	PVSI	0.1214 sec	

Table 2.4: Computation time of ranking for ΔQ_k

2.4.3 Change in active and reactive power both at multiple buses

In this case, complex power perturbation is considered at multiple buses, and their effect on change in voltage at the observer bus is determined on the basis of PVSI, JDE and traditional MCS. Perturbation in complex power is modeled as bi-variate normal random variable as provided in (2.50), (2.51) and (2.52). The active and reactive power of inverter-based distributed generation is negatively correlated. So, the correlation coefficient of active and reactive power perturbation (ρ_{pq}) is taken as -0.1. For considering the correlation among the complex power perturbation at all the available DGs in the distribution system, the active and reactive power correlation coefficient ρ_p and ρ_q is considered as 0.2.

$$\begin{bmatrix} \Delta P_k \\ \Delta Q_k \end{bmatrix} \sim \mathcal{N} \left(\begin{bmatrix} 0 \\ 0 \end{bmatrix}, \begin{bmatrix} 10 & -.4472 \\ -.4472 & 2 \end{bmatrix} \right), k \in \{2, 8..\}$$
 (2.50)



(a) 69 bus distribution system

(b) 141-bus distribution system

Fig. 2.7: The PVSI of active buses for (a) change in voltage at bus 27, (b) change in voltage at bus 141 due to complex power perturbation at active buses

$$\begin{bmatrix} \Delta P_k \\ \Delta Q_k \end{bmatrix} \sim \mathcal{N} \left(\begin{bmatrix} 0 \\ 0 \end{bmatrix}, \begin{bmatrix} 20 & -.8944 \\ -.8944 & 4 \end{bmatrix} \right), k \in \{4, 10...\}$$
 (2.51)

$$\begin{bmatrix} \Delta P_k \\ \Delta Q_k \end{bmatrix} \sim \mathcal{N} \left(\begin{bmatrix} 0 \\ 0 \end{bmatrix}, \begin{bmatrix} 30 & -1.341 \\ -1.341 & 6 \end{bmatrix} \right), k \in \{6, 12..\}$$
 (2.52)

2.4.3.1 69-bus distribution system

Complex power perturbation (ΔS_k) is considered at thirty-four active buses as given in (2.50), (2.51) and (2.52); where $k \in \{2, 4, 6,68\}$ and for observing their effect on change in voltage, bus-27, bus-45 and bus-51 are selected as observer buses.

2.4.3.2 141-bus distribution system

Complex power perturbation (ΔS_k) is considered at seventy active buses as shown in (2.50), (2.51) and (2.52), where $k \in \{2, 4, 6, ..., 140\}$ and for observing their effect on change in voltage bus 59, bus 129 and bus 141 is selected as observer bus.

2.4.3.3 Discussion

Ranking of active buses for complex power perturbation at active buses is done using the proposed PVSI, JDE [26] and traditional MCS method. The ranking of active buses for complex power perturbation is the same as active power perturbation and reactive power perturbation at active buses, as shown in Table 2.1 and Table 5.5. The computation time is given in Table 2.5. After comparing all three methods in terms of accuracy and computation time, it is observed that the PVSI gives a similar ranking as traditional MCS in less computation time than JDE due to their simplistic and analytic formulation.

In this case, PVSI is the maximum variance of a two-dimensional data point $(\Delta V_{oak}^r, \Delta V_o^r)$, $(\Delta V_{oak}^i, \Delta V_o^i)$ and $(\Delta V_{oak}, \Delta V_o)$ along the principal component axis due to perturbation in complex power at active buses. Here, ΔV_{oak}^r , ΔV_{oak}^r and ΔV_{oak} are the real part of change in voltage, imaginary part of change in voltage and absolute change in voltage at observer bus O due to

Distribution-system	Method	Computation time
69-bus	Traditional MCS	3373.31sec
69-bus	JDE	0.8799 sec
69-bus	PVSI	0.1253 sec
141-bus	Traditional MCS	10956sec
141-bus	JDE	0.9912 sec
141-bus	PVSI	0.1407 sec

Table 2.5: Computation time of ranking for ΔS_i

complex power perturbation at k^{th} active buses and ΔV_o^r , ΔV_o^i and ΔV_o are the cumulative real part of change in voltage, imaginary part of change in voltage and absolute change in voltage at the observer bus due to complex power perturbation at the active bus together.

Fig. 2.7 shows *PVSI* values for all the active buses due to complex power perturbation at active buses. Considering bus 27 as the observer bus of the 69 bus system, *PVSI* values are shown in Fig. 2.7-(a) and considering bus 141 as the observer bus of the 141 bus system, the *PVSI* value are shown in Fig. 2.7-(b).

In Fig. 2.7-(a), shows the maximum value of PVSI observed at bus 24. Therefore, in the case of the 69-bus distribution system, complex power perturbation at bus 24 is selected as the most impactful bus for change in voltage at bus 27. Similarly, the highest value of PVSI is observed at bus 66 for observer buses 45 and 51. Therefore, active bus 66 is selected as the most impactful bus for observer buses 45 and 51 due to complex power perturbation at active buses.

Similarly, in Fig. 2.7-(b), the maximum variation in PVSI occurs at bus 132. Therefore, in the case of the 141-bus distribution system, complex power perturbation at bus 132 is considered as the most impactful bus for change in voltage bus 141. Similarly, for the observer bus 59 and 129, the higher value of PVSI is observed at bus 54 and 126, respectively. Therefore, active bus 54 and 126 is selected as the most impactful bus for observer buses 59 and 129 due to complex power perturbation at active buses. From all three cases, it is observed that the active bus near to observer bus, where the largest power perturbation is considered, has the highest impact on the change in voltage at that observer bus. It happens due to the impact of power perturbation on voltage deviation depending on the size and location of the perturbation. In Fig. 2.7, it is seen that the value of $PVSI_{k_r}$ is more than $PVSI_{k_i}$, because perturbation of active power is dominant over reactive power perturbation due to its size.

2.5 Conclusion

- The traditional Monte Carlo Simulation (MCS) method for evaluating the impact of power perturbation at active buses on bus voltage is computationally intensive. A Principal Component Analysis-based novel Probabilistic Voltage Sensitivity Index (PVSI) is introduced to reduce computation time. The effectiveness of the proposed method is validated on the 69-bus and 141-bus distribution systems by comparing it with established Joint Differential Entropy (JDE) and traditional MCS methods.
- To evaluate the impact of power perturbation at active buses on voltage deviation at observer buses, active, reactive and complex power perturbations are considered at multiple active buses in three different cases. From all these cases, it is observed that PVSI gives a similar ranking as the traditional MCS and JDE methods in 85.75% and 85.8% less computation time than the JDE for 69-bus and 141-bus systems, respectively.

- Due to the advantage in computation time and accuracy, PVSI can be utilized in many applications, such as identifying the DG responsible for voltage fluctuation in the distribution system to enhance grid reliability and clustering the distribution network to implement the decentralized voltage control.
- One of the strengths of the proposed PVSI is that in the simulation, not only unidirectional but also bidirectional power flows are taken into account at several active buses. It is done by taking the variance of power perturbation more than the load at that active bus. Therefore, the ranking proposed by PVSI is valid for the distribution system where DGs are feeding power back to the grid.

Chapter 3

Optimal Selection of Voltage
Controlling Parameter in
Uncertain Active Distribution
Network

3.1 Introduction

The increasing integration of Converter-Based Generation (CBG), such as solar and wind power, along with the expansion of Electric Vehicle (EV) charging infrastructure, introduces significant uncertainty into the distribution network. This uncertainty arises from the variable nature of CBG outputs, the unpredictable number of EVs arriving at Charging Stations (CS), and the fluctuating power demands from consumers. As a result, maintaining a stable voltage profile within the distribution system becomes more complex and challenging.

To address these challenges, this work focuses on improving the voltage profile by optimizing voltage-controlling parameters. It is achieved through formulating a comprehensive Multi-Objective Optimal Power Flow (OPF) problem that considers various aspects of the distribution network. The analysis incorporates CBG sources and aims to balance multiple objectives, such as minimizing line losses, reducing voltage deviation, and maximizing the output power of CBG sources.

The Modified Jaya (M-Jaya) algorithm is used to solve the optimization problem. This algorithm is adept at converting multiple objectives into a single objective function, which simplifies the optimization process while ensuring that all key objectives are considered. The M-Jaya algorithm iteratively adjusts the voltage-controlling parameters to find the optimal balance that meets all objectives. Additionally, we integrate a state-based probabilistic model to accurately account for the inherent uncertainties in the distribution network. This model considers the intermittent nature of CBG outputs, the varying number of EVs at charging stations, and the dynamic power demand from the load. By incorporating these uncertainties into the OPF analysis, we ensure that the solutions are robust and reliable under different operating conditions. To validate our approach, we conducted numerical tests on two benchmark distribution systems: the enhanced IEEE-33 bus system and the unbalanced IEEE-123 bus system. These tests involved determining the optimal settings for voltage-controlling parameters over a 24-hour period, reflecting the typical daily variations in generation and load.

This approach provides a robust framework for managing the complexities and uncertainties associated with modern distribution networks, ensuring stable and efficient operation in the face of increasing renewable energy penetration and EV adoption.

This chapter is organized as follows. In Section 3.2, the modeling of the distribution network is

presented. The problem formulation for OPF with their constraints is explained in Section 3.3. The M-Jaya algorithm is used to solve the OPF, and it is explained in Section 3.4. The numerical test of the multi-objective optimal power flow with the state-based probabilistic model is done on enhanced IEEE-33 and unbalanced IEEE-123 test system, and their result is explained in Section 3.5. The conclusion of the work is given in Section 3.6.

3.2 Modeling of distribution network

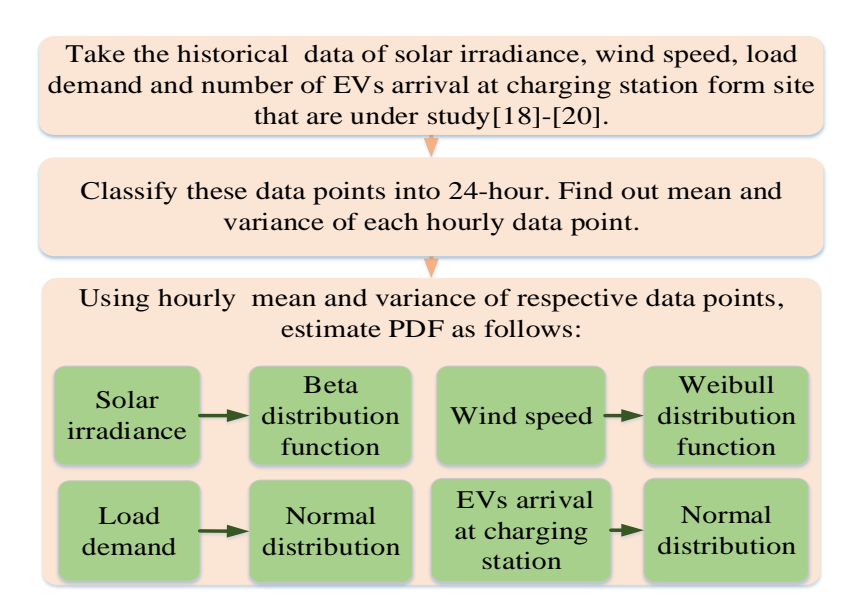


Fig. 3.1: Steps to model PDF

In this section, formulation for power generation from wind and solar-based energy resources, load demand and number of EVs arriving at charging stations using respective Probability Density Function (PDF) has been explained. Simultaneously, the modeling of EVs present at charging stations as load and charging/discharging of Battery Energy Storage System (BESS) installed at a charging station is also presented.

3.2.1 Modeling of hourly solar irradiation and power output

Mainly solar irradiation is estimated by Beta distribution. The PDF of solar irradiance is expressed as shown in equation (3.1).

$$f_b(r) = \begin{cases} \frac{\Gamma(aa+b)}{\Gamma(aa) \times \Gamma(b)} \times r^{aa-1} \times (1-r)^{b-1}, 0 \le r \le 1, a \ge 0, b \ge 0\\ 0 & Otherwise \end{cases}$$
(3.1)

where r is normalized solar irradiation, $f_b(r)$ is Beta distribution function. aa, b are shape parameter of Beta distribution. As explained in Fig. 3.1, hourly solar irradiance is modeled by the Beta distribution function using 5-years $(365 \times 5 \times 24)$ of solar irradiance data [96]. Fig. 3.2-(a) shows the estimation of 13h solar irradiance by Beta distribution function with shape parameters aa = 8.9 and b = 3.56.

$$b = (1 - \mu) \times \left(\frac{\mu \times (1 - \mu)}{\sigma^2} - 1\right), aa = \frac{\mu b}{1 - \mu}$$
 (3.2)

For considering the uncertainty, the continuous hourly PDF of solar irradiation has been classified into several states. Classification of states is crucial, the high number of states increases accuracy but it also increases complexity while calculating output power. The probability of solar irradiance

for any state is calculated from the corresponding continuous PDF as shown in the (3.3).

$$p_{sy} = \int_{s_{y1}}^{s_{y2}} f_b(r) dr \tag{3.3}$$

 p_{sy} is probability of solar irradiance in state y. s_{y1} and s_{y2} are limits of solar irradiation probability for state y. The output power from the PV module depends upon solar irradiance, site temperature and characteristics of the PV module. For each state of the hourly time segment, the calculation of output power from PV module is shown from (3.4) to (3.8).

$$T_{C_y} = T_A + r_{ay} \left(\frac{N_{OT} - 20}{0.8} \right) \tag{3.4}$$

$$I_y = r_{ay} \left[I_{sc} + K_i (T_c - 25) \right]$$
 (3.5)

$$V_y = V_{oc} - K_v * T_{C_y} \tag{3.6}$$

$$P_{r_{ay}}(t) = N * FF * V_y * I_y \tag{3.7}$$

$$P_{r_{ay}}(t) = N * FF * V_y * I_y$$

$$FF = \frac{V_{MPP} * I_{MPP}}{V_{oc} * I_{oc}}$$

$$(3.7)$$

where T_{cy} is cell temperature $^{\circ}C$ during state y. T_A is ambient temperature $^{\circ}C$. K_v is voltage temperature coefficient. K_i is current temperature coefficient. N_{OT} is nominal operating temperature of cell in ${}^{\circ}C$. FF is ill factor. V_{oc} is open-circuit voltage in V. I_{sc} is short-circuit current in A, I_{MPP} is current at maximum power point in A. V_{MPP} is voltage at maximum power point in V. $P_{r_{ay}}(t)$ is output power of PV module during state y of time segment Δt . And r_{ay} is average irradiation of state y.

3.2.2Modeling of wind speed and output power

Wind speed is modeled as Weibull distribution. As shown in (3.9)

$$f_w(v) = \frac{k}{c} \times \left(\frac{v}{c}\right)^{k-1} \times e^{\left[-\left(\frac{v}{c}\right)^k\right]}$$
(3.9)

where v is normalized wind speed. $f_w(v)$ is Weibull distribution function. k is shape parameter of Weibull distribution. c is scale parameter of Weibull distribution. As explained in Fig. 3.1, hourly wind speed is modeled by the Weibull distribution function using 5-years $(365 \times 5 \times 24)$ of wind speed data [96]. In Fig. 3.2-(b), the estimation of 15h wind speed data by Weibull distribution function with shape parameters k = 0.77 and c = 8.56 is shown.

$$k = \left(\frac{\sigma}{\mu}\right)^{-1.86}, c = \frac{\mu}{\Gamma(1 + \frac{1}{\mu})}$$
 (3.10)

For considering the uncertainty of wind speed, their continuous hourly PDF is classified into several states. The probability of wind speed for any state is calculated from the corresponding continuous PDF as shown in the equation (3.11).

$$p_{vz} = \int_{w_{z1}}^{w_{z2}} f_w(v) dv \tag{3.11}$$

where p_{vz} is probability of wind speed in state z. w_{z1} and w_{z2} are limits of wind speed probability for state z. The output power from a wind turbine mainly depends upon wind velocity, the size of the turbine and the length of its blade. For each state of the hourly time segment, the calculation

of output power from the wind turbine is provided in (3.12).

$$P_{V_z}(t) = \begin{cases} 0 & 0 \le v_{az} \le v_{ci} \\ P_{rated} * \frac{(v_{az} - v_{ci})}{v_{az} - v_{ci}} & v_{ci} \le v_{az} \le v_r \\ P_{rated} & v_r \le v_{az} \le v_{co} \\ 0 & v_{co} \le v_{az} \end{cases}$$
(3.12)

where v_{ci} , v_r and v_{co} is cut in speed, rated speed and cut-off speed of wind turbine respectively. P_{V_z} is out put power of wind turbine during state z for time segment Δt . v_{az} is average wind speed of state z.

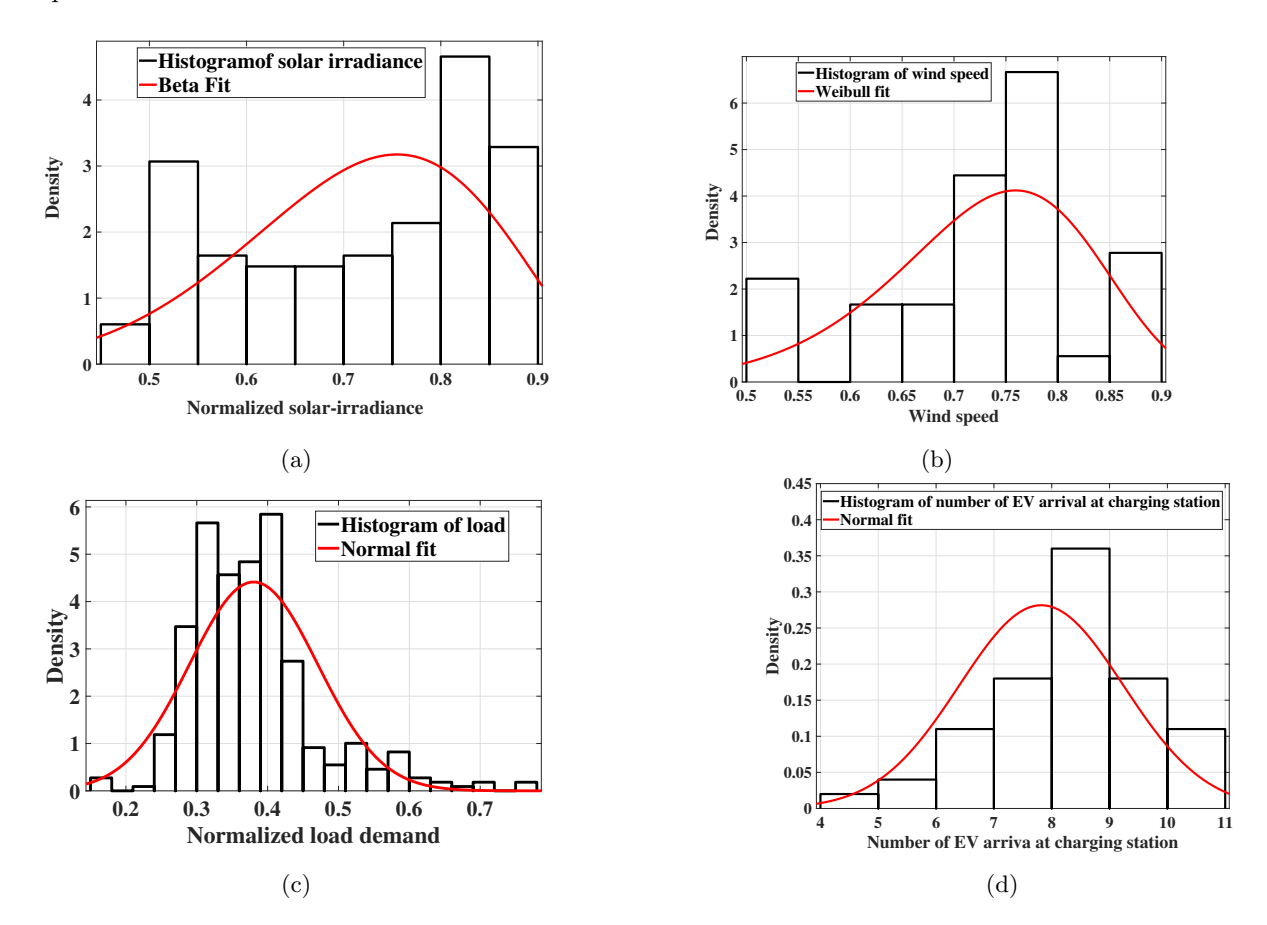


Fig. 3.2: PDF of (a) Solar irradiation of 13h (b) wind speed of 15h (c) load of 13h (d) number of EVs arrival of 13h

3.2.3 Modeling of Load

The load demand is estimated by the normal distribution function. The PDF of load demand is expressed as shown in (3.13).

$$f_L(l) = \frac{e^{\frac{-(l-\mu_l)^2}{2(\sigma_l)^2}}}{\sigma_l \sqrt{2\pi}}$$
(3.13)

where μ_l , and σ_l are mean and stander deviation of load for hourly time period. As explained in Fig. 3.1, hourly load demand is modeled by the Normal distribution function using 5-years $(365 \times 5 \times 24)$ of load demand data [97]. Fig. 3.2-(c) shows the estimation of 13h load demand by Normal distribution function with $\mu_l = 0.39$ and $\mu_l = 0.098$. For considering the uncertainty of load demand, their continuous hourly PDF is classified into several states. The probability of load demand for any state is calculated from the corresponding continuous PDF as shown in the

(3.14).

$$p_{L_s} = \int_{s_{11}}^{s_{12}} f_L(l) dl \tag{3.14}$$

where s_{l1} and s_{l2} are lower and upper limits of load demand power for state s.

3.2.4 Modeling of EVs as load

The State Of Charge (SOC) of an Electric Vehicle (EV) battery changes with time when the EV is connected to the distribution network. It is updated for each time interval as shown in (3.15).

$$SOC_{E,n,s}(t) = SOC_{E,n,s}(t-1) + \eta_{Ech,n} P_{Ech,n,s}(t) \Delta t$$

$$(3.15)$$

where $SOC_{E,n,s}(t)$ and $SOC_{E,n,s}(t-1)$ are the present and previous SOC of n^{th} EV available in the charging station for state s. $P_{Ech,n,s}(t)$ is the charging power of n^{th} EV for state s. Δt is the time segment of charging. The charging power of an EV is a chunk of the total power of the charging station. $\eta_{Ech,n}$ represents efficiency of charging power for n^{th} EV. The charging power of EVs is expressed in the (3.16).

$$P_{Ech,n,s}(t) = \frac{(C_{batt,n} - SOC_{n,s}(t)C_{batt,n})P_{CS,s}(t)}{T_{rem,n} \times \sum_{j=1}^{m} (\frac{1}{T_{rem,j}})(C_{batt,j} - SOC_{j,s}(t) \times C_{batt,j})}$$
(3.16)

where $T_{rem,n} = T_{d,n} - T_{arr,n}$, $C_{batt,n}$ represents battery capacity. $T_{arr,n}$ represents arrival time of n^{th} EV.

3.2.4.1 Stochastic Nature of EV

The EVs are composed of many random variables, such as (i) Traveling distance during the day, (ii) Parking time, (iii) Arrival time, and (iv) Driving methods. These variables should be taken into account in the optimization model. The arrival time of EVs at charging stations is a random variable, and it is modeled by a normal pdf [98] as described in (3.17).

$$f_{E_n}(T_{arr}) = \frac{e^{-(\frac{T_{arr} - \mu_{T_{arr}}}{2\sigma_{T_{arr}}})^2}}{\sigma_{T_{arr}}\sqrt{2\pi}}$$
(3.17)

where $T_{arr,n}$ represents the arrival time of n^{th} EV. μ_{arr} and $\sigma_{T_{arr}}$ are the mean and standard deviation of the daily arrival time of EV at the charging station. The starting SOC depend on many factors, such as (1) Daily traveled distance d_n (2) All-Electric Range (AER_n) (3) Battery SOC at the departure time. The mathematical expression of starting SOC of the EV battery is shown in (3.18).

$$SOC_{start,n}(\%) = \left(1 - \frac{d_n}{AER_n}\right) \times 100$$

$$AER = \frac{C_{batt,n}}{E_{cons/mile,n}}$$
(3.18)

Daily distance traveled by EVs is arbitrary in nature, and it is estimated by lognormal pdf as shown in (3.19).

$$f_{E_d}(d_n) = \frac{1}{d_n \sqrt{2\pi(\sigma_{d_n})^2}} \times e^{-\frac{(\ln(d_n) - \mu_{d_n})}{2(\sigma_{d_n})}}, d_n > 0$$
(3.19)

where μ_{d_n} and σ_{d_n} are mean and stander-deviation of daily distance traveled by EVs.

3.2.4.2 Evaluation of Number of EVs at Charging station

The number of EVs at charging stations is determined by using a state-based probabilistic method using equation (3.20).

$$N_{EV}(T_{arr}) = 100 \times \int_{t1}^{t2} f_{E_n}(T_{arr}) dT_{arr}$$
(3.20)

where N_{EV} represents number of EVs arrival at time segment T_{arr} . Considering the stochastic nature of the number of EVs arrival at a charging station in time segment Δt is modeled by normal random variable as given (3.21) with mean and variance as N_{EV} and $0.2N_{EV}$, respectively.

$$f_{n_{EV}}(n_{EV}) = \frac{e^{\frac{-(n_{EV} - \mu_{EV}^t)^2}{2(\sigma_{EV}^t)^2}}}{\sigma_{EV}^t \sqrt{2\pi})}$$
(3.21)

The probability $p_{n_{EV_s}}$ of EVs arrival in state s is calculated as given equation (3.22).

$$p_{n_{EV_s}} = \int_{s_{EV_1}}^{s_{EV_2}} f_{n_{EV}}(n_{EV}) dn_{EV}$$
(3.22)

where s_{EV_1} and s_{EV_2} are upper and lower limit of EVs arrival at charging station in state s. As explained in Fig. 3.1, EVs arrival at the charging station is modeled by Normal distribution using 5-years $(365 \times 5 \times 24)$ of travelling end time data given in [99]. Fig. 3.2-(d) shows the estimation of 13h EVs arrival at the charging station by Normal distribution function with $\mu_l = 8$ and $\sigma_{EV}^2 = 4$.

3.2.5 Modeling of BESS at Charging Station

The installation of BESS at the charging station mitigates the voltage fluctuation due to uncertain load demand by EV-load. It assists in maintaining the bus voltage by optimal planning of their charging and discharging. The mathematical modeling of charging-discharging is shown in [100] (3.23)

$$SOC_{B,s}(t) = SOC_{B,s}(t-1) + \eta_{Bch} P_{Bch,s}(t) \Delta t\alpha - \frac{P_{Bdc,s}(t) \Delta t\beta}{\eta_{Bdc}}$$
(3.23)

where α and $\beta \in (0,1)$, and $\alpha\beta = 0$, because both charge and discharge of the battery are not possible at a time. η_{Bch} and η_{Bdc} are charging and discharging efficiency of BESS. $P_{Bch,s}$ and $P_{Bdc,s}$ represents the charging and discharging power of BESS for state s. $SOC_{B,s}(t)$ and $SOC_{B,s}(t-1)$ represents the present and previous SOC of BESS for state s.

3.2.5.1 Charging of BESS

BESS stores a fraction of the power generated by DG if the load at the charging station integrated bus at time t is less than DG generation as shown (3.24)

$$P_{Bch,s}(t) = \eta_{Bch} K_{Bch,s}(t) PV_s(t), K_{Bch,s}(t) > 0$$
(3.24)

where PV(t) represents available DG power in time segment Δt . $K_{Bch}(t)$ represents fraction of DG power, which is stored by BESS in time segment Δt for state s.

3.2.5.2 Discharging of BESS

BESS release a fraction of the stored power if the load at the charging station integrated bus at time t is more than DG generation as shown (3.25).

$$P_{Bdc,s}(t) = \frac{\eta_{BdcK_{Bdc,s}}SOC_{B,s}(t-1)C_{BESS}}{\Delta t}$$
(3.25)

where C_{BESS} represents total capacity of BESS. $K_{Bdc,s}(t)$ is fraction of BESS power, which is release by BESS in time segment Δt for state s.

3.3 Problem Formulation

OPF is used to determine the optimal solution for control variables by satisfying certain objective functions. While determining an optimal solution, it also satisfies all constraints. Therefore, in this work, OPF has been used to determine optimal rating of voltage controlling devices while considering the objective function as minimization of power losses, minimization of voltage deviation and maximization of power output from DG in the distribution power network.

3.3.1 Objective Function

The multi-objective function for the OPF problems under consideration aims to minimize network losses, voltage deviations, and reactive power absorption by the available CBG, as given in (3.26).

$$minf = \sum_{t=1}^{N_t} \sum_{k=1}^{N_s} \left(P_{Loss,s}^{abc}(t) + K_v \left(\sum_{T_b} (\Delta V_s^{abc}(t)) \right)^2 + K_q \left(\sum_{DG_b} (\Delta Q_s^{abc}(t)) \right)^2 \right)$$
(3.26)

where f is a multi-variable objective function. N_t and N_s are the total number of time segments and the total number of states for each time segment. K_v and K_q is penalty factors. In this work K_v and K_q have been selected as 10^3 . $\Delta V_s^{abc}(t)$ represents phase a,b and c bus voltage limit violations in state s for a time segment Δt . ΔQ_s^{abc} represents the reactive power provided by a CBG in state s during a time segment Δt across phases a,b and c. T_b and DG_b are used to represent the total number of buses and the total number of CBG-integrated buses in the network, respectively.

3.3.1.1 Constraints

Two types of constraints has been taken into account, which are explained as following

3.3.1.2 Equality Constraints

$$\begin{split} P_{ij,s}^{abc}(t) &= -\kappa(s,1) P_{PV_{j}}^{abc}(t) - \kappa(s,2) P_{WT_{j}}^{abc}(t) + \kappa(s,3) P_{L_{j}}^{abc}(t) \\ &+ \kappa(s,4) P_{E_{ch_{j,s}}}^{abc}(t) + P_{jk,s}^{abc}(t) \pm P_{Bdc/sc,j,s}^{abc}(t) \\ Q_{ij,s}^{abc}(t) &= \pm Q_{PV_{j,s}}^{abc}(t) \pm Q_{WT_{j,s}}^{abc}(t) + \kappa(s,3) Q_{L_{j,s}}^{abc}(t) \\ &+ Q_{sh,j,s}^{abc}(t) + Q_{jk,s}^{abc}(t) \\ (V_{i,s}^{abc}(t))^{2} &= (V_{j,s}^{abc}(t))^{2} + 2(R_{ij}^{abc}P_{ij,s}^{abc}(t) + X_{ij}^{abc}Q_{ij,s}^{abc}(t)) \\ &+ Z_{ij}^{2}I_{ij}^{abc}(t) \\ I_{ij}^{abc}(t) &= \frac{(P_{ij,s}^{abc}(t))^{2} + (Q_{ij,s}^{abc}(t))^{2}}{(V_{i,s}^{abc}(t))^{2}} \\ Q_{PV,i,s}^{abc}(t) &= \sqrt{(S_{PV_{abc},i,s}^{comp}(t))^{2} - P_{PV,s,i}^{abc}(t))^{2}} \\ Q_{WT,i,s}^{abc}(t) &= \sqrt{(S_{WT_{abc},i,s}^{comp}(t))^{2} - P_{WT,s,i}^{abc}(t))^{2}} \end{split}$$

where κ is a matrix with four columns, which comprises all the combination of the states of wind, solar, the number of EVs arriving at the charging station and load demand. i, j and k represent

three consecutive buses of the network. $P_{PV_{j,s}}^{abc}(t)$ and $P_{WT_{j,s}}^{abc}(t)$ are active power generated by solar and wind type generation in phase a,b and c during time segment Δt for state s. $P_{L_{j,s}}^{abc}(t)$ is load demand of phase a,b and c during of time segment Δt for state s at j^{th} bus. $P_{E_{ch_j}}^{abc}(t)$ is phase power demand by EVs for time segment Δt of state s. $P_{Bch/dc,j,s}^{abc}(t)$ is the phase charging-discharging power of BESS installed at a charging station for state s of time segment Δt . $Q_{PV_{j,s}}^{abc}(t)$, $Q_{WT_{j,s}}^{abc}(t)$, $Q_{PV_{j,s}}^{abc}(t)$ and $S_{WT_{j,s}}^{comp}(t)$ are active, reactive power and complex power generated by solar and wind type converter-based generation integrated in phase a,b and c during time segment Δt for state s. $Q_{j,s}^{abc}(t)$ is reactive power supplied in each phase a,b and c by reactive power compensator for a time segment Δt of state s. $P_{ij,s}^{abc}(t)$ and $Q_{ij,s}^{abc}(t)$ are phase a,b and c active and reactive power coming from i^{th} to j^{th} bus. $P_{jk,s}^{abc}(t)$ and $Q_{jk,s}^{abc}(t)$ are outgoing active and reactive power from j^{th} to j^{th} bus. $V_{i,s}^{abc}(t)$ and $V_{i,s}^{abc}(t)$ represent phase a,b and c voltage of i^{th} and j^{th} bus during time segment Δt for state s. $I_{ij}^{abc}(t)$ is current flowing in each phase a,b and c from i^{th} h to j^{th} buses during time segment Δt for state s. $R_{ij}^{abc}(t)$ is current flowing in each phase a,b and c from i^{th} h to j^{th} buses during time segment Δt for state s. $R_{ij}^{abc}(t)$ and $P_{ij}^{abc}(t)$ buses, respectively.

3.3.1.3 Inequality Constraints

$$P_{PV_{abc}}^{min} \leq P_{PV,j,s}^{abc}(t) \leq P_{PV_{abc}}^{max}$$

$$P_{WT_{abc}}^{min} \leq P_{WT,j,s}^{abc}(t) \leq P_{WT_{abc}}^{max}$$

$$Q_{PV_{abc}}^{min} \leq Q_{PV,j,s}^{abc}(t) \leq Q_{PV_{abc}}^{max}$$

$$Q_{WT_{abc}}^{min} \leq Q_{WT,j,s}^{abc}(t) \leq Q_{WT_{abc}}^{max}$$

$$V_{abc}^{min} \leq V_{j,abc,s}(t) \leq V_{abc}^{max}$$

$$T_{tap}^{min} \leq T_{tap,i} \leq T_{tap}^{max}$$

$$Q_{C,abc}^{min} \leq Q_{C,s}^{abc}(t) \leq Q_{C,abc}^{max}$$

$$Q_{C,abc}^{cos}(t) \leq 0.2C_{batt,n}$$

$$SOC_{Emin,n}^{abc} \leq SOC_{E,n,s,j}(t) \leq SOC_{Emax,n}^{abc}$$

$$P_{Bch_{min}}^{abc} \leq P_{Bch,s}^{abc}(t) \leq P_{Bch_{max}}^{abc}$$

$$P_{Bdc_{min}}^{abc} \leq P_{Bdc,s}^{abc}(t) \leq P_{Bdc_{max}}^{abc}$$

$$SOC_{Bmin}^{abc} \leq SOC_{B,s}^{abc}(t) \leq SOC_{Bmax}^{abc}$$

$$SOC_{Bmin}^{abc} \leq SOC_{B,s}^{abc}(t) \leq SOC_{Bmax}^{abc}$$

where $P_{PV_{abc}}^{max}$, $P_{PV_{abc}}^{min}$, $P_{WT_{abc}}^{max}$ and $P_{WT_i}^{min}$ are maximum and minimum active power generation from solar and wind type generation integrated in phase a,b and c, respectively. T_{tap}^{max} and T_{tap}^{min} are minimum and maximum OLTC tap settings limit. $Q_{C,abc}^{min}$ and $Q_{C,abc}^{max}$ are shunt compensator limits integrated in phase a,b and c. $Q_{PV_{abc}}^{max}$, $Q_{WT_{abc}}^{max}$, $Q_{PV_{abc}}^{min}$ and $Q_{WT_{abc}}^{min}$ are reactive power limits of CBG solar and wind type generation integrate in phase a,b and c, respectively. $P_{Ech,n,s}^{abc}(t)$ charging power of n^{th} EV connected in phase a,b and c. SOC_{Emin}^{abc} and SOC_{Emax}^{abc} are the limit of state of charge of EVs battery integrated in phase a,b and c. $P_{Bch_{max}}^{abc}$, $P_{Bch_{max}}^{abc}$, $P_{Bdc_{min}}^{abc}$ and $P_{Bdc_{max}}^{abc}$ are charging and discharging power limit of battery installed at the charging station in phase a,b and c. SOC_{Bmax} and SOC_{Bmin} are the limit of the state of charge of the battery installed at the charging station in phase a,b and c.

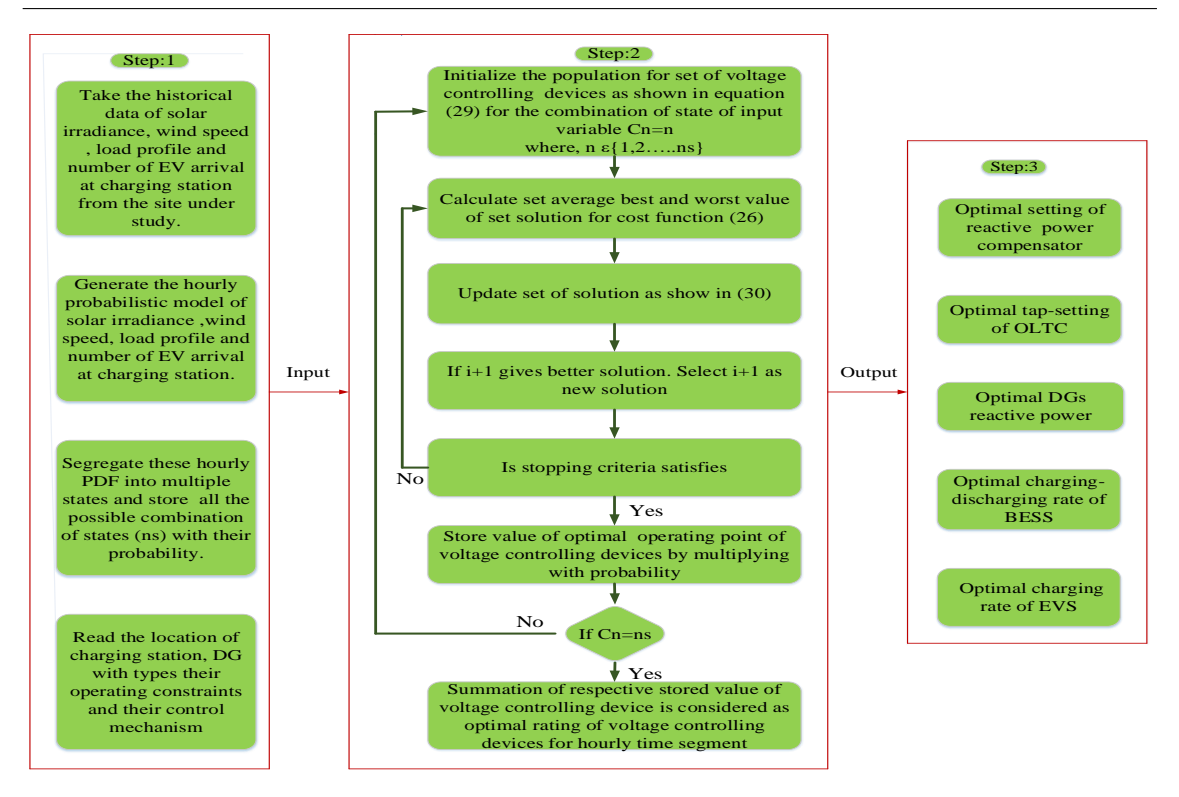


Fig. 3.3: Steps to determine optimal setting of voltage controlling parameters

Jaya algorithm for solving OPF 3.4

Jaya algorithm retains the feature of evolutionary algorithm and swarm-based intelligence. Jaya algorithm has certain merits over the population-based algorithms, such as it does not require derivative information for the initial search and algorithmic specific parameters. Java algorithm search for a solution by getting closer to the global best solution and eliminating the worst solution as shown in equation (3.30) to (3.31).

$$\bar{x}_0 = \bar{x}_{min} + c_0(\bar{x}_{max} - \bar{x}_{min})$$
 (3.29)

$$\bar{x}_{k}^{i+1} = \bar{x}_{k}^{i} + c_{1} \times (\bar{x}^{b} - |\bar{x}_{k}^{i}|) - c_{2} \times (\bar{x}^{w} - |\bar{x}_{k}^{i}|)$$

$$\bar{x}_{k}^{ab} = \frac{\bar{x}^{b1} + \bar{x}^{b2} + \bar{x}^{b3}}{3}$$

$$(3.30)$$

$$\bar{x}^{ab} = \frac{\bar{x}^{b1} + \bar{x}^{b2} + \bar{x}^{b3}}{3} \tag{3.31}$$

where \bar{x}_0 is an initial set of solutions. \bar{x}_k^{i+1} is set of updated solution. k is population size. i is the number of iterations. In this work, population size and number of iteration are considered as 20 and 100 respectively. c_0 , c_1 and c_2 are random variables and their values lies between [0,1]. \bar{x}^b and \bar{x}^w is set of best and worst solution for i^t h iteration. \bar{x}^{ab} is average best solution. In this work, the best solution of the Jaya algorithm has been modified by taking the average of the top three best solution as shown in (3.31). It improves the convergence rate for the cost function. The number iteration is considered as convergence criteria for solving the OPF problem. The basic steps to solve the OPF problem by the Jaya algorithm have been explained in step: 2 of Fig. (3.3).

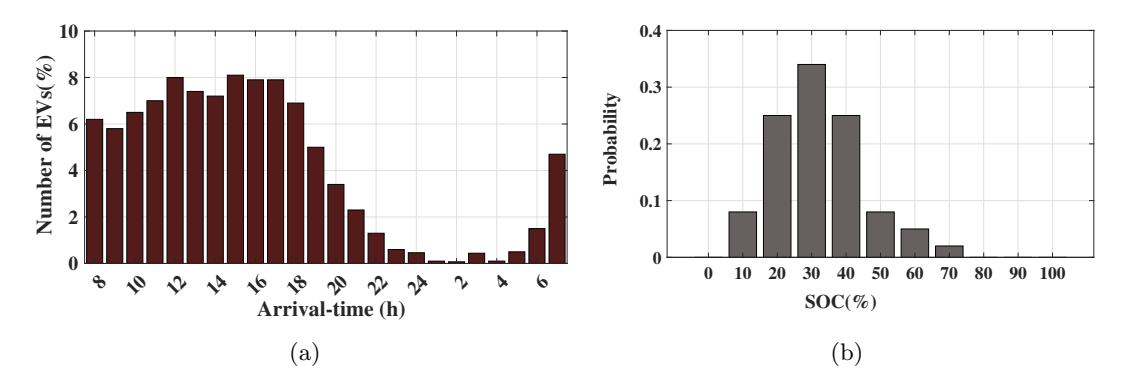


Fig. 3.4: (a) EVs arrival at charging station in hourly time segment for $100 \mathrm{EVs}$, (b) PDF of initial SOC for EV batteries

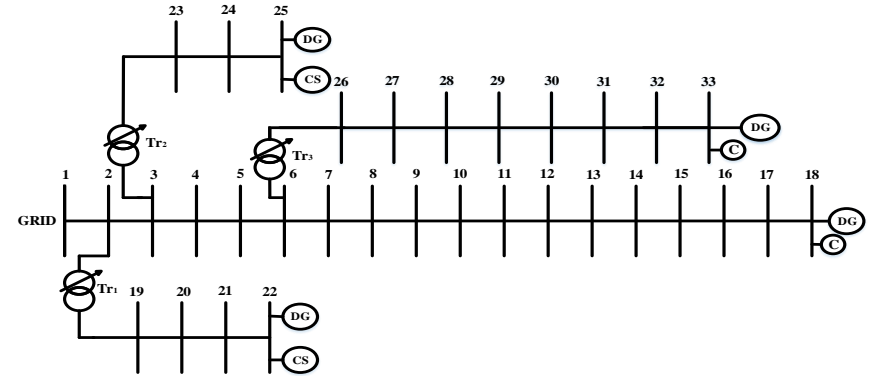


Fig. 3.5: Enhanced IEEE-33 test system

3.5 Results and Discussion

The optimal setting of the voltage-controlling parameters is determined for the enhanced IEEE-33 [101] and unbalanced IEEE-123 [102] distribution system. For evaluating the optimal setting of the voltage-controlling parameters for both systems, MATLAB R2019b with the system configuration Intel-Core i7-8700, CPU @ 3.20GHz, is used. Base power and voltage for IEEE-33; 100 MVA, 12.66 kV and IEEE-123 distribution; 100 kW, 4.16 kV.

3.5.1 Enhanced IEEE-33 distribution system

In this test system, the optimal setting of the voltage-controlling parameters are determined in three scenarios of power generation by renewable-based generation as follows, (1) Only solar-based generation, (2) Only wind-based generation, (3) Solar and wind generation together. considering the impact of the tap changer on voltage control, at three locations, the transformer equipped with a tap-changer has been considered as shown in Fig. 3.5. The maximum and minimum tap settings are considered as -5 and 5. At buses 18, 22, 25, and 33 DG of rating 800 kW is considered based on voltage sensitivity [101]. At buses 18 and 33, reactive power compensators of rating 400 kVAR and 600 kVAR are considered, respectively. At buses 22 and 25, a charging station is considered. Both charging stations can accommodate 100 EVs during the day. It is assumed that each EV and charging station is installed with 85 kWh and 500 kWh battery, respectively. Simultaneously, the initial SOC of installed BESS at CS is assumed to be 0.45 pu. The number of EVs arriving for each hourly time segment of the 24 h time period is determined from end time data given in [99] using (3.17) and it is shown in Fig. 3.4-(a). The initial SOC of the EV battery is determined by daily distance traveled data given in [99] using (3.17) to (3.18), and it is shown in Fig. 3.4-(b). The parking time of EVs is considered 5 h [103]. For finding out the optimal setting of voltage controlling parameters for maintain the bus voltage variation within the limits of $\pm 5\%$ [104], OPF given in (3.26) to (3.28) has been solved using the M-Jaya algorithm.

Table 3.1: State with their Probability of Input Variables for 13 h in case of Solar type DGs

State	DG output	Prob	Load	Prob	EVs	Prob
1	$0 \le p_s < 0.6$	0.267	$0 \le l < 0.5$	0.8919	$4 \le E < 9$	0.71
2	$0.6 \le p_s < 1$	0.73983	$0.5 \le l < 1$	0.1081	$9 \le E < 11$	0.29

Table 3.2: Combination of States of Input Variable for 13 h in case of Solar type DGs

State	Combination of DG-output, number of EVs	Probability
	arrival at CS and load demand	
1	$0 \le p_s < 0.6, 0 \le l < 0.5, 4 \le E < 9$	0.1690
2	$0 \le p_s < 0.6, 0 \le l < 0.5, 9 \le E < 11$	0.0695
3	$0 \le p_s < 0.6, 0.5 \le l < 1, 4 \le E < 9$	0.0204
4	$0 \le p_s < 0.6, 0.5 \le l < 1, 9 \le E < 11$	0.0837
5	$0.6 \le p_s < 1, 0 \le l < 0.5, 4 \le E < 9$	0.460
6	$0.6 \le p_s < 1, 0 \le l < 0.5, 9 \le E < 11$	0.1913
7	$0.6 \le p_s < 1, 0.5 \le l < 1, 4 \le E < 9$	0.0576
8	$0.6 \le p_s < 1, 0.5 \le l < 1, 9 \le E < 11$	0.02391

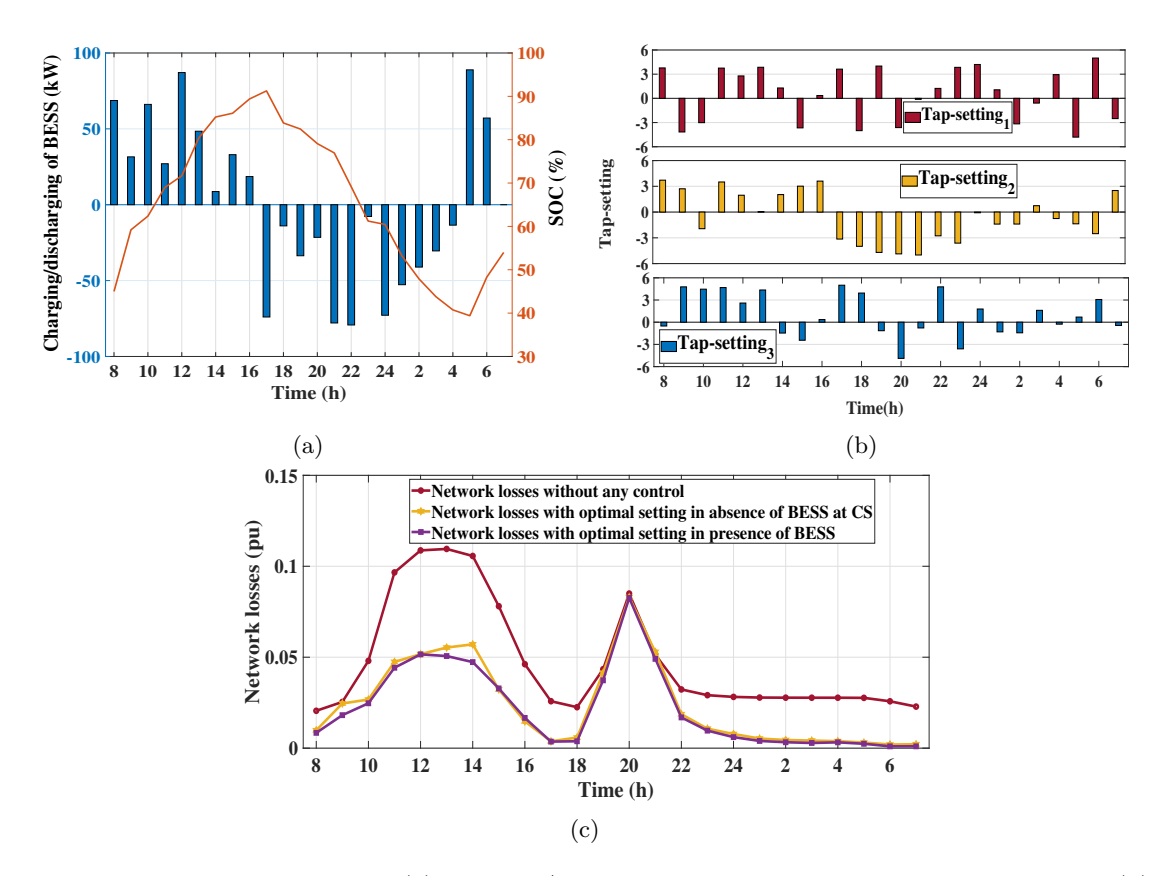


Fig. 3.6: In case Solar type DGs (a) charging/discharging power with SOC of BESS at bus 22 (b) tap-setting of OLTC (c) network losses for 24 h time period

3.5.2 Solar Generation

In this case, solar-based generation has been considered for power generation. The stochastic characteristics of solar generation, load, and number of EVs arriving at the charging station have

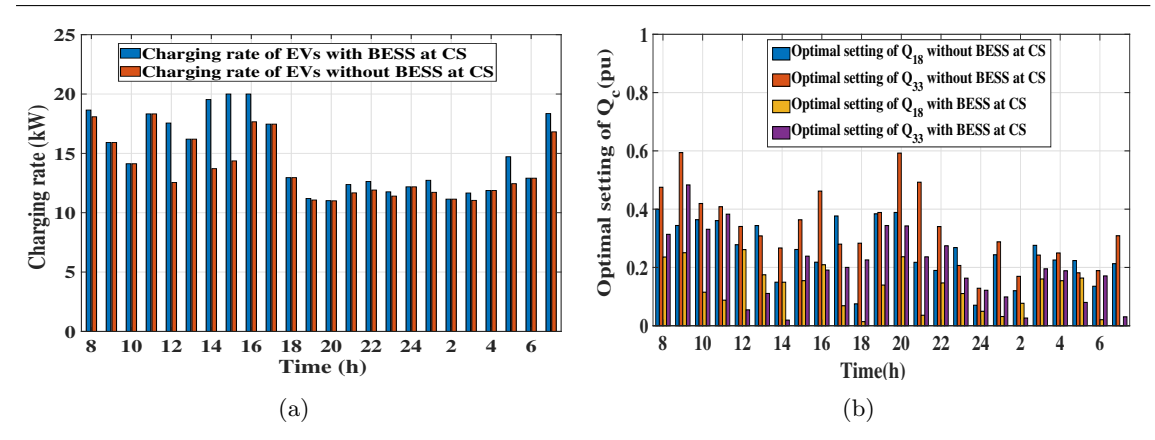


Fig. 3.7: In case Solar type DGs (a) charging rate of EVs at bus 22 (b) optimal VAR setting of reactive power compensator

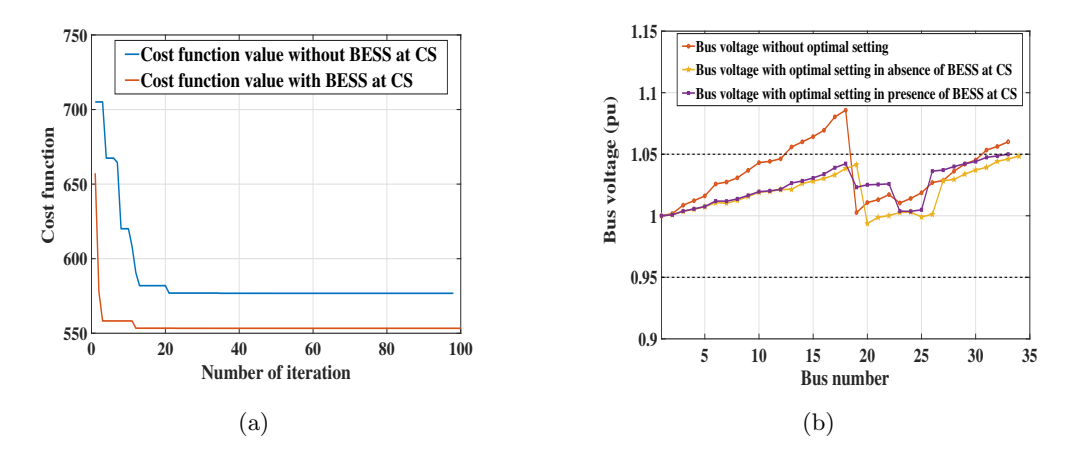


Fig. 3.8: In case Solar type DGs (a) cost Function (b) voltage Levels at all buses with and without optimal setting for $13~\rm h$

been taken into account while determining the optimal setting of voltage-controlling parameters. As shown in Fig. 3.3, for implementing the stochastic characteristics of the solar generation, load, and number of EVs arriving at the charging station in the OPF problem, at first, utilizing respective five years of historical data of these input variables given in [96]-[99], their hourly probability density function is formulated, as explained in Section II. The PDF of solar irradiation, load, and number of EVs arriving at the charging station for 13 h are shown in Fig. 3.2-(a), (b) and, (d), respectively. Further, hourly PDFs of these variables are segregated into three states. In Table 3.1, states of solar generation, load, and number of EVs arriving at the CS with their probability for 13 h have been given. Further, all the combination of these states has been given in Table 3.2. All these combinations are taken as input for the OPF problem. For all eight combinations, the optimal rating of voltage controlling parameter is determined by the Jaya algorithm. The sum of the multiplication between the optimal rating of the voltage-controlling parameter of all eight states with their probability is considered as the optimal rating of the voltage-controlling parameter of the 13 h time segment. Similarly, the optimal rating of voltage-controlling parameters is determined for the entire 24 h time period. The optimal charging-discharging power with their SOC of BESS installed in CS at bus 22 is shown in Fig. 3.6-(a). The BESS takes power from (5 h to 16 h) due to DG generating more power than the required power by the load at this hour. Similarly, BESS discharges power from (15 h to 4 h) due to the power required by the load is higher than the power generated by DGs. All three tap changer installed between (2-19), (3-23) and (6-26) is shown in Fig.3.6-(b), respectively. In both the cases with and without BESS at CS, almost similar tap-setting is observed. The losses of the distribution network with and without optimal settings of voltage-controlling devices show in Fig. 3.6-(c). The total losses of the distribution network for 24 h, without the optimal setting of voltage-controlling parameters is .0114 pu (1140 kW), and with the optimal setting of the voltage controlling parameter in the presence and absence of BESS at CS are 0.005211 pu (521.1 kW) and 0.005686 pu (568.6 kW), respectively. BESS observes active power penetration generation by DGs, which improves the operating power factor of DGs. Consequently, the losses of the network get reduced. Fig. 3.7-(a), the optimal charging power of EVs is shown. The presence of BESS at CS improves the charging rate of EVs. The optimal reactive power supplied by the reactive power compensator installed at bus 18 and 33 with and without BESS at CS is shown in Fig. 3.7-(b). The cumulative reactive power supplied by the reactive power compensator for the 24 h time period with and without BESS at CS is 11.93 pu and 10.05 pu, respectively. BESS reduces the demand of reactive power in the network by supplying active power in high load power demand condition. The value of the cost function and voltage profile of the network is shown in Fig. 3.8. The cost function with and without BESS at CS is shown in Fig. 3.8-(a). The value of the cost function is lesser in the case of BESS installed at CS because it reduces losses as well as improves the power factor of DGs. In the case of solar generation, the highest generation-to-load ratio is observed at 14 h. Therefore, at this hour, the highest value of voltage is observed at all buses. The bus voltage at this hour with and without optimal setting of voltage controlling parameter is shown in Fig. 3.8-(b). The optimal setting of the voltage-controlling parameter improves the voltage profile of the network by managing the active and reactive power demand of the network.

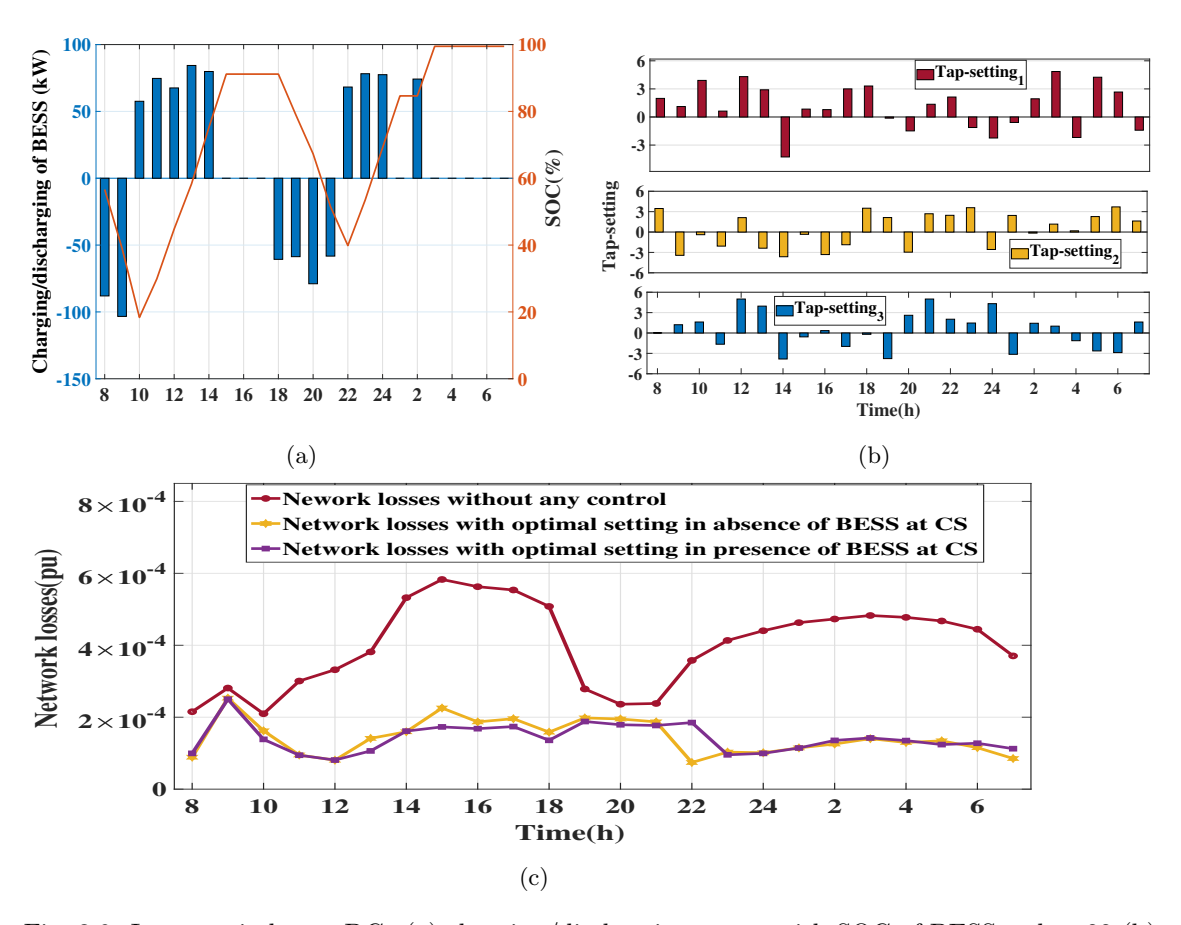


Fig. 3.9: In case wind type DGs (a) charging/discharging power with SOC of BESS at bus 22 (b) tap-setting of OLTC (c) network losses for 24 h time period

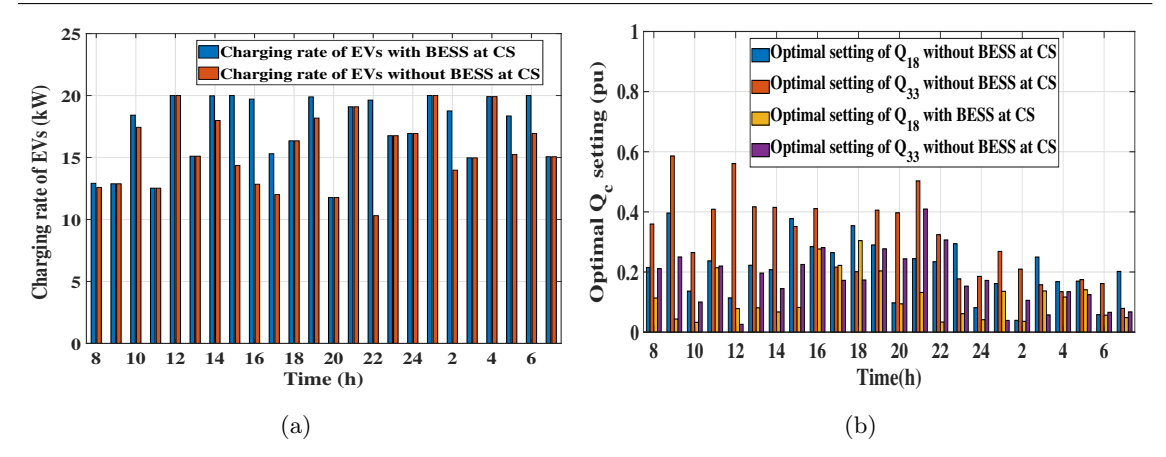


Fig. 3.10: In case wind type DGs (a) charging rate of EVs at bus 22 (b) optimal VAR setting of reactive power compensator

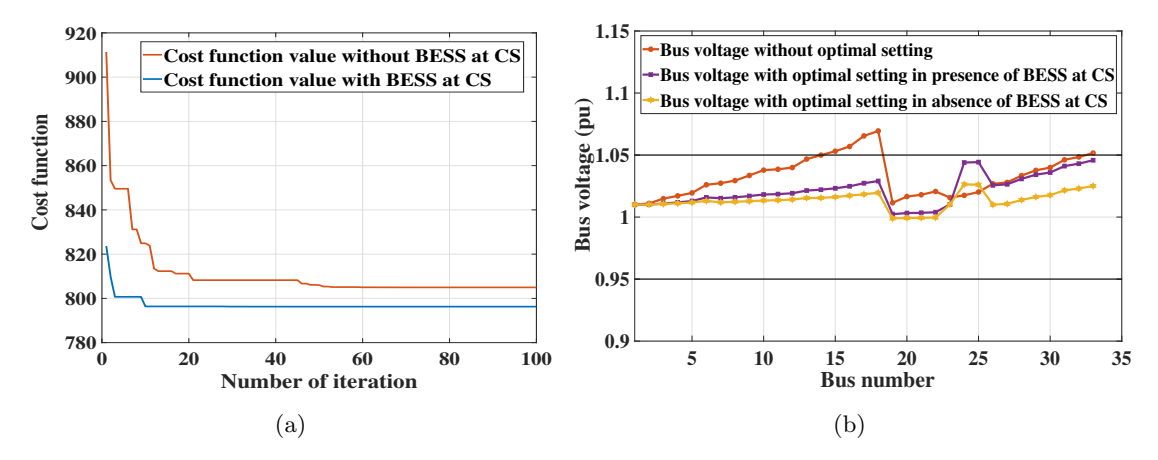


Fig. 3.11: In case wind type DGs (a) cost Function (b) voltage Levels at all buses with and without optimal setting for $15~\rm h$

3.5.3 Wind Generation

In this case, wind-type generation has been considered for power generation. solar-type generation, in this case, also the stochastic characteristics of wind generation, load, and number of EVs arriving at the charging station have been incorporated into the OPF problem while determining the optimal setting of voltage-controlling parameters. The optimal charging-discharging power with their SOC of BESS installed in CS at bus 22 is shown in Fig. 3.9-(a). The BESS takes power from (18 h to 21 h) and (18 h to 21 h) due to surplus of power generation than the load demand at this hour. Between (15 h to 17 h), BESS neither takes power nor discharges power because, at this time period, power generation is equal to load demand. All three tap changer installed between (2-19), (3-23) and (6-26) is shown in Fig. 3.9-(b), respectively. The losses of the distribution network with and without optimal settings of voltage-controlling devices show in Fig. 3.9-(c). The total losses of the distribution network for 24 h, without the optimal setting of voltage-controlling parameters is 0.0105 pu (1050 kW), and with the optimal setting of the voltage controlling parameter in the presence and absence of BESS at CS are 0.003396 pu (339.6 kW) and 0.003449 pu (344.9 kW), respectively. Fig. 3.10-(a), the optimal charging power of EVs is shown. The presence of BESS at CS improves the charging rate of EVs. The optimal reactive power supplied by the reactive power compensator installed at bus 18 and 33 with and without BESS at CS is shown in Fig. 3.10-(a). The cumulative reactive power supplied by the reactive power compensator for the 24 h time period with and without BESS at CS is 10.53 pu and 8.941 pu, respectively. The cumulative active power generation by wind-type generation is relatively higher than a solar-type generation and also consistent. Therefore, the reactive power supplied by the reactive power compensator and network losses is less in the case of wind-type generation than in solar-type generation. The value of the cost function and voltage profile of the network is shown in Fig. 3.11. The cost function with and without BESS at CS is shown in Fig. 3.11-(a). The cost function with and without BESS at CS is shown in Fig. 3.11-(a). In the case of wind-type generation, the highest generation-to-load ratio is observed at the instant of 15 h. Therefore, at this hour, the highest value of voltage is observed at all buses. The bus voltage at this hour with and without optimal setting of voltage controlling parameter is shown in Fig. 3.11-(b). The optimal setting of the voltage-controlling parameter improves the voltage profile of the network.

3.5.4 Mixed Type generation

In this case, both the equal rating of solar and wind types of generation is considered for power generation. Similar to solar-type generation, in this case, also the stochastic characteristics of solar-type generation, wind generation, load, and the number of EVs arriving at the charging station have been incorporated into the OPF problem while determining the optimal setting of voltage-controlling parameters. In this case, both solar and wind-type generation is considered together, input variable gets increased. Therefore, for each hourly time segment, all sixteen combinations of input variables are considered to determine the optimal rating of the voltage-controlling parameter. The optimal charging-discharging power with their SOC of BESS

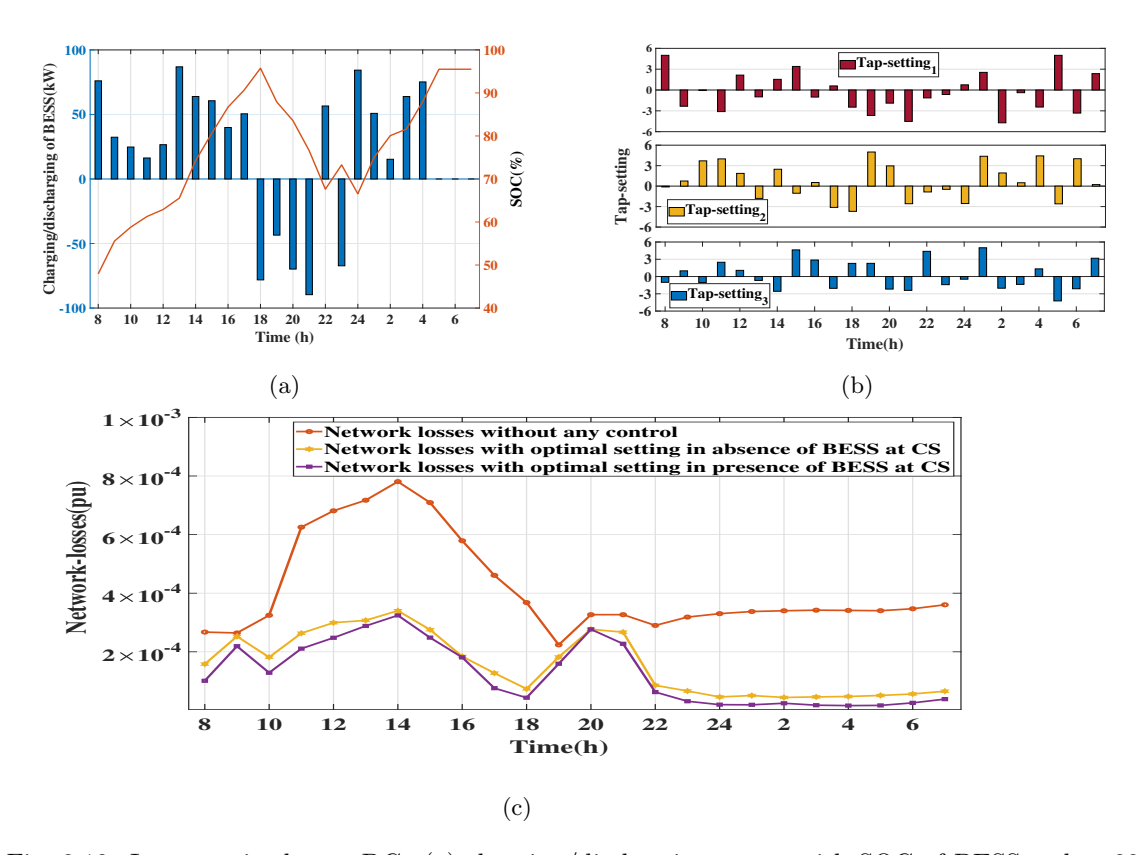


Fig. 3.12: In case mixed type DGs (a) charging/discharging power with SOC of BESS at bus 22 (b) tap-setting of OLTC (c) network losses for 24h time period

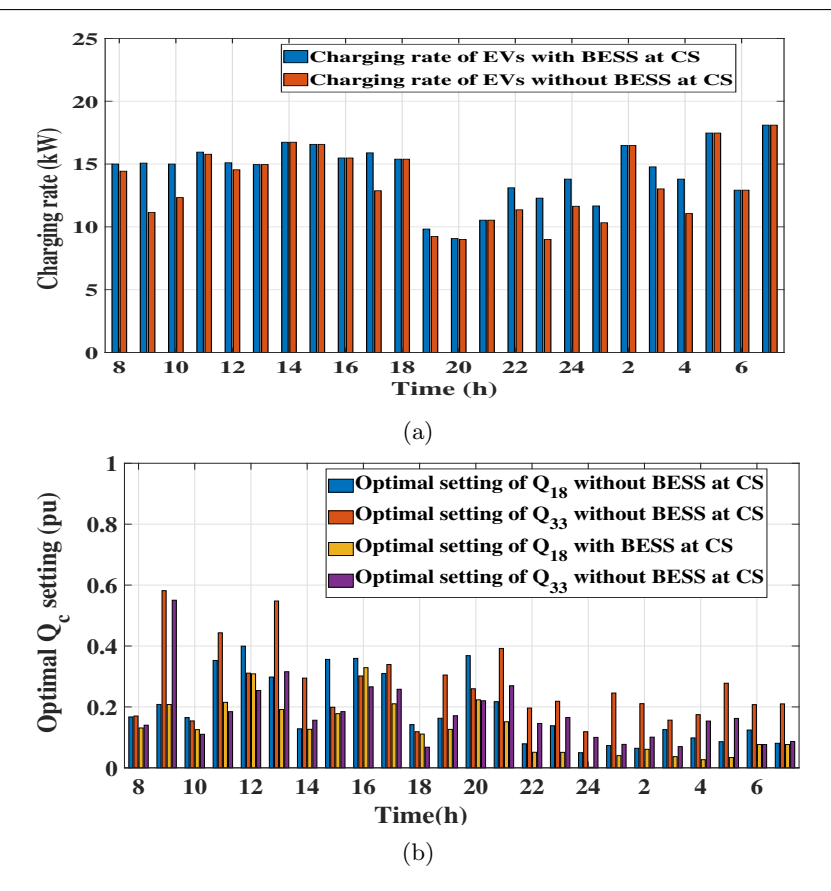


Fig. 3.13: In case mixed type DGs (a) charging rate of EVs at bus 22 (b) optimal VAR setting of reactive power compensator for 24 h time period

installed in CS at bus 22 is shown in Fig. 3.12-(a). BESS takes power from (18 h to 22 h) and 24 h due to higher power generation than the load demand at this hour. In this case, the charging time segment is less in comparison to individual power generation by solar and wind type generation. The optimal tap setting is shown in Fig. 3.12-(b). The losses of the distribution network with and without optimal settings of voltage-controlling devices show in Fig. 3.12-(c). The total losses of the distribution network over 24 h duration, without the optimal setting of voltage-controlling parameters is 0.0096 pu (960 kW), and with the optimal setting of the voltage controlling parameter in the presence and absence of BESS at CS are 0.003366 pu (336.6 kW) and 0.3243 pu (324.3 kW), respectively. The cumulative active power generation by mixed-type generation is relatively higher than the individual power generation by solar and wind-type generation also consistent. Therefore, the reactive power supplied by the reactive power compensator, which is shown in Fig. 3.13-(b) and network losses is lesser than the individual power generation by solar and wind type generation. The BESS at CS improves the charging rate of EVs. The optimal reactive power supplied by the reactive power compensator installed at bus 18 and 33 with and without BESS at CS is shown in Fig. 3.13-(b). The cumulative reactive power supplied by the reactive power compensator for the 24h time period with and without BESS at CS is 10.1 pu and 8.1 pu, respectively. The value of the cost function and voltage profile of the network is shown in Fig. 3.14. The cost function with and without BESS at CS is shown in Fig. 3.14-(a). The cost function with and without BESS at CS is shown in Fig. 3.14-(a). In the case of mixed-type generation, the highest generation-to-load ratio is observed at 14 h. Therefore, at this hour, the highest value of voltage is observed at all buses. The bus voltage at this hour with and without optimal setting of voltage controlling parameter is shown in Fig. 3.14-(b). The optimal setting of the voltage-controlling parameter improves the voltage profile of the network.

To evaluate the effectiveness of the proposed M-Jaya algorithm, it has been compared with other

Table 3.3: Comparison of M-Jaya algorithm with PSO and GWO algorithm for 14h on IEEE-33

Para-	M-Jaya	M-Jaya	PSO	PSO	GWO	GWO
meter	with	without	with	without	with	without
	BESS	BESS	BESS	BESS	BESS	BESS
cost-	377.21	608.98	407.21	658.518	397.21	658.98
function						
losses	24.7	25.13	27.1	28.68	25.1	25.9
(kW)						
(kVAR)						
Q_{18}	175.5	275.2	193.2	296	187.4	275.4
Q_{33}	177.3	296	215.4	300.13	197.56	306.4
$OLTC_1$	1.03	1.03	1.01	1.03	1.02	1.02
$OLTC_2$	0.98	0.997	0.987	0.99	099	1.01
$OLTC_3$	1.02	1.013	1.01	1.012	1.01	0.986
SOC(%)						
$BESS_{22}$	73.5		73.4		74.2	
$BESS_{25}$	80.4		72.7		75.23.	
Charging						
rate of						
EVs in CS(kW)						
CS_{22}	19.62	14.1	17.8	13.3	18.4	11.9
CS_{25}	14.34	12.4	13.4	12.8	14.1	13.6

algorithms, such as particle swarm optimization (PSO)[105] and grey wolf optimizer (GWO)[106] in terms of the cost function, optimal setting of voltage controlling parameter, and network losses. It is compared in two cases: (a) with BESS at the charging station and (2). without BESS at a charging station. All these comparing parameters are given in the TABLE 3.3. The value of the cost function for both the cases by M-Jaya algorithm, PSO and GWO is shown in Fig.3.14-(a). The value of the objective function for both the cases with and without BESS are 377.21 and 608.981, respectively, which is lesser than the value of the objective function by PSO and GWO without violating any constraints.

3.5.5 Unbalanced IEEE-123 distribution system

In this test system, the optimal setting of the voltage-controlling parameters is determined by considering both solar and wind-type generation together. For considering the impact of the tap changer on voltage control, at four locations, the transformer equipped with a tap-changer has been considered as shown in Fig. 3.5. The maximum and minimum tap settings are considered as -5 and 5. In the different phases of test system, at eleven buses, DGs of rating 800 kW, at four buses, the reactive power compensator of rating 200 kVAR and Charging Station (CS) are considered. The location of DGs, reactive power compensator of rating 200 kVAR and CS are shown in Fig. 3.5. All the charging stations can accommodate 100 EVs during the day. It is assumed that each EV

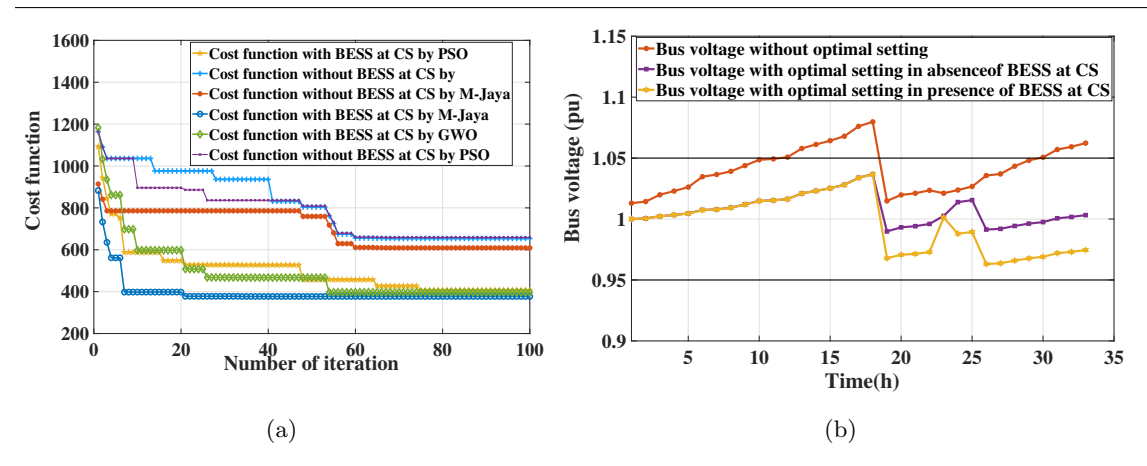


Fig. 3.14: In case mixed type DGs (a) comparison of cost function by M-Jaya algorithm with PSO and GWO algorithm (b) voltage levels at all buses with and without optimal setting for 14 h

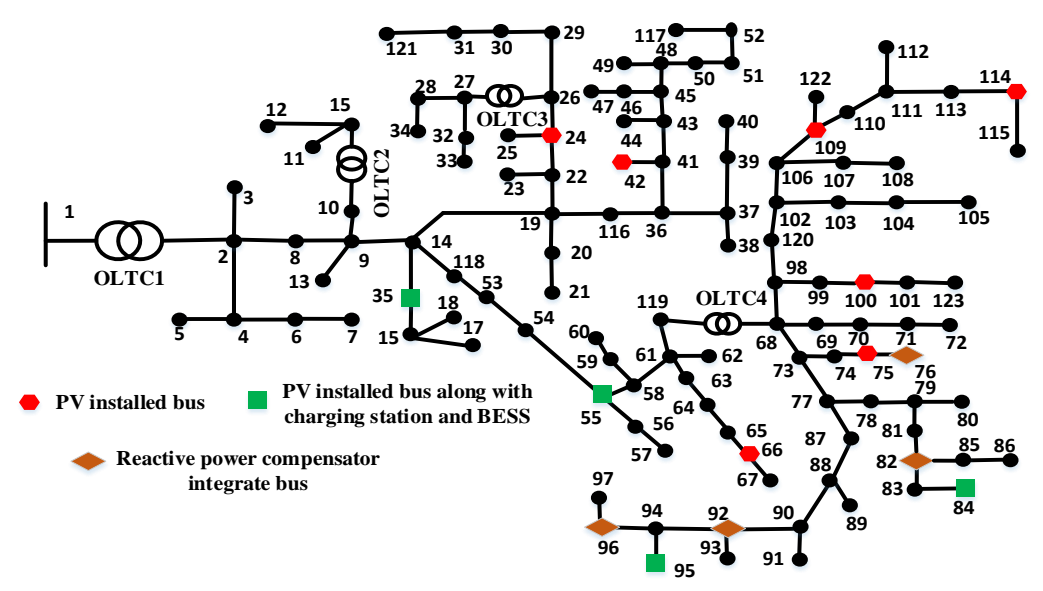


Fig. 3.15: IEEE-123 test system

and Charging Station is installed with 85 kWh and 500 kWh battery, respectively. Simultaneously, the initial SOC of installed BESS at CS is assumed to be 0.45 pu. For this test system also, the number of EVs arriving for each hourly time segment of the 24 h time period is determined from end time data given in [99] using (3.17) and it is shown in Fig. 3.4-(a). The initial SOC of the EV battery is derived from the daily distance travelled data provided in [99], utilizing equations (3.17) to (3.18). The outcome is depicted in Fig. 3.4-(b). The parking time of EVs is considered 5 h [103]. For finding out the optimal setting of voltage controlling parameters, OPF given in (3.26) to (3.28) has been solved using the M-Jaya algorithm.

3.5.6 Discussion

In this case, both the equal rating of solar and wind types of generation is considered for power generation. The stochastic characteristics of solar-type generation, wind-type generation, load, and the number of EVs arriving at the charging station have been incorporated into the OPF problem while determining the optimal setting of voltage-controlling parameters. In this case, both solar and wind-type generation is considered together. Therefore, for each hourly time segment, all sixteen combinations of input variables are considered to determine the optimal rating of the voltage-controlling parameter. The optimal charging-discharging power with their SOC of BESS

Table 3.4: Bus present in each phases

Phases	Present Buses
a	1,2,8,9,10,11,12,14,15,19,20,21,22,24,26,27,28,29,30,31,34,41,43
	45, 46, 47, 48, 49, 50, 51, 52, 53, 54, 55, 56, 57, 58, 59, 61, 62, 63, 64, 65,
	66,67,6870,71,72,73,77,78,79,80,81,82,83,84,87,88,89,90,92
	94,95,96,98,99,100,101,102,106,109,110,111,112,113,114
	$115,\!116,\!118119,\!120,\!121,\!122,\!123$
b	1,2,8,13,14,19,22,23,24,26,29,30,31,36,37,39,40,41,43,44,45,48,49
	50,51,52,53,54,55,56,57,58,59,60,61,62,63,64,65,66,67,68,73,77
	78, 79, 80, 81, 82, 83, 84, 87, 88, 90, 91, 92, 94, 96, 97, 98, 99, 100, 101, 102,
	$106,\!107,\!108,\!109,\!116,\!118,\!119,\!120,\!121,\!122,\!123$
c	1, 2, 4, 5, 6, 7, 8, 9, 14, 16, 17, 18, 19, 22, 24, 25, 26, 27, 28, 29, 30, 31, 32
	33, 34, 35, 36, 41, 42, 43, 45, 48, 49, 50, 51, 52, 53, 54, 55, 56, 57, 58, 61, 62
	$ \begin{vmatrix} 63,64,65,66,67,68,73,7475,76,77,78,79,80,81,82,83,84,85,86,87,88 \end{vmatrix} $
	89, 92, 93, 94, 95, 96, 98, 99, 100, 101, 102, 103, 104, 105, 106, 109, 116, 118
	119,120,121,122,123

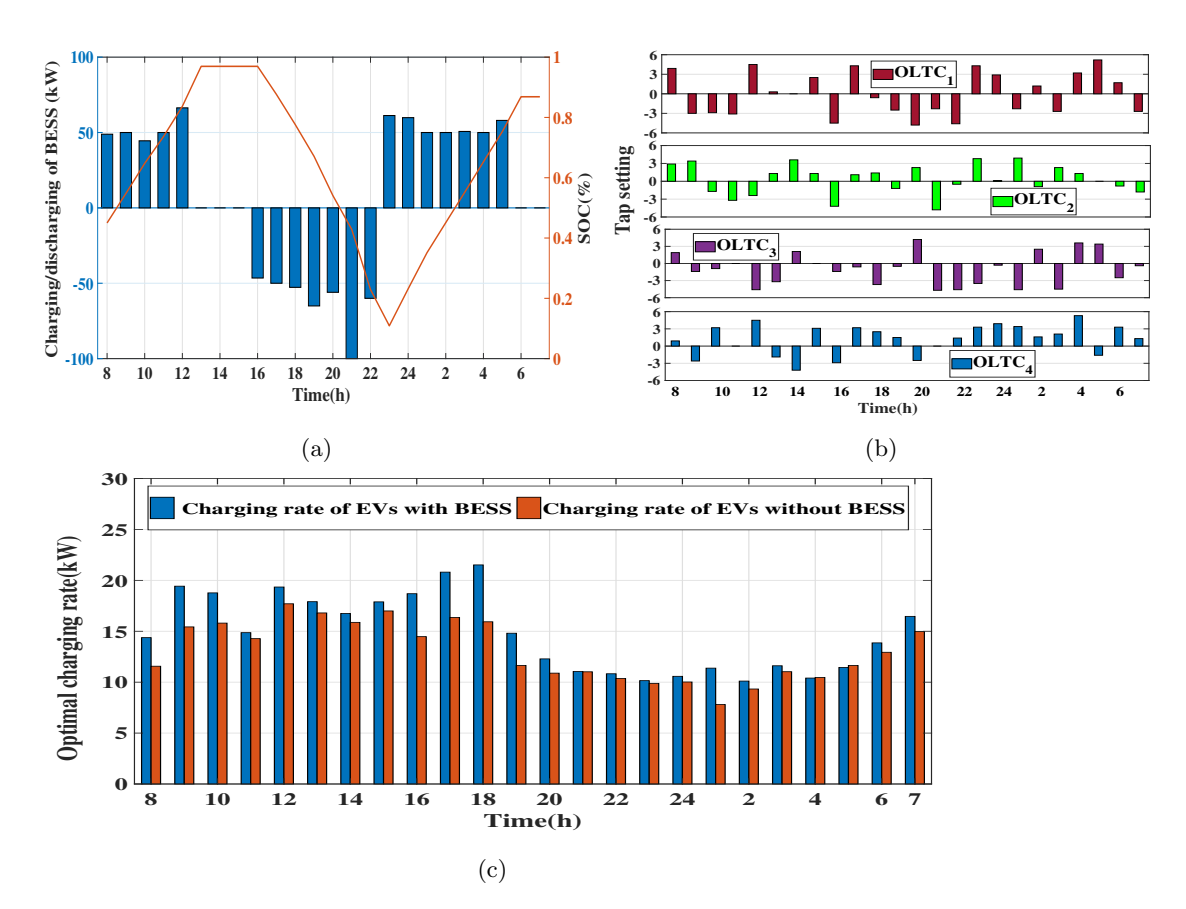


Fig. 3.16: In case mixed type DGs in IEEE-123 test system (a) charging/discharging power with SOC of BESS at bus 35 (b)tap-setting of OLTC (c) charging rate of EVs at bus 35

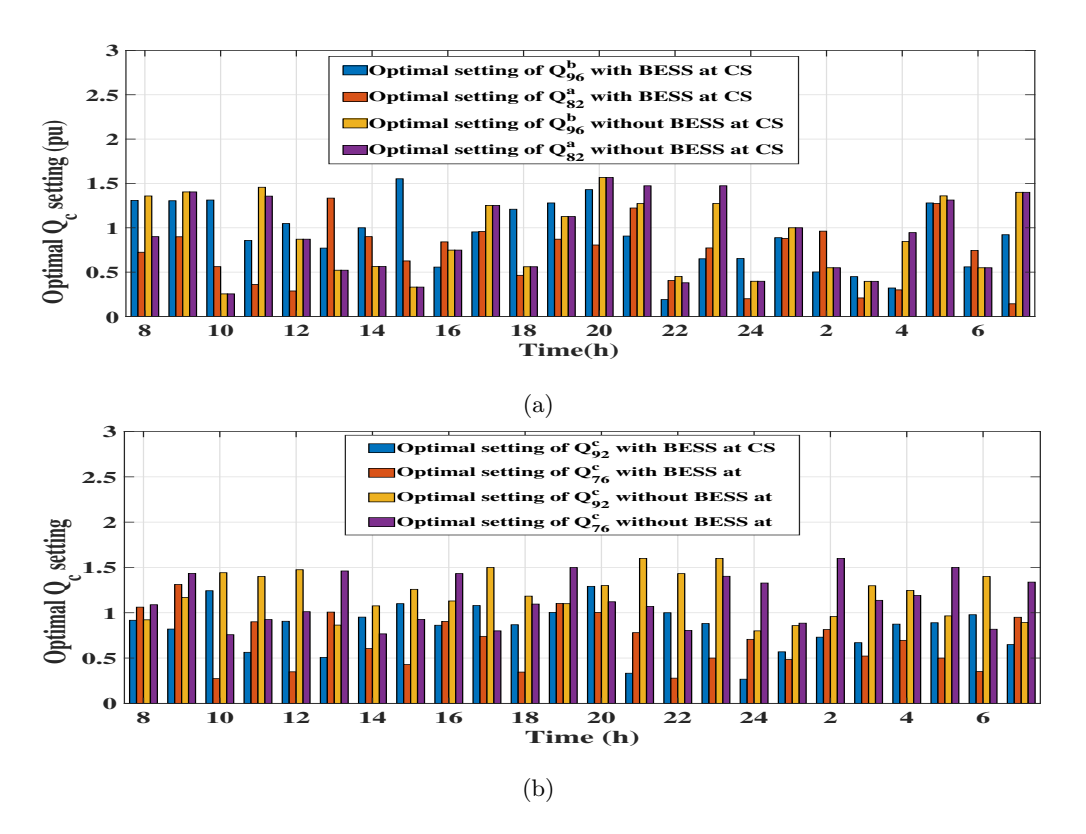


Fig. 3.17: In case mixed type DGs in IEEE-123 test system (a) optimal VAR setting of reactive power compensator at bus 82-a and 96-b (b) optimal VAR setting of reactive power compensator at bus 76-a and 92-b

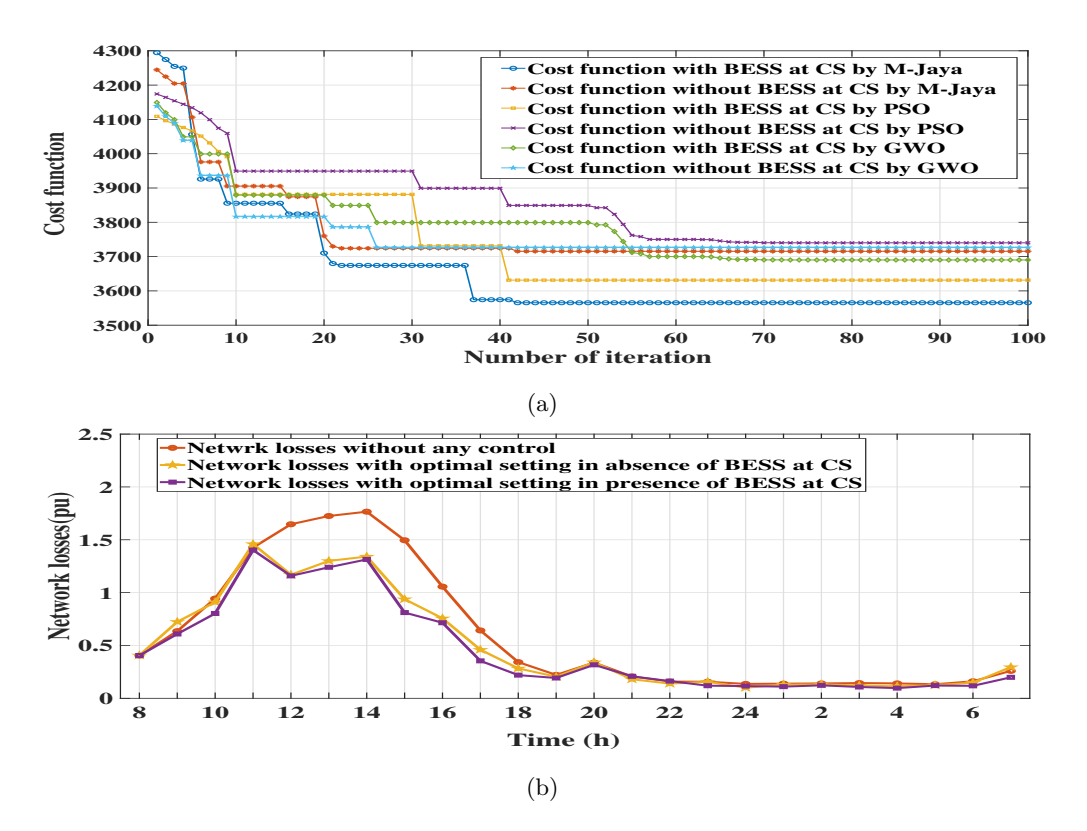


Fig. 3.18: In case mixed type DGs (a) Comparison of cost function by M-Jaya algorithm with PSO and GWO algorithm (b) voltage Levels at all buses with and without Optimal setting for 14 h

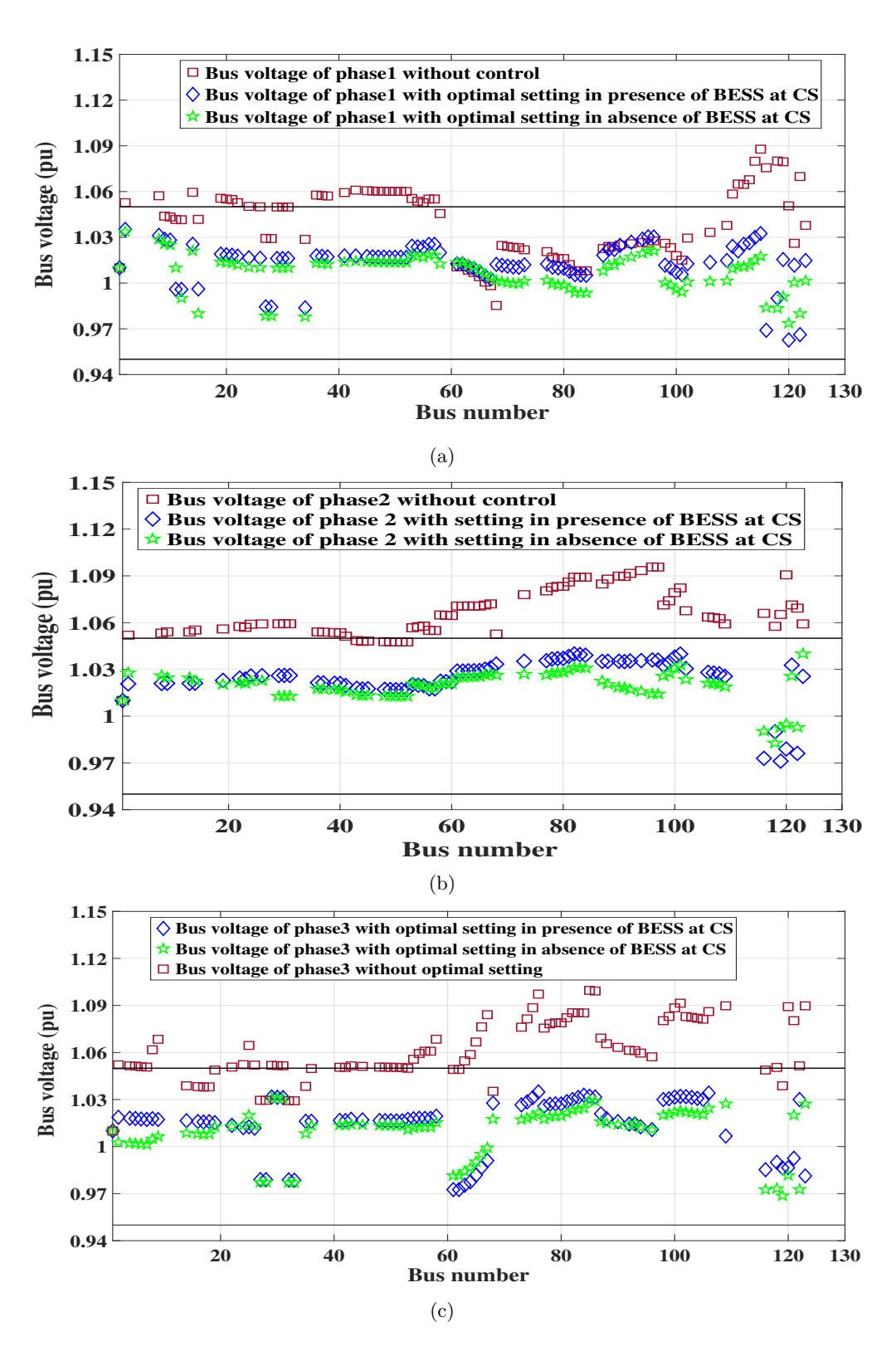


Fig. 3.19: In case mixed type DGs in IEEE-123 test system for 14 h with and without optimal setting (a) voltage level of present buses in phase-a (b) voltage level of present buses in phase-b (c) voltage level of present buses in phase-c

installed in CS at bus 35 of phase a is shown in Fig. 3.16-(a). BESS takes power from (1 h to 12 h) and (23 h to 24 h) due to higher power generation than the load demand at this hour. Similarly, BESS supplies power from (16 h to 22 h) due to generation being lesser than load. The optimal tap setting and optimal charging rate of EVs are shown in Fig. 3.16b-(b) and (c), respectively. The BESS at CS improves the charging rate of EVs. The optimal reactive power supplied for a 24 h time period by the reactive power compensator installed at phase-a of bus 82, phase-b of bus 92, phase-c of bus 76 and phase-c of bus 92 with and without BESS at CS is shown in Fig. 3.17-(a) and (b). The cumulative reactive power supplied by the reactive power compensator for the 24 h time period with and without BESS at CS is 81.24 pu and 104.85 pu, respectively. The losses of the distribution network with and without optimal settings of voltage-controlling devices show in Fig. 3.18-(a). The total losses of the distribution network for 24 h, without the optimal setting of voltage-controlling parameters, is 14.41 pu, and with the optimal setting of the voltage controlling parameter in the presence and absence of BESS at CS are 11.92 pu and 10.82 pu, respectively. In the case of mixed-type generation, the highest generation-to-load ratio is observed at 14 h. Therefore, at this hour, the highest value of voltage is observed at all buses. In the case of mixed-type generation, the highest generation-to-load ratio is observed at 14 h. Therefore, at this hour, the highest value of voltage deviation is observed on all buses. The bus voltage of all the phases at this hour with and without optimal setting of voltage controlling parameter is shown in Fig. 3.19-(a), (b) and (c), respectively. The available buses in phases a, b, and c are listed in Table 3.4, and their respective voltage profile is shown in Fig. 3.19. The over-voltage phenomenon is observed in all three phases at different buses without any control. The optimal setting of the voltage-controlling parameter improves the voltage profile of the network. The result of the M-Jaya algorithm is compared with Particle Swarm Optimization (PSO) [105] and Grey Wolf Optimizer (GWO) [106] in terms of the cost function, optimal setting of voltage controlling parameter, and network losses. The value of the cost function for both the cases by M-Jaya algorithm, PSO and GWO is shown in Fig. 3.18b-(b). The value of objective function for both the cases with and without BESS are 3565.46 and 3715.26, respectively, which is lesser than the value of the objective function by PSO and GWO without violating any constraints.

3.6 Conclusion

- The increasing integration of renewable energy generation and charging infrastructure into the distribution network heightens uncertainty within the distribution network. To maintain voltage profile of the distribution network, these factors must be incorporated while determining the setting of voltage-controlling parameters.
- This work determines the optimal settings for voltage-controlling parameters over a 24-hour period by considering stochastic characteristics of various types of Converter-Based Generation (CBG), such as solar, wind, and mixed generation, power demand by loads, and the number of Electric Vehicles (EVs) arriving at charging stations using an hourly state-based probabilistic model incorporated into the OPF problem.
- The enhanced IEEE 33 and an unbalanced IEEE 123 test system are used to determine the effectiveness of the proposed method.
- Optimal settings of voltage-controlling parameters enhance the voltage profile and reduce losses in the distribution system.

- Installing BESS at charging stations improves the charging rate of EVs and decreases network losses by improving the power factor of distributed generation.
- The M-Jaya algorithm achieves better convergence for proposed objective functions without violating any operating constraints.
- The proposed work provides insights into forecasting the optimal settings of voltage-controlling parameters for any period in the presence of renewable generation and charging infrastructure in the distribution network.

Chapter 4

Dual-Stage Voltage Control For Active Distribution Network With High Penetration of Photovoltaic Distributed Generators Using Spectral Clustering

4.1 Introduction

The high penetration of power from renewable-based DGs causes reverse power flow, due to which overvoltage is observed in the Active Distribution Network (ADN). The overvoltage issue not only causes harm to the electrical equipment present in the ADN but also restricts the hosting capacity of the network. Hence, addressing the overvoltage issue is imperative to ensure the stable and reliable operation of the ADN.

In the past, Photovoltaic Distributed Generations (PV-DGs) used to operate at unity power factor without active and reactive power control capabilities, which restricted PV inverters from contributing to power dispatching. In this scenario, traditional voltage control techniques are not considered an optimal solution due to their higher cost, sluggish response times, and lack of suitability for bidirectional power flow [8]-[107].

With the advancement of power-electronic inverter technology, voltage control by regulating the active and reactive power of PV-DGs offers optimistic solutions to mitigate the overvoltage issues in ADN [17]. Active Power Curtailment (APC) and Reactive Power Compensation (RPC) are widely adopted strategies that can enable PV inverters to address the overvoltage problem. However, centralized curtailment of active power from available PV-DGs in the network is not considered an optimal solution for utility grids. In this work, a two-stage voltage control technique is proposed to deal with this issue. In the primary stage, using state-based probabilistic modeling of the load-generation scenario and Electric-Vehicles (EVs) present in the Charging Station (CS), the optimal rating of the On-load Tap changer (OLTC), optimal charging and discharging of Battery Energy Storage Systems (BESSs) and optimal charging of EVs are estimated for the entire 24 hour(h) planning horizon with the objective of minimization of overvoltage and network losses. When the optimal hourly setting of the available voltage-controlling device in the network fails to maintain the voltage profile due to a high generation-to-load ratio, the voltage profile is restored by implementing CBVC in the secondary stage. To implement CBVC, the ADN is divided into multiple clusters using a probabilistic voltage sensitivity index-based spectral clustering method, ensuring that the available PV-DGs within each cluster can maintain the

bus voltage within the designated cluster. Further, the optimal operating power of PV-DGs is determined by independently solving the OPF for each cluster with the objective of reducing the active power curtailment and reactive power absorption by the available PV-DGs in the cluster. The proficiency of the proposed method is validated by comparing it with the Centralized Voltage Control (CVC) method in terms of voltage profile, cumulative active power curtailment and reactive power absorption by PV-DGs, network losses and computation time.

The remaining sections of the chapter are arranged as follows. In Section 4.2, modeling the active distribution network is presented. Two-stage voltage control strategy is elucidated in Section 4.3. The implementation of the proposed two-stage voltage control technique on the 37-bus and modified IEEE 123-bus system is elucidated in section 4.4. The conclusion is presented in section 4.5.

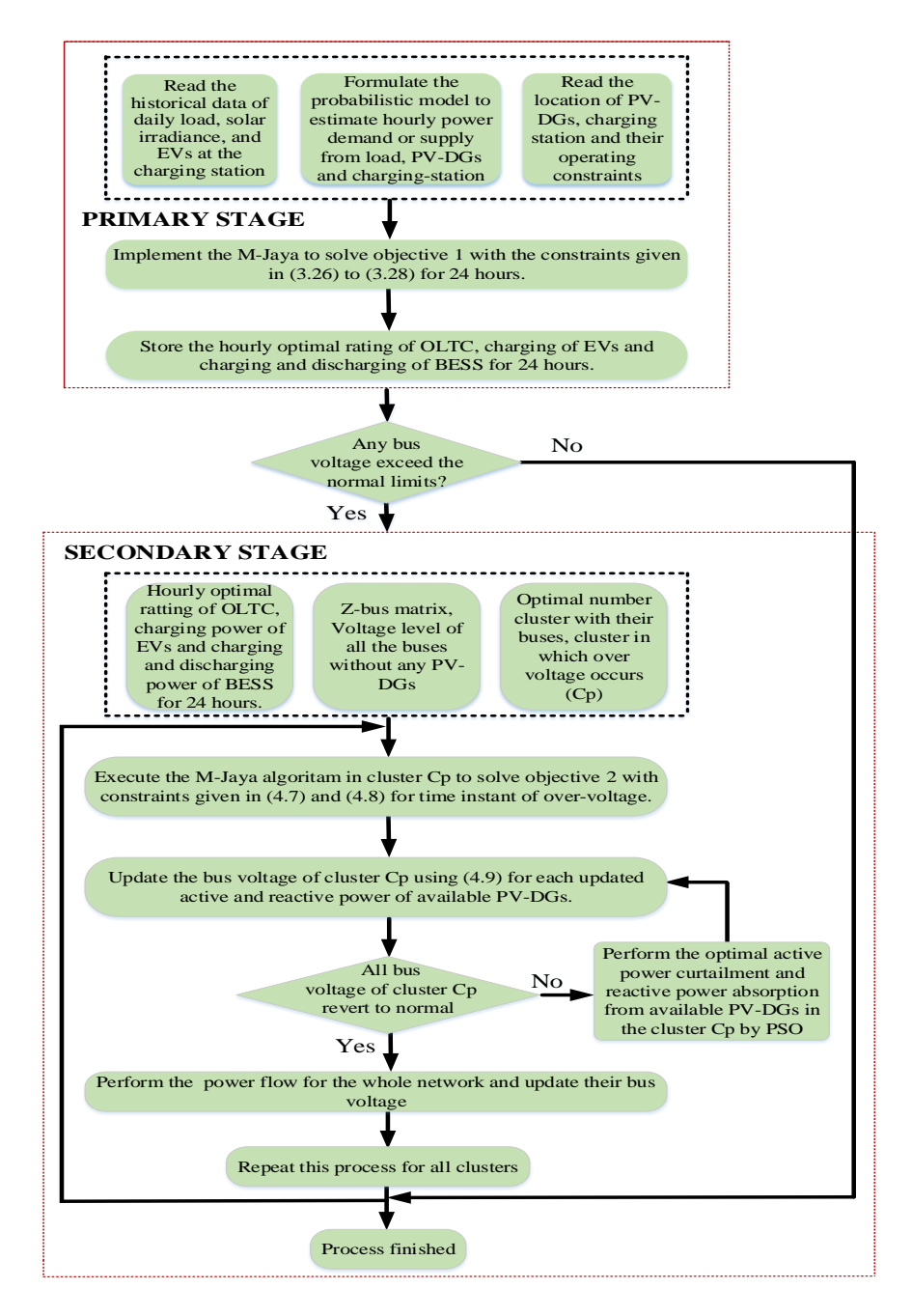


Fig. 4.1: Flowchart of two-stage voltage control

4.2 ADN modeling Strategy

The state-based probabilistic modeling of hourly output from PV-DGs, load demand, available EVs in the Charging Station(CS), and the operating of BESS with time-varying load and generation is explained in section 3.2.

4.3 Voltage Control Strategy

In this section two-stage voltage control technique shown in Fig. 4.1 is elaborated. In the primary stage, the optimal hourly setting of the voltage-controlling device is determined for the 24 h time period. In case the optimal hourly setting voltage-controlling device fails to maintain the voltage profile, the secondary stage of voltage control comes into action. It is implemented in clustered ADN by utilizing voltage-controlling capabilities of available PV-DGs in each cluster independently.

4.3.1 Primary Stage Voltage Control

In this stage, utilizing the probabilistic model of PV-DG output and available EVs in the charging station, optimal setting of OLTC, charging-discharging of BESS and charging of EVs are planned for a 24 h planning horizon. The minimization of overvoltage and network losses is considered as an objective function, as explained in section 3.3. Modified –Jaya (M-Jaya) algorithm is used to solve hourly optimal power flow problems, as explained in section 3.4.

4.3.2 Secondary Stage voltage Control

In the secondary stage, CBVC is implemented. To execute this, at first, ADN is segregated into different clusters based on the impact of power perturbation at PV-DGs integrated bus in the network on bus voltage. It is assessed in terms of the Probabilistic Voltage Sensitivity Index (PVSI). While calculating PVSI, the analytic formula of voltage sensitivity is utilized. Further, using spectral clustering, ADN is segregated into multiple clusters. It segregates the ADN in such a way that existing PV-DGs in the cluster are able to retain the bus voltage within the cluster. Further, the optimal operating point of available PV-DGs in each cluster is determined by solving the OPF problem to minimize their active power curtailment and reactive power absorption.

4.3.2.1 Clustering of ADN Using PVSI

4.3.2.2 Formulation of Probabilistic Voltage Sensitivity Index (PVSI)

In this work PVSI is used to determine the impact available PV-DGs on bus voltage. The formulation of PVSI is explained in section 2.3.

4.3.2.3 Steps of spectral clustering

Spectral clustering is a graph-based algorithm that segregates $m \times n$ data matrix into a k cluster. The steps to execute clustering are explained below.

Step 1: Create the data matrix $(\Omega_{m\times n})$, the PVSI of each bus voltage due to power perturbation at individual DG is arranged in the column of the data matrix. If the size of the network is m, and the number of PV-DG present in AND is n, then the size of the data matrix becomes $m \times n$.

Further, spectral clustering is performed for the data matrix to cluster of the ADN.

$$\Omega_{(m \times n)} = \begin{bmatrix}
PVSI_{11} & PVSI_{12} & \dots PVSI_{1n} \\
\vdots & \ddots & \\
PVSI_{m1} & PVSI_{m2} & \dots PVSI_{mn}
\end{bmatrix}$$
(4.1)

Step 2: For $\Omega_{m\times m}$, evaluate the Euclidean distance between the buses of the network utilizing (4.2) to create the distance matrix $\lambda_{m\times m}$.

$$\lambda_{ij} = \begin{cases} \left(\sum_{i,j=1}^{m} (PVSI_{ik} - PVSI_{jk})^2\right)^{\frac{1}{2}}, & if i \neq j \\ 0 & otherwise \end{cases}$$

$$(4.2)$$

Step 3: Formulate the unnormalized and normalized Laplacian matrices, (L_{un}) and (L_n) , respectively, as given in (4.3).

$$L_{un} = D_g - \lambda, \qquad L_n = D_g^{-\frac{1}{2}} L D_g^{\frac{1}{2}}$$
 (4.3)

 D_g is a symmetric diagonal matrix. The element of D_g is determined by summing up the row of distance matrix (λ) as given (4.4).

$$D_{g_{ii}} = \sum_{i,j=1}^{m} \lambda_{ij} \tag{4.4}$$

Step 4: Formulate the eigenvector matrix $V_{m \times k}$ from normalized Laplacian matrix as given in (4.5).

$$V_{m \times k} = \begin{bmatrix} v_1 & v_2 & \dots & v_k \end{bmatrix} \tag{4.5}$$

where v_k is eigenvector that corresponding to the smallest eigenvalues of L_n

Step 5: Implement the K-mean clustering for eigenvector-matrix by considering each row as a data point. Allocate the actual data points of Ω to the same clusters as their respective rows in the eigenvector matrix $V_{m \times k}$.

4.3.2.4 Quality of Cluster Index (QCI)

The quality of the cluster is determined by the Silhouette index. It gives the degree of coupling among the member of the cluster, given in (4.6).

$$SI(i) = \frac{d(i) - g(i)}{\max[d(i), g(i)]}$$

$$d(i) = \frac{1}{N_p} \binom{\sum_{i,j \in C_p, i \neq j, j=1}^{N_p} S_{i_{C_p} j_{C_p}}}{\sum_{i,j \in C_p, i \neq j, j=1}^{N_l} S_{i_{C_p} j_{C_p}}}$$

$$f(i) = \min_{\substack{1 \leq i \leq k \\ l \neq p}} \frac{1}{N_l} \binom{\sum_{m \in C_l, m=1}^{N_l} S_{i_{C_p} m_{C_l}}}{\sum_{m \in C_l, m=1}^{N_l} S_{i_{C_p} m_{C_l}}}$$

$$QCI = \frac{1}{k} \sum_{i=1}^{k} \left(\frac{1}{N_p} \sum_{i=1}^{N_p} SI_i(j)\right)$$

$$(4.6)$$

where d(i) and g(i) are the average differential entropy between i^{th} DG integrated bus with all other buses in the same cluster C_p and different clusters, respectively. N_p and N_l are total number of buses in cluster C_p and C_l , respectively. Values of QCI lie between zero to one. The highest value of QCI indicates defines perfect clustering [108].

4.3.2.5 Optimization problem for secondary stage voltage control

To determine the optimal operating point of available PV-DGs, OPF is solved for each cluster individually. The minimization of active power curtailment and reactive power absorption is taken as the objective function, and active and reactive power output from PV-DGs is taken as the decision variable. The objective function and their operating constraints are detailed in (4.7) and (4.8), respectively.

$$obj2 = \sum_{i=1}^{M_p} \left[(\Delta P_{curt}^{p_i})^2 + \Delta Q_{obs}^{p_i})^2 \right]$$
 (4.7)

$$0.95pu \le V_{C_p}^i \le 1.05pu$$

$$P_{min}^{p_i} \le \Delta P_{curt}^{p_i} \le P_{max}^{p_i}$$

$$Q_{min}^{p_i} \le \Delta Q_{obs}^{p_i} \le Q_{max}^{p_i}$$

$$-0.95 \le pf_{DG_{p_i}} \le 0.95$$
(4.8)

where p_i represents the i^{th} PV-DG of cluster C_p . M_p represents total number of PV-DG in the cluster C_p . $\Delta P_{curt}^{p_i}$ and $\Delta Q_{obs}^{p_i}$ are the active and reactive power curtailed and observed by the i^{th} PV-DG of cluster C_p . $P_{max}^{p_i}$, $P_{min}^{p_i}$, $Q_{min}^{p_i}$ and $Q_{max}^{p_i}$ are maximum and minimum curtailed active and observed reactive power limit from i^{th} PV-DG of cluster C_p and $pf_{DG_{p_i}}$ represents their power factor. $V_{C_p}^i$ represents updated i^{th} bus voltage of p^{th} cluster. To solve the OPF problem for C_p , PSO is utilized. However, validation of voltage constraints given in (4.8) by full load flow calculation for each updated active and reactive power of PV-DGs becomes a computational process.

Consequently, the analytic formula of voltage sensitivity (subsection-2.2.2) is utilized for updating the bus voltage as given in (4.9).

$$\begin{bmatrix} v_{C_{p_i}} \\ \vdots \\ v_{C_{p_k}} \\ \vdots \\ v_{C_{p_n}} \end{bmatrix} = \begin{bmatrix} v_{C_{p_{i_0}}} \\ \vdots \\ v_{C_{p_{k_0}}} \\ \vdots \\ v_{C_{p_{n_0}}} \end{bmatrix} + \begin{bmatrix} Z_{C_{p_i}1} & \dots & Z_{C_{p_i}C_{p_i}} & \dots & Z_{C_{p_i}n} \\ \dots & \ddots & \vdots & \dots & \vdots \\ Z_{C_{p_k}1} & \vdots & Z_{C_{p_k}C_{p_i}} & \dots & Z_{C_{p_k}n} \\ \vdots & \vdots & \vdots & \ddots & \vdots \\ Z_{C_{p_n}1} & \vdots & \ddots & \dots & Z_{C_{p_n}C_{p_n}} \end{bmatrix} \begin{bmatrix} \Delta S^{C_{p_i}} \\ \vdots \\ \Delta S^{C_{p_k}} \\ \vdots \\ \Delta S^{C_{p_k}} \end{bmatrix}$$

$$(4.9)$$

where $v_{C_{p_i}}$ and $v_{C_{p_{i_0}}}$ represents bus voltage of i^{th} bus in cluster p, before and after disturbance at all the available PV-DGs in the cluster p. $Z_{C_{p_i}n}$ represents the mutual impedance between i^{th} bus of cluster p and n^{th} bus of the network. $\Delta S^{C_{p_i}}$ is complex power perturbation at i^{th} PV-DG integrated bus in cluster p.

The impedance matrix size decreases in cluster-based control, leading to a reduction in the computation time required to determine the optimal operating point of available PV-DGs in the cluster. The M-Jaya algorithm is used to solve the OPF problem for the second stage.

In the second stage, the set of variables corresponds to the curtailed active power ΔP_{DG} and the absorbed reactive power ΔQ_{DG} from the available PV-DGs in the clusters. The size of the set of variables is $d=2n_{DG}$. n_{DG} is the total number of DGs participating in voltage control.

4.4 Results and Discussion

For implementing the two-stage voltage control, a practical three-phase balanced 37-bus and modified IEEE-123 test system are taken into account. It is implemented in MATLAB R2019b with Intel-Core i7-8700, CPU @ 3.20GHz configuration.

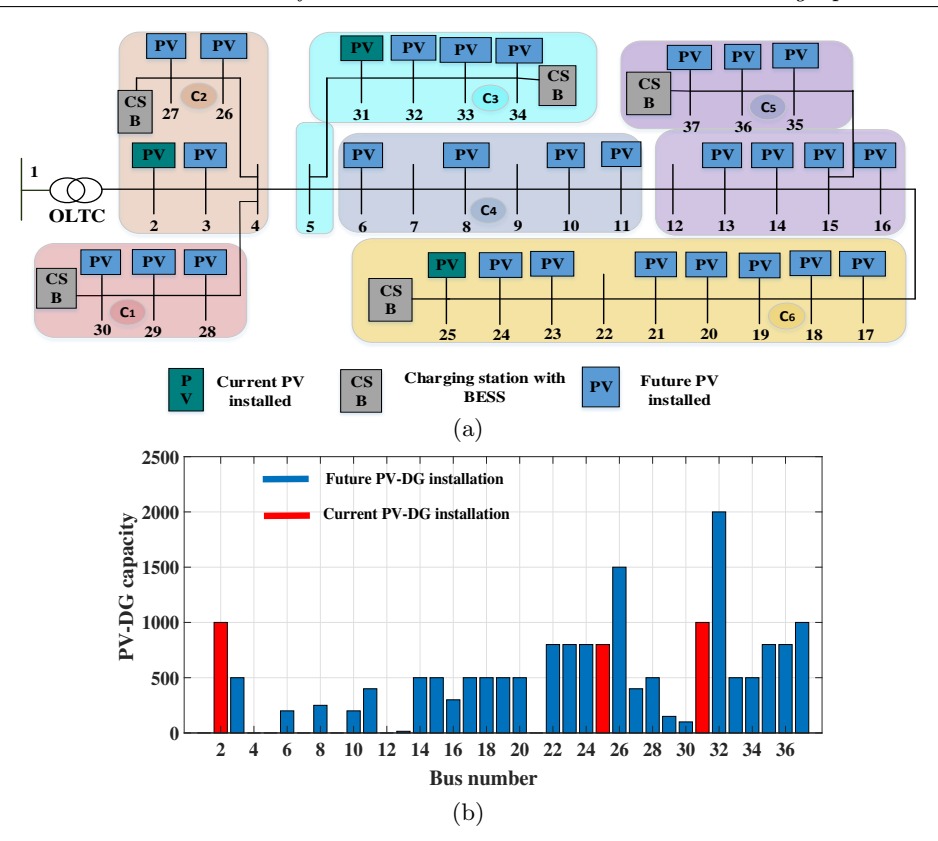


Fig. 4.2: (a) 37-bus ADN (b) current and future PV-DG installation

4.4.1 37-bus distribution system

The system parameter of the 37-bus system, such as the line impedance, load demand present and future PV-DG capacity of each bus, are taken from [36]. As shown in Figure 4.2-(a), bus one is considered as a reference bus with a transformer equipped with OLTC. The minimum and maximum tap positions are considered as -5 and 5, respectively. As observed by [104], bus voltage of the network for previously installed PV-DGs stay within the acceptable $\pm 5\%$ of the base bus voltage, indicating no violations of voltage limits. It is assumed that 18.315 MW is going to be installed into the distribution system. The present and future values of installed PV-DGs on all buses are shown in Fig. 4.2-(b). Increasing EVs in the market significantly impacts the voltage level of the distribution network. Thus, as shown in Fig. 4.2-(a), five charging stations with BESS are considered at five different locations. Each charging station accommodates 100 EVs during the day. It is assumed that each EV is installed with an 85 kWh battery and rating of BESS at the charging station is 500 kWh. The initial SOC and distribution of EVs arrival for each hour are determined using (3.20)-(3.22) from 2009 NHTS data [109] as shown Fig. 3.4. The maximum EV charging rate and the separation period from arrival to departure are considered as $0.2C_{EV}$ and 5 h, respectively [110].

$$\begin{bmatrix} \Delta P_i \\ \Delta Q_i \end{bmatrix} \sim \mathcal{N} \left(\begin{bmatrix} 0 \\ 0 \end{bmatrix} \begin{bmatrix} S_i & -0.05S_i \\ -0.05S_i & 0.31S_i \end{bmatrix} \right)$$
 (4.10)

where S_i is rating of PV-DG integrated at i^{th} bus.

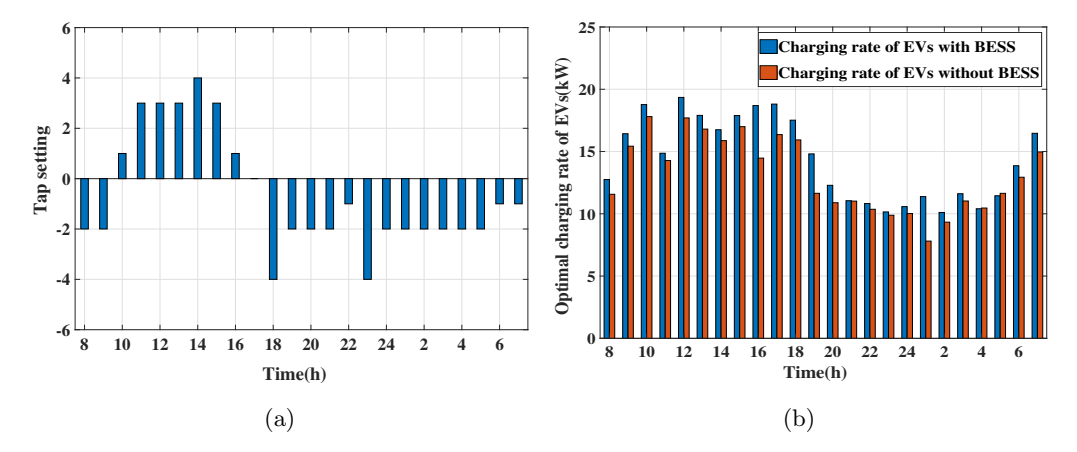


Fig. 4.3: In 37-bus system,(a) optimal tap setting of OLTC, (b) optimal charging rate of EVs, for 24 h time segment

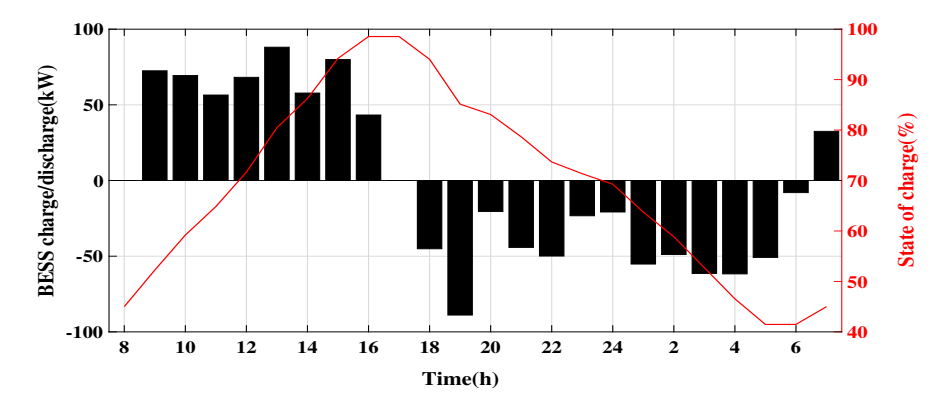


Fig. 4.4: Charging/discharging rate of BESS installed at bus 25 with CS in 37-bus system Table 4.1: State with their probability of solar irradiance, number of EVs arrival at CS and load for 13 h

State	PV-DG output	Prob	Load	Prob	EVs	Prob
1	$0 \le p_s < 0.5$	0.0137	$0 \le l < 0.3$	0.23	$0 \le E < 5$	0.083
2	$0.5 \le p_s < 0.7$		$0.3 \le l < 0.6$		_	
3	$0.7 \le p_s < 1$	0.6262	$0.6 \le l < 1$	0.0728	$8 \le E < 12$	0.35

Primary Stage 4.4.1.1

As shown in Fig. 4.1, in the primary stage, the hourly load demand, power generation by PV-DGs and the number of EVs arrival in the charging station are taken as input to determine the optimal setting of OLTC, charging rate of available EVs in the charging station and charging-discharging of BESS. The hourly PV-DG output, load, and EV arrival data are estimated from five years of historical data [109]-[111] using beta and normal PDFs as explained in section 3.2. Initially $(5 \times 365 \times 24)$ historical data is classified into 24 h time segment. Then, utilizing respective hourly $(5 \times 365 \times 24)$ data, their hourly PDF is estimated. For 13 h, PDF of solar irradiance, load demand and the total EVs entering at the CS are depicted in Figs. 3.2-(a), 3.2-(c) and 3.2-(d), respectively. To consider all input scenarios, their respective PDFs are classified into three states (Table 4.1). For each state of solar irradiance, the corresponding PV-DG output is calculated using (3.4)-(3.8) with PV module parameters from [112]. Using states of these input variable, state matrix ($\tau_{27\times3}$) is formulated. It consists of all the combination input variable scenarios, which is used in optimization formulation as shown (3.27) to determine the optimal hourly setting of OLTC, charging rate of available EVs in the charging station and charging-discharging of BESS for the entire 24 h planning horizon.

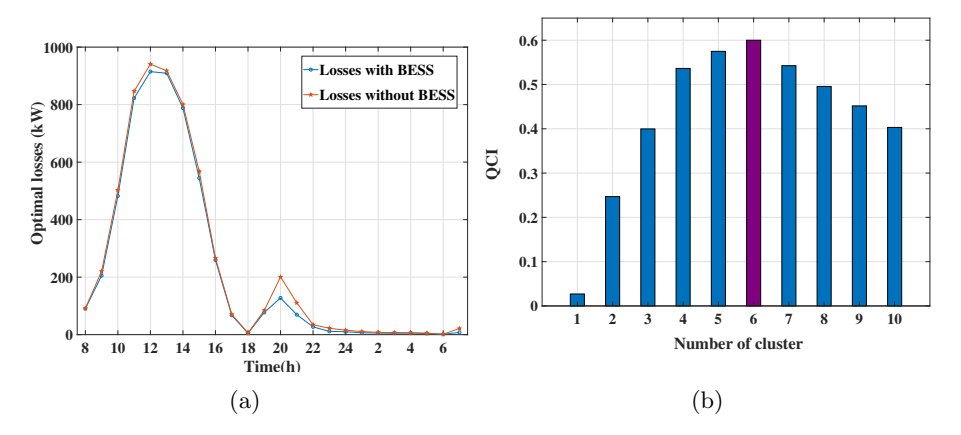


Fig. 4.5: In 37-bus system, (a) optimal hourly losses (pu), (b) Quality of Cluster Index (QCI) for different number of clusters

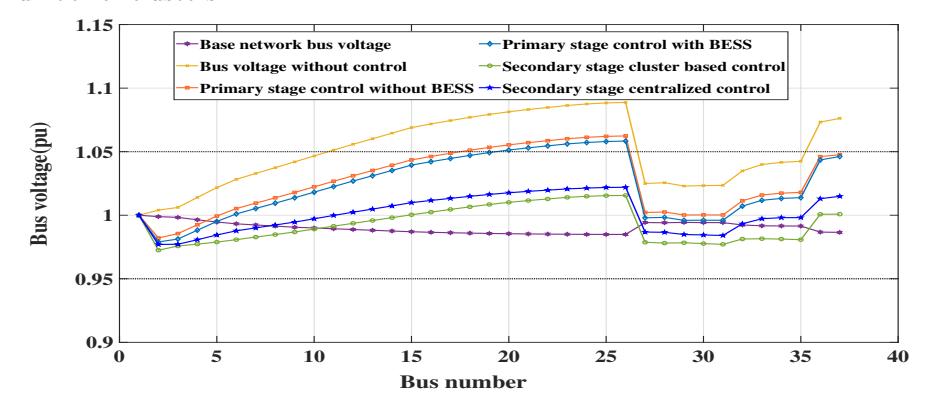


Fig. 4.6: In 37-bus system, voltage profile of all buses with and without two-stage voltage control technique for $13~\mathrm{h}$

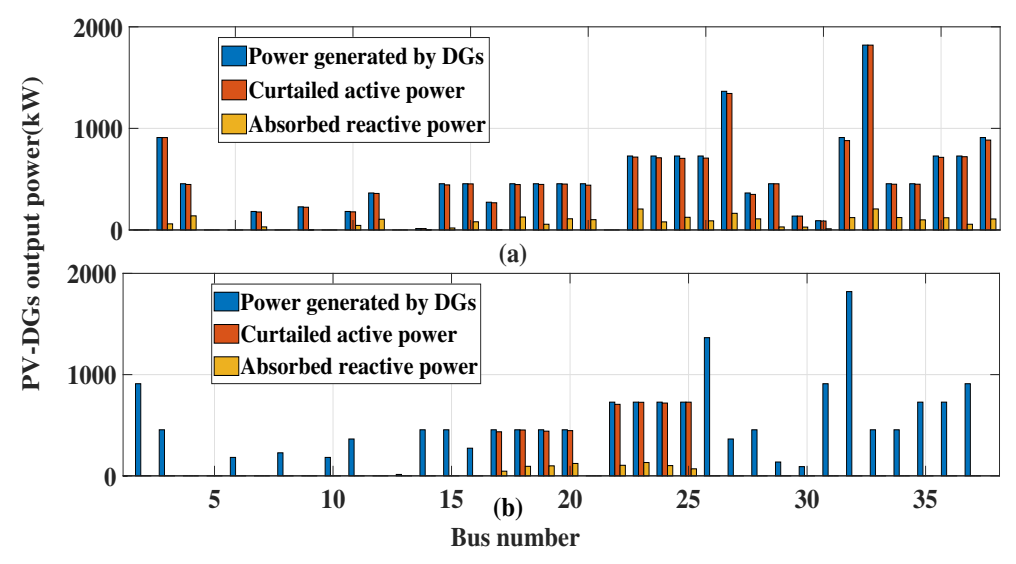


Fig. 4.7: In 37-bus system, (a) DGs output power in CVC, (b) DGs output power in CBVC

The optimization problem is solved by M-Jaya algorithm, as elaborated in section 3.4. The optimal tap setting and charging rate of EVs with and without BESS are shown by in Fig. 4.3-(a) and Fig. 4.3-(b), respectively. In both cases, similar tap positions are observed, but in the case of a charging station with a BESS, the charging rate of EVs is improved. The charging-discharging of BESS depends on generation to load ratio. Fig. 4.4 illustrates the charging-discharging characteristics of BESS installed with the charging station at bus 25 in terms of their SOC and charging-discharging

rate. This figure depicts the BESS getting charged from the 8^{th} h to the 16^{th} h due to higher generation than the load at that bus. Similarly, BESS getting discharged from the 8^{th} h to the 16^{th} h due to lower generation than the load at that bus. BESS stores the power in high-generation periods and supplies power in low-generation periods. Thus, it enhance the voltage profile of the network and also reduces network losses. The voltage profile and network losses for both cases are illustrated in Fig. 4.6 and Fig. 4.5-(a), respectively. The cumulative losses for 24 h with and without BESS are 5448.3 kW and 5750 kW, respectively. Placement of BESS in charging station reduces 6% losses than the charging station without BESS. The voltage profile of all the buses with and without implementing a two-stage voltage control method for 13 h is shown in Fig. 4.6. Due to the high power penetration by available PV-DGs with respect to load demand at 13 h, the optimal hourly setting of voltage-controlling devices is not able to maintain the voltage profile in the network. Thus, a secondary stage of voltage control is required.

$$\begin{bmatrix} \Delta P_i \\ \Delta Q_i \end{bmatrix} \sim \mathcal{N} \left(\begin{bmatrix} 0 \\ 0 \end{bmatrix} \begin{bmatrix} S_i & -0.05S_i \\ -0.05S_i & 0.31S_i \end{bmatrix} \right)$$
(4.11)

where S_i is rating of PV-DG integrated at i^{th} bus.

0.6. Therefore, ADN is segregated into six clusters.

4.4.1.2 Secondary Stage

A Cluster-Based Voltage Control (CBVC) technique is implemented in the secondary stage. Before implementing the CBVC, PVSI-based spectral clustering is implemented to separate the ADN into several clusters. It segregates the ADN into several clusters based on the impact of PV-DGs on bus voltages, as explained in the section 4.3.2.1. While performing the clustering, the power perturbation at the PV-DG integrated bus is modelled by zero mean normal random variables [89] as given in the (4.11). The optimal number of clusters is selected on the basis of the Quality Cluster Index (QCI). In Fig. 4.5-(b), QCI for the combination of different number of clusters is shown. The highest value of QCI is obtained for a combination of six clusters which is

Utilizing the cluster information, the Distribution System Operator (DSO) implements the CBVC to mitigate the overvoltage in the network, as illustrated in Fig. 4.1. In Fig. 4.6, overvoltage occurs from bus 16 to 24 without BESS and from bus 18 to 24 with BESS. From Fig. 4.2-(a), it is clear that these buses belongs to C_6 . Further, to mitigate the overvoltage issues, available PV-DGs in cluster C_6 are utilized. The optimal setting of available PV-DGs in cluster C_6 is determined by solving the OPF problem independently with the objective of minimization of active power curtailment and reactive power absorption from these PV-DGs, as illustrated in section 4.3.2.5. M-Jaya algorithm solves the OPF problem with the same parameter, which is taken in the primary stage. The analytic formula of voltage deviation given in (4.9) is used to update the bus voltage for each iteration, thereby minimizing computation time. Fig. 4.7-(b) illustrate the optimal curtailed active and observed reactive power from available PV-DGs in the cluster C_6 . Further, load flow is solved for the optimal active and reactive power of available PV-DGs in the cluster C_6 with the optimal setting of OLTC, the optimal charging rate of EVs and the optimal discharging rate of BESS of 13 h, it is observed that the voltage profile of all the buses comes within the limit, depicted in Fig. 4.6.

For the comparison, the whole network is considered as one cluster, and all the available PV-DGs in the network are utilized to mitigate the overvoltage issue. Which is called Centralized Voltage Control (CVC). A similar OPF problem is solved as CBVC by M-Jaya algorithm to evaluate the optimal operating point of all the available PV-DGs in the network. The optimal operating point of all the available PV-DGs by CVC is shown in Fig. 4.7-(a). Furthermore, solving the load flow for

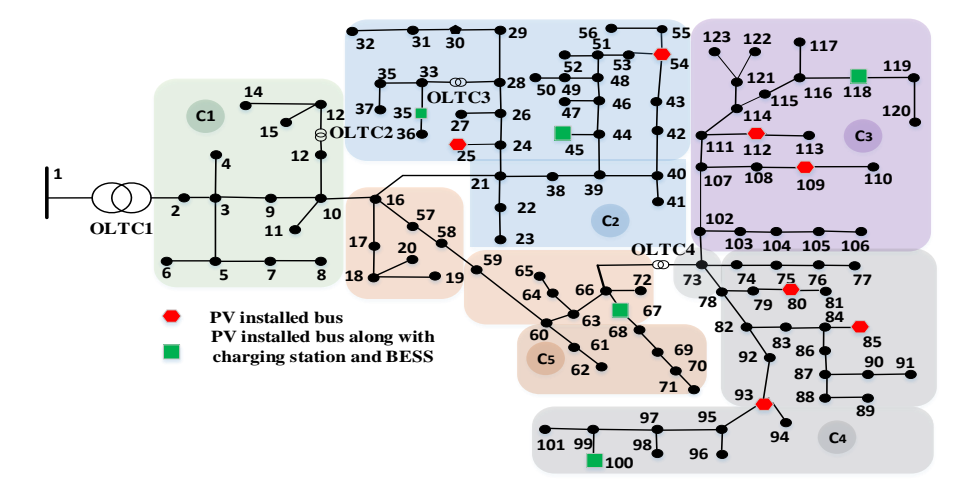


Fig. 4.8: Modified IEEE 123-bus system

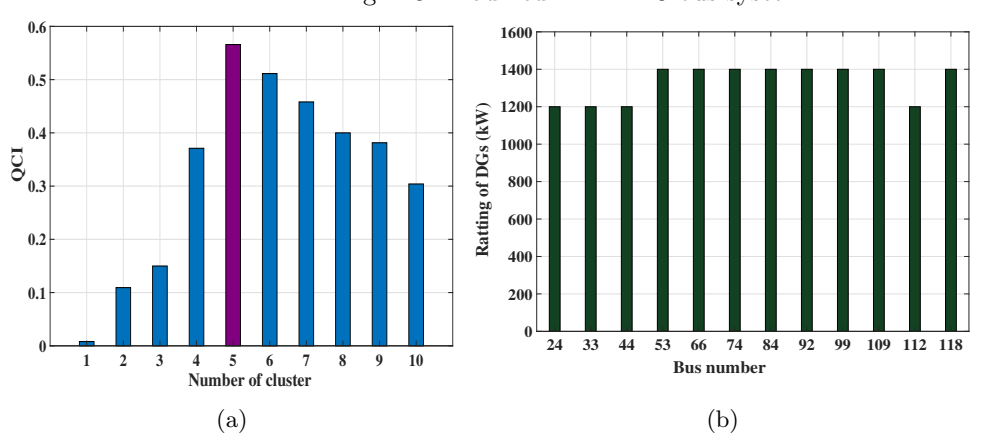


Fig. 4.9: In, IEEE 123-bus system, (a) Quality of Cluster Index (QCI) for different number of clusters, (b) rating of DGs with locations

the optimal setting of all the available PV-DGs in the network with the optimal setting of voltage controlling devices of 13 h, it is observed that in this case also the voltage level of all the buses comes under the limit, as shown in Fig. 4.6 by Centralized Voltage Control. In Table 4.2, a comparison between CBVC and CVC in terms of total active power curtailment and reactive power absorption from the PV-DGs, network losses and computation time is presented. In CBVC, overvoltage is mitigated by lesser cumulative active power curtailment and reactive power absorption from the available PV-DGs in the network than CVC. As a result, CBVC gives a better voltage profile with less amount network losses. In CBVC, OPF is solved for each cluster independently. Therefore, it minimizes huge computation time.

Table 4.2: Comparison table on 37-bus system for 13 h

	Total APC of	Total RPA of	Total	Computation
Methods	DGs in (kW)	DGs (kVAR)	Losses (kW)	time(sec)
CVC	301.9	1996.3	710.1	11.39
CBVC	76.2	728.7	558.1	3.1

4.4.2 Modified IEEE 123-bus system

In order to verify the proposed CBVC on a larger test system, the modified IEEE 123-bus [102] system is taken into account. The original IEEE 123-bus system is designed as a multi-phase

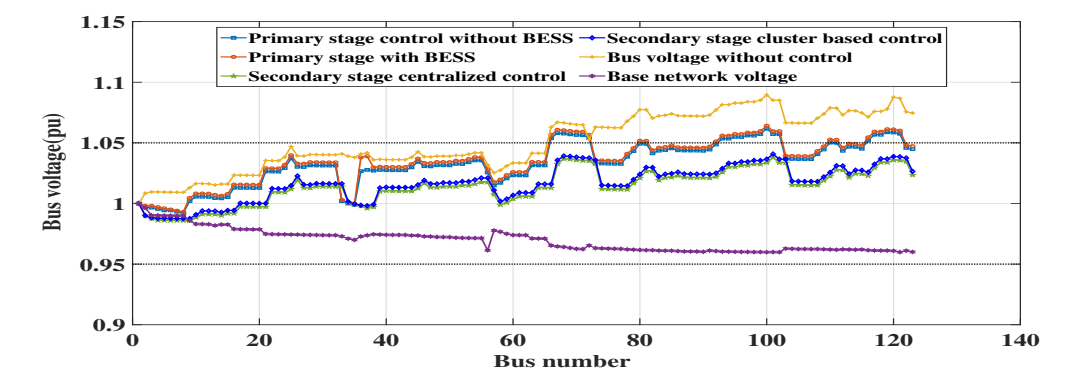


Fig. 4.10: In modified IEEE 123-bus, voltage profile of all buses with and without two-stage voltage control method for 13 h

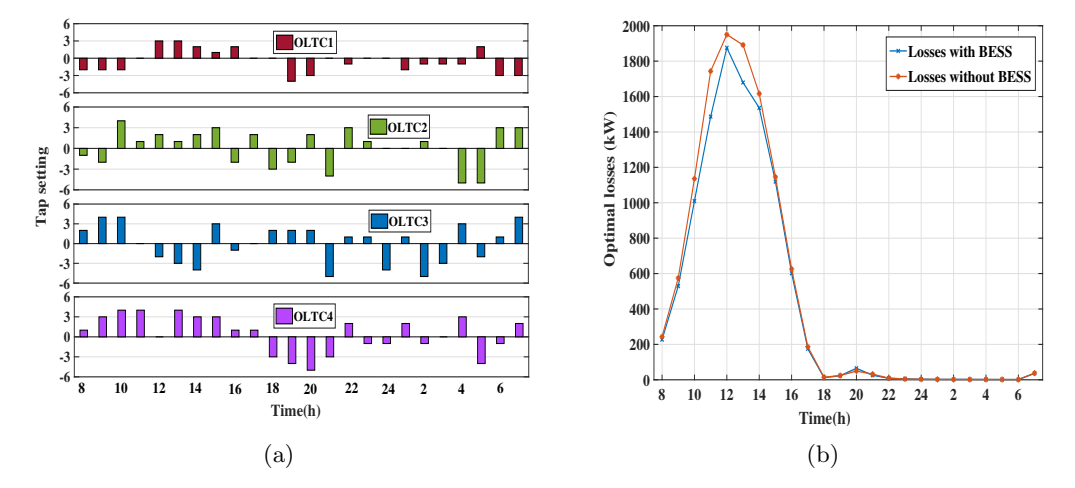


Fig. 4.11: In modified IEEE 123-bus system, (a) Optimal tap setting of OLTCs, (b) Optimal network losses, for each hourly time segment

unbalanced test system, but in this work, it is modified to be a three-phase balanced system. The numbering of all the buses is rearranged, and it is shown in Fig. 4.8. The rating of integrated PV-DGs is shown in Fig. 4.9-(b). The hourly output power from PV-DGs, load profile and number of EVs arriving at the charging station is calculated from their hourly probabilistic model.

Fig. 4.10 illustrates the voltage profile of all the buses with and without two-stage voltage control for 13 h. The voltage profile with PV-DGs without any control is represented by bus voltage without control. The overvoltage is observed from bus 66 to 123. Operating the distribution network with the optimal hourly setting of available voltage-controlling devices in the network, which is determined in the primary stage of voltage control, improves the voltage profile but is not able to mitigate the overvoltage issue from all the buses in the network. Therefore, the secondary stage of voltage control is implemented as explained in Fig. 4.1. The optimal tap setting of all the available PV-DGs in the network is shown in Fig. 4.11-(a). Further, Fig. 4.11-(b) illustrate the hourly losses of the network with and without BESS in the charging station. Cumulative losses for 24 h with and without BESS are 10428 kW and 11298 kW, respectively. BESS in the charging station reduces 8% losses than the charging station without BESS.

To implement the secondary stage of voltage control, the network is segregated into five clusters, as shown in Fig. 4.8, based on the highest value of QCI, and it is observed for the combination of five clusters, as shown in Fig. 4.9-(a). From Fig. 4.10, it is observed that overvoltage occurs in C_3 , C_4 and C_5 . Solving OPF for each cluster independently, the optimal setting of PV-DGs are determined. Further, Solving the load flow for the obtained optimal operating point of available PV-DGs in cluster C_3 , C_4 and C_5 with 13 h optimal setting of available voltage controlling devices in the network, it is observed that voltage profile of all the buses comes under the limit as shown in Fig. 4.10 by secondary stage cluster based voltage control. For comparison, in this case also centralized voltage control is implemented as a 37-bus system. The observed voltage profile is represented in Fig. 4.10 as a secondary stage centralized voltage control. From the comparison Table 4.3 and Fig. 4.10, it is observed that CBVC mitigate the overvoltage by less amount of cumulative active power curtailment and reactive power absorption from the available PV-DGs in the network than CVC. As a result, CBVC gives a better voltage profile with lesser network losses. Simultaneously, CBVC solves OPF for each cluster independently. Therefore, it reduces significant computation time.

	Total APC of	Total RPA of	Total	Computation
Methods	DGs in (kW)	DGs (kVAR)	Losses (kW)	time(sec)
CVC	419.1	2673.4	1702.4	160.6
CBVC	310.2	1023 5	15/0.2	11 02

Table 4.3: Comparison table on IEEE 123-bus system for 13 h

4.5 Conclusion

- Maintaining the voltage profile in the distribution network with increasing penetration of PV-DGs requires an economical and fast solution. Thus, in this work is proposed a two-stage voltage control technique.
- Primary Stage determines the optimal hourly setting of the voltage-controlling parameter for the entire 24-hour planning horizon, considering the stochastic characteristics of load demand, power generation from PV-DGs, and the number of EVs arriving at the charging station.
- Secondary Stage applies the CBVC control technique if the optimal hourly setting fails to maintain the voltage profile. The network is segregated using entropy-based spectral clustering, ensuring that the available PV-DGs within each cluster can maintain the voltage profile. The optimal operating power of PV-DGs is then determined by independently solving the OPF problem. The effectiveness of proposed method is evaluated on 37-bus and modified IEEE 123-bus systems, comparing it with the CVC method.
- Simulation results show that CBVC reduces the operation of PV-DGs at lagging power factor by 70% in the 37-bus system and by 30% in the modified IEEE-123 test system. Consequently, CBVC also achieves a reduction in losses by 21.1% in the 37-bus system and by 10% in the modified IEEE-123 test system compared to the CVC method.
- CBVC solves OPF on a cluster basis, therefore, it reduces 73.1% and 92.5% computation time for the 37-bus and modified IEEE-123 test system, respectively.

Chapter 5

Enhancement of Hosting Capacity of Active Distribution Network Utilizing Optimal Placement of Battery Energy Storage System

5.1 Introduction

The increasing demand for power necessitates improvements in the hosting capacity of distribution networks. The hosting capacity refers to the volume of distributed energy resources that the network can support without negatively affecting its operational limits.

Solar-Based Distributed Generations (PV-DGs) into the network meet power demands but also push the network beyond its normal operational limits. This creates significant challenges in maintaining a stable voltage profile due to the intermittent nature of renewable energy sources and load. Consequently, the hosting capacity of the network gets reduced.

Battery Energy Storage System (BESS) can effectively handle the fluctuations in renewable energy generation by storing surplus energy during periods of high power generation and discharging it when power generation is low. This capability helps stabilize the network and supports the integration of more renewable energy sources without compromising network reliability. The installation of BESS into the active distribution network increases the cost of operation for utility grids. Therefore, optimal utilization of BESS is a very crucial factor. In this work, the hosting capacity of the distribution network is improved by installing the BESS with the most dominant PV-DG. The Sobol voltage sensitivity index is used to determine the dominant PV-DG in the active distribution network. Further, the optimal setting of available voltage-controlling parameters is determined to maximize the network's hosting capacity by keeping network voltage under the limit by the Modified-Jaya algorithm (M-Jaya). State-based probabilistic modeling is used to incorporate the stochastic nature of load and generation into the OPF problem. IEEE-33 balanced and IEEE-13 unbalanced distribution network is utilized to validate the proposed strategies. From the simulation, it is observed that placing the BESS with the dominant PV-DGs not only enhances the hosting capacity of the network but also reduces the network's losses.

This chapter is organized as follows.

In Section 3.2, the modeling of the distribution network is presented. The problem formulation for OPF with their constraints is explained in Section 3.3. The M-Jaya algorithm is used to solve the OPF, and it is explained in Section 3.4. The numerical test of the multi-objective optimal power flow with the state-based probabilistic model is done on enhanced IEEE-33 and unbalanced IEEE-13 test system, and their result is explained in Section 3.5. The conclusion of the work is given in Section 3.6.

5.2 Formulation of load, generation and Battery Energy Storage System (BESS)

5.2.1 Modeling of load, generation and BESS

The state-based probabilistic modeling is used to determine hourly output from PV-DGs and load demand is explained in section 3.2.

5.2.2 Modeling of BESS

The BESS mitigates the stochastic behavior of the PV-DGs by optimal charging and discharging properties. It supports voltage stability and boosts the network's hosting capacity [113]. The mathematical modeling of charging-discharging is shown in (3.23)

$$SOC_{B,s}(t) = SOC_{B,s}(t-1) + \eta_{Bch} P_{Bch,s}(t) \Delta t\alpha - \frac{P_{Bdc,s}(t) \Delta t\beta}{\eta_{Bdc}}$$
(5.1)

where α and $\beta \in (0,1)$, and $\alpha\beta = 0$, because both charge and discharge of the battery are not possible at a time. η_{Bch} and η_{Bdc} are charging and discharging efficiency of BESS. $P_{Bch,s}$ and $P_{Bdc,s}$ represents the charging and discharging power of BESS for state s. $SOC_{B,s}(t)$ and $SOC_{B,s}(t-1)$ represents the present and previous SOC of BESS for state s.

5.2.3 Charging of BESS

BESS stores a fraction of the cumulative power generated by PV-DG where BESS is installed at time t, if the load in the network is less than the power generated by PV-DGs, as given (5.2)-(5.3)

$$P_{Bch,s}(t) = \eta_{Bch} K_{Bch,s} PV_{n_s}(t), K_{Bch,s}(t) > 0$$
(5.2)

$$P_{PV_j}(t) > P_{l_j}(t) \tag{5.3}$$

where $P_{PV_j}(t)$ represents available PV-DG power in time segment Δt . $K_{Bch}(t)$ represents fraction of power generated by available PV-DG, where BESS is installed in the network, which is stored by BESS in time segment Δt for state s.

5.2.4 Discharging of BESS

BESS release a fraction of the stored power at time t if the load power of the network is higher than the power generated by PV-DGs in the network, as given (5.4).

$$P_{Bdc,s}(t) = \frac{\eta_{BdcK_{Bdc,s}}SOC_{B,s}(t-1)C_{BESS}}{\Delta t}$$
(5.4)

where C_{BESS} represents total capacity of BESS. $K_{Bdc,s}(t)$ is fraction of BESS power, which is release by BESS in time segment Δt for state s.

5.3 Impact of PV-DGs in the active distribution network

Power perturbation at any bus and bus voltage are interconnected and closely linked to one another. The stochastic nature of PV-DGs impacts bus voltage but is not uniform across the network, which also impacts the hosting capacity of the network. BESS mitigate the stochastic nature of PV-DG

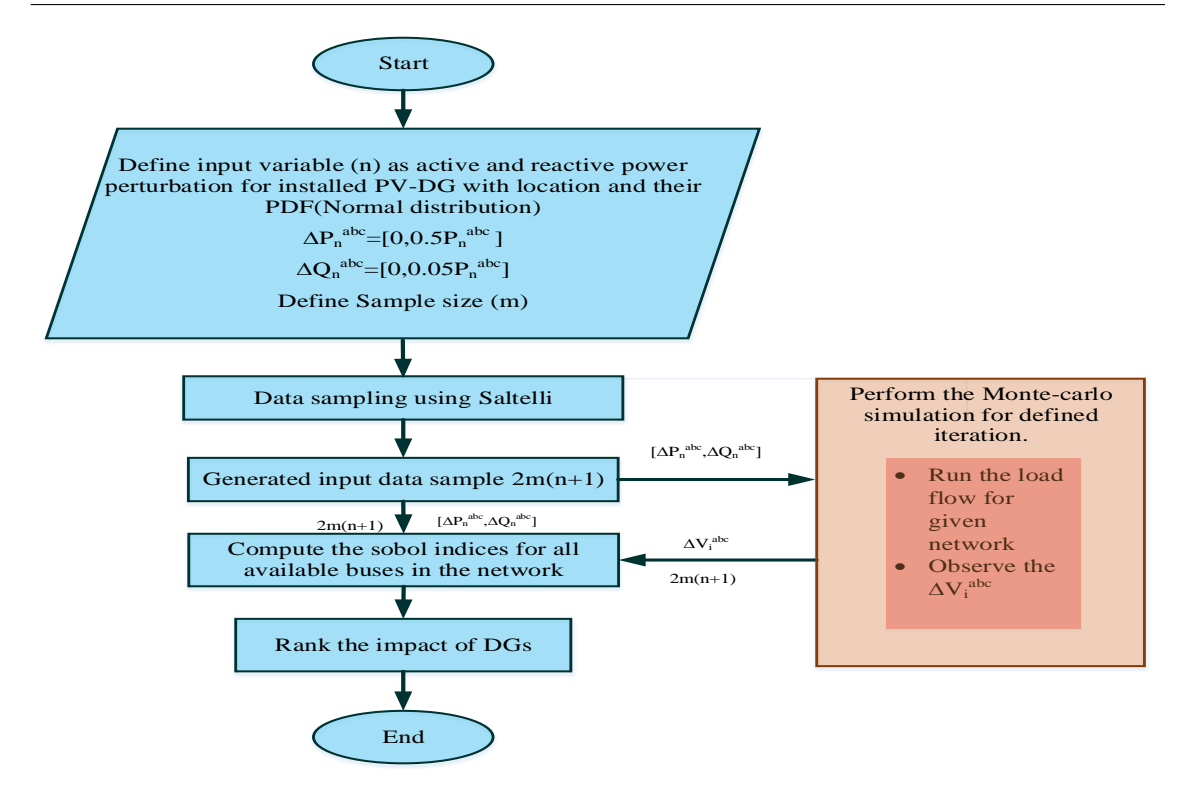


Fig. 5.1: Steps to perform sobol indexing method

by their charging and discharging properties. The integration of BESS alongside all the PV-DGs is not feasible because of economic constraints. Thus, the most dominant PV-DGs are appropriate for the placement of DGs. In this work, the Sobol sensitivity index is utilized to determine the dominance of PV-DGs on the bus voltage.

5.3.1 Sobol sensitivity

Sobol indices serve as the data-driven established method for conducting global sensitivity analyses. Derived from decomposing the model output variance, it enable the attribution of the impact of uncertain inputs to the variability observed in the model's output [114]. Let the $y = f(X_1, X_2...X_n)$ be square integrable with its definition pertaining to the n-dimensional unit hypercube and $X = (X_1, X_2...X_n)$ is set of input parameters. According to function decomposition scheme [114], $y = f(X_1, X_2, \dots X_n)$ can be decomposed in term of variance as shown (5.5)

$$V(Y) = \sum_{i=1} V_i + \sum_{i} \sum_{i \le j} V_{ij} + \sum_{i} \sum_{i \le j \le l} V_{ijl} \dots$$
(5.5)

$$V_{i} = V_{i}([E(y/X_{i})])$$

$$V_{ij} = V_{X_{i}X_{j}}(E[(y/X_{i}X_{j})]) - V_{X_{i}}(E[(y/X_{i})])$$

$$-V_{X_{i}}(E[(y/X_{j})])$$
(5.6)

where $E(y/X_i X_j...X_n)$ represents expectation of output in terms of input variable for decomposed subfunction, V(Y) variance of output variable and V_{ij} variance of decomposed subfunction of output variable. Divide (2.8) by V(Y),

$$1 = \sum_{i=1}^{N} \frac{V_i}{V(y)} + \sum_{i} \sum_{i \le j} \frac{V_{ij}}{V(y)} + \sum_{i} \sum_{i \le j \le l} \frac{V_{ijl}}{V(y)} \dots$$

$$1 = \sum_{i=1}^{N} S_i + \sum_{i} \sum_{i \le j} S_{ij} + \sum_{i} \sum_{i \le j \le l} S_{ijl} \dots$$

$$(5.7)$$

In (5.7), S_i , S_{ijl} presents first-order and total-order Sobol sensitivity indices. The first-order index gives the impact of individual input parameter changes, whereas the total-order sensitivity index accounts for both the individual input parameter changes and other input parameter changes. In this work, Sobol sensitivity index has been implemented into multiple steps using a Multiobjective Evolutionary Algorithm (MOEA) framework [115], as shown in Fig. 5.1. In the first step, the total number of PV-DGs in the network, their location and power perturbation range ($\Delta P_n = [0, 0.5\Delta P_n]$, $\Delta Q_n = [0, 0.5\Delta Q_n]$) with their PDF (Normal distribution) is defined. Further, sampling is performed using Saltelli for $(n \times m)$ data set. n and m are the number of input variables and sample size. It gives 2m(n+1) data set, which is a combination of different scenarios of power generated by PV-DGs. Utilizing 2m(n+1) data sample, Monte-Carlo simulation is performed and 2m(n+1) data sample of output variable (ΔV) is observed. Finally, 2m(n+1) data set of input and output are set to the MOEA framework format to obtain the first and total

order Sobol sensitivity index. The highest value of the total order Sobol sensitivity index S_{ijl} is

considered as the highest dominant PV-DGs in the network.

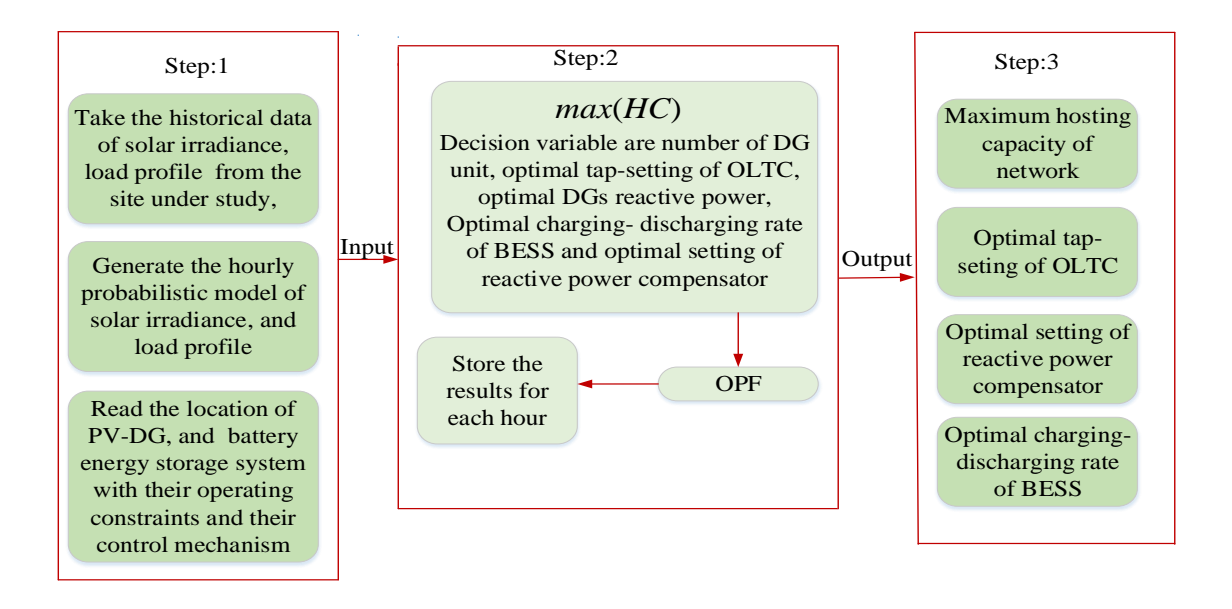


Fig. 5.2: Steps to determine the hosting capacity of the network

5.4 Problem Formulation

Optimal Power Flow (OPF) refers to the computational process of determining the most efficient operating conditions with certain objective functions. Therefore, in this work, OPF has been used to determine the optimal rating of voltage-controlling devices while considering the objective function of maximizing the hosting capacity of the network. The M-Jaya algoritam has been used to solve the OPF problem.

5.4.0.1 Objective Function

The objective function of the OPF problems under consideration is the maximization of the Hosting Capacity of the network, which is shown in (5.8).

$$HC = \max(\sum_{t=1}^{n_t} \sum_{s=1}^{n_s} \sum_{i=1}^{n_{pv}} P_{pv,s,j}^{t,abc})$$
(5.8)

5.4.0.2 Equality Constraints

$$\begin{split} P_{ij,s}^{abc}(t) &= -k(s,1) P_{PV_j}^{abc}(t) + k(s,2) P_{L_j}^{abc}(t) \pm P_{B_{ch/dc,j,s}}^{abc}(t) \\ Q_{ij,s}^{abc}(t) &= Q_{PV_j}^{abc}(t) + Q_{L_j}^{abc}(t) + Q_{C_{i,s}}^{abc}(t) \\ (V_{i,s}^{abc}(t))^2 &= (V_{j,s}^{abc}(t))^2 + Z_{ij}^2 I_{ij}^{abc}(t) \\ &+ 2(R_{ij}^{abc} P_{ij,s}^{abc}(t) + X_{ij}^{abc} Q_{ij,s}^{abc}(t)) \\ I_{ij}^{abc}(t) &= \frac{(P_{ij,s}^{abc}(t))^2 + (Q_{ij,s}^{abc}(t))^2}{(V_{i,s}^{abc}(t))^2} \\ Q_{PV,s}(t) &= \sqrt{(S_{PV,s}^{inv_{abc}}(t))^2 - P_{PV,s}^{abc}(t))^2} \end{split}$$
 (5.9)

where κ is a matrix with two columns, which comprises all the combination of the states of solar irradiance and load demand. $P_{PV_{i,s}}^{abc}(t)$ are active power generated by solar type generation for a time segment Δt of state s. $P_{L_{i,s}}^{abc}(t)$ is load demand for state s of time segment Δt . $P_{B_{ch/dc,j,s}}^{abc}(t)$ is the charging-discharging power of BESS installed at a charging station for state s of time segment Δt . $Q_{PV_{i,s}}^{abc}(t)$, and $S_{PV_{i,s}}^{inv_{abc}}(t)$ are reactive power and complex power generated by solar type converter-based generation. $Q_{C_{i,s}}^{abc}(t)$ is reactive power supplied by reactive power compensator for a time segment Δt of state s. $V_{i,s}^{abc}(t)$ and $V_{k,s}^{abc}(t)$ are bus voltage of i^{th} and k^{th} bus respectively for time segment Δt of state s. $\delta_{ki,s}^{abc}$ represents voltage angle difference between i^{th} and k^{th} bus on time segment Δt for state s. G_{ki} and G_{ki} are real and imaginary part of admittance between $K_{i,s}^{th}$ and $K_{i,s}^{th}$ bus on time segment $K_{i,s}^{th}$ for state $K_{i,s}^{th}$ and $K_{i,s}^{th}$ a

5.4.0.3 Inequality Constraints

$$\begin{aligned} P_{PV_{max_{i}}}^{abc} &\leq P_{PV,s}^{abc}(t) \leq P_{PV_{min_{i}}}^{abc} \\ Q_{PV_{max_{i}}}^{abc} &\leq Q_{PV,s}^{abc}(t) \leq Q_{PV_{min_{i}}}^{abc} \\ V_{min}^{abc} &\leq V_{i,s}^{abc}(t) \leq V_{max}^{abc} \\ T_{tap}^{min} &\leq T_{tap,i} \leq T_{tap}^{max} \\ Q_{C_{min}}^{abc} &\leq Q_{C,s}(t)^{abc} \leq Q_{C_{max}}^{abc} \\ P_{B,n,s}^{abc}(t) &\leq 0.2C_{batt,n} \\ P_{Bch_{min}}^{abc} &\leq P_{Bch,s}^{abc}(t) \leq P_{Bch_{max}}^{abc} \\ P_{Bdc_{min}}^{abc} &\leq P_{Bdc,s}^{abc}(t) \leq P_{Bdc_{max}}^{abc} \\ SOC_{Bmin}^{abc} &\leq SOC_{B,s}^{abc}(t) \leq SOC_{Bmax}^{abc} \end{aligned}$$

$$(5.10)$$

where $P_{PV_{max_i}}^{abc}$, and $P_{PV_{min_i}}^{abc}$ are maximum and minimum active power generation from solar based generation, respectively. T_{tap}^{max} and T_{tap}^{min} are minimum and maximum transformer tap

settings limit. $Q_{C_{min}}^{abc}$ and $Q_{C_{max}}^{abc}$ are shunt compensator limit. $Q_{PV_{max}}^{abc}$, and $Q_{PV_{min}}^{abc}$ are reactive power limits of solar type generation. $P_{Bch_{max}}^{abc}$, $P_{Bch_{min}}^{abc}$, $P_{Bdc_{min}}^{abc}$ and $P_{Bdc_{max}}^{abc}$ are charging and discharging power limit of battery installed at the charging station. SOC_{Bmax}^{abc} and SOC_{Bmin}^{abc} are the limit of the state of charge of the battery installed at the charging station.

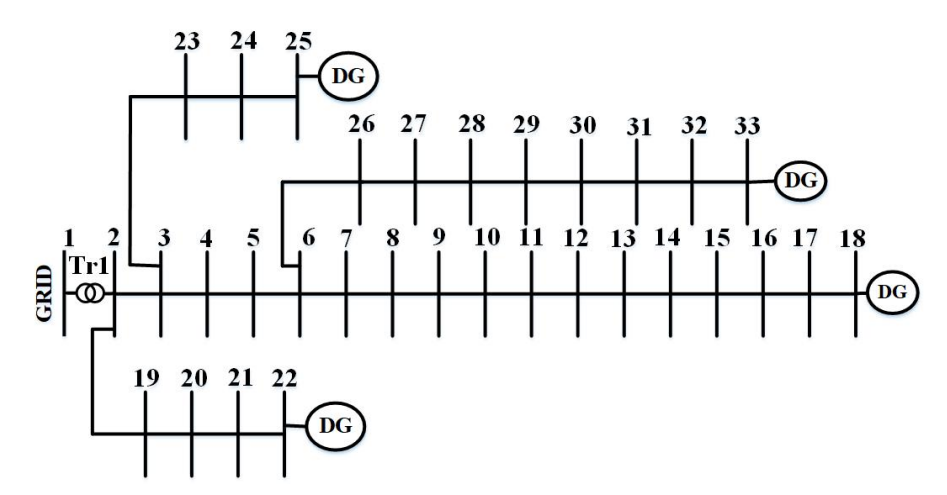


Fig. 5.3: IEEE-33 system

Table 5.1: State with their probability of solar power generation, and load for 13 h

State	PV-DG output	Prob	Load	Prob
1	$0 \le p_s < 0.5$	0.0137	$0 \le l < 0.3$	0.23
2	$0.5 \le p_s < 0.7$	0.35	$0.3 \le l < 0.6$	0.6972
3	$0.7 \le p_s < 1$	0.6262	$0.6 \le l < 1$	0.0728

Table 5.2: Combination of States of Input Variable for 13 h in case of Solar type DGs

State	Combination of PV-DG output,	Probability
	and load demand	
1	$0 \le p_s < 0.5, 0 \le p_l < 0.3$	0.003151
2	$0 \le p_s < 0.5, 0.3 \le p_l < 0.6$	0.0099551
3	$0 \le p_s < 0.5, 0.6 \le p_l < 1$	0.0009738
4	$0 \le p_s < 0.7, 0 \le p_l < 0.3$	0.0805
5	$0 \le p_s < 0.7, 0.3 \le p_l < 0.6$	0.2440
6	$0 \le p_s < 0.7, 0.6 \le p_l < 1$	0.02548
7	$0.7 \le p_s < 1, 0 \le p_l < 0.3$	0.144
8	$0.7 \le p_s < 1, 0.3 \le p_l < 0.6$	0.4365
9	$0.7 \le p_s < 1, 0.6 \le p_l < 1$	0.045591

5.5 Results and Discussion

In this work, to enhance the hosting capacity of the network, the battery energy storage system is installed with the most dominant PV-DGs in the network. Further, by utilizing the optimal setting of the voltage-controlling parameters of the network and the optimal charging and discharging of BESS, the hosting capacity of the network is enhanced. To determine the optimal setting of voltage controlling parameter and optimal charging-discharging of BESS, OPF for the objective of maximizing the hosting capacity of the network is solved using the Modified–Jaya (M-Jaya) algorithm. The implementation of the proposed method is done on IEEE-33 [101]

and unbalanced IEEE-13 [116] distribution system using MATLAB R2019b with the system configuration Intel-Core i7-8700, CPU @ 3.20 GHz. Base power and voltage for IEEE-33: 100 MVA, 12.66 kV and IEEE-13 distribution: 100 kW, 4.16 kV. In both the test systems, the optimal setting of the OLTC, reactive power compensation by DGs, and the charging-discharging profile of the BESS is determined for improving the hosting capacity of the network in three cases: (a) without any control (a) BESS is installed with most dominant PV-DGs (c) BESS is installed with random PV-DGs.

Bus number	Value of Sobol index	Ranking
with PV-DG		
18	0.3672	1
22	0.2575	4
25	0.2970	3
22	0.3057	2

Table 5.3: Ranking of PV-DGs by Sobol index for IEEE 33 test system

5.5.1 IEEE-33 test system

In this test system, at four locations far end feeders (i.e., in bus no 18, 22, 25, 33) rating of 800 kW solar-based distributed generation is considered as shown in Fig. 2.5. Between buses 1 and 2, the on-load tap changer is considered, and their maximum and minimum tap settings are set to -5 and 5. The BESS of the rating 500 kW is considered for enhancing the hosting capacity, and their initial state of charge is taken as 0.45 pu.

5.5.1.1 Discussion

To enhance the hosting capacity of the BESS with dominant PV-DGs in the network is considered. To determine the dominant PV-DGs, the sobol index has been used, as explained in section 5.3. In this case, the highest value of the sobol index is observed in bus 18, as shown in the Table 5.3. Thus, bus 18 is considered as the optimal position for installing BESS in the network. Further, by utilizing the optimal setting of an available voltage-controlling parameter, such as an on-load tap changer with charging and discharging rate of installed BESS, the hosting capacity of the network is determined. In Fig. 5.2, steps to determine the optimal setting of voltage controlling parameter and charging-discharging of BESS to enhance the hosting capacity of the network are explained. In the first step,, for considering the stochastic characteristics of load and generation, state-based probabilistic modeling is utilized as explained in section 3.2. In this work, the hourly PDF of PV-DGs and load is divided into three states, and their combination is given as input to the OPF problem to determine the optimal setting of voltage-controlling devices and charging-discharging of installed BESS. For 13th h, all three states of output power from PV-DGs and load with their probability is given in Table 5.1 and their nine combinations with their probability is given in Table 5.2. Further, this combination of load and generation is given as input to the OPF problem. In the second step, the OPF with the objective of maximizing the hosting capacity of the network, as shown given (5.8)-(5.10) is solved using the M-Jaya algorithm for each combination of PV-DG output power and load demand to determine the optimal setting of voltage-controlling parameters and charging and discharging of installed BESS in the network. Furthermore, the summation of the obtained optimal setting multiplied for each combination of load and generation by their probability is considered as the hourly optimal setting. The optimal hourly setting of the voltage-controlling parameter and charging-discharging of BESS is stored in the third step. In this test system, the

hosting capacity of the network is determined in all three cases given in Table 5.4. The cumulative hosting capacity for 13th h without any control is 2200.74 kW, BESS installed at bus 22 is 2468 kW and BESS installed at bus 18 is 2662 kW The impact of PV-DGs on bus voltage depends on common impedance sharing. Thus, PV-DG installed on bus 18 is considered to be the dominant bus. The BESS enhance the hosting capacity by mitigating the stochastic characteristics of PV-DGs by observing and releasing the active power from PV-DGs. The PV-DG installed on bus 18 has a cumulative higher impact on the voltage level on all buses than on all three buses. Thus, BESS installed on bus 18 improves the hosting capacity more than BESS installed on bus 22. For all three cases, the voltage profile for 13^{th} h is shown in Fig. 5.6. In all three cases, voltage profiles are under limits. The optimal charging-discharging power with their SOC is shown in Fig. 5.4. For BESS installed at bus 22 is shown in Fig. 5.4-(a), and for the bus location 18 is shown in Fig. 5.4-(b). The charging rate is higher in the case of BESS installed at bus 22 because PV-DG installed at that bus has the highest cumulative impact on the bus voltage of the network. The optimal setting of OLTC for BESS installed at bus 22 is shown in Fig. 5.5. A similar, optimal setting of OLTC is observed for BESS installed at bus 18. The losses of the network for all three cases are shown in Fig. 5.7. In all three cases, it is observed that BESS installed with dominant PV-DG not only improved the hosting capacity of the network but also reduced the network losses.

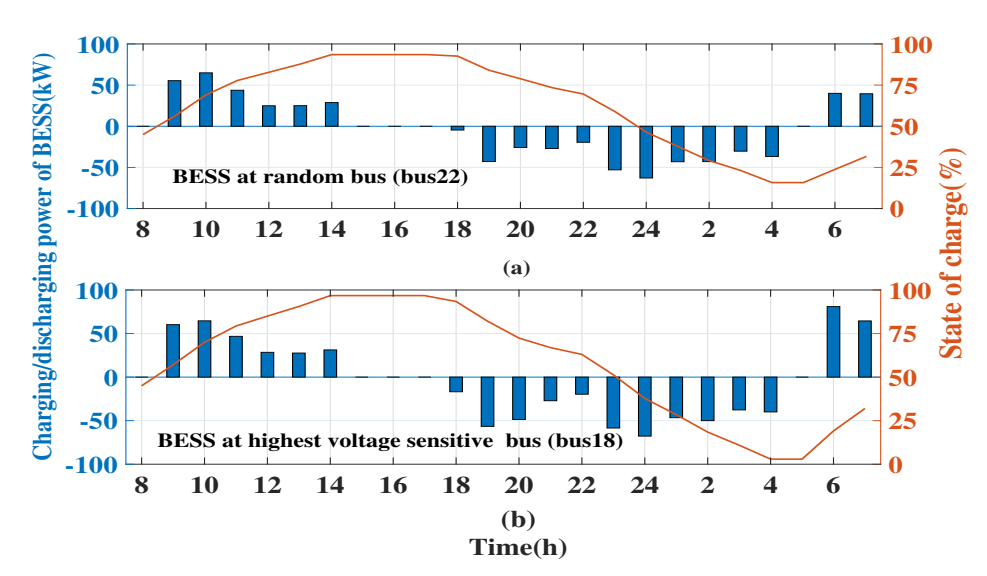


Fig. 5.4: Charging/discharging profile of BESS for 24 h time period

Table 5.4: Comparative analysis of different approaches for enhancing hosting capacity

Test case	Hosting Capacity of buses (kW)				Losses(kW)
1est case	Bus18	Bus22	Bus25	Bus33	LOSSES(KW)
Without any control	590.34	510.1	535.21	565.4	261.23
BESS at bus-18	759.7	597.14	610.23	695.3	240.71
BESS at bus-22	637.1	625.23	595.3	611.23	225.13

5.5.2 IEEE-13 unbalanced test system

In this test system, at each phase of three locations, such as buses 634, 652, and 671 rating of 500 kW solar-based distributed generation is considered as shown in Fig. 5.9. Between bus 650, and bus 632, the on-load tap changer is considered, and their maximum and minimum tap settings are considered as -5 and 5. The BESS of the rating 250 kW for each phase at the installed location is

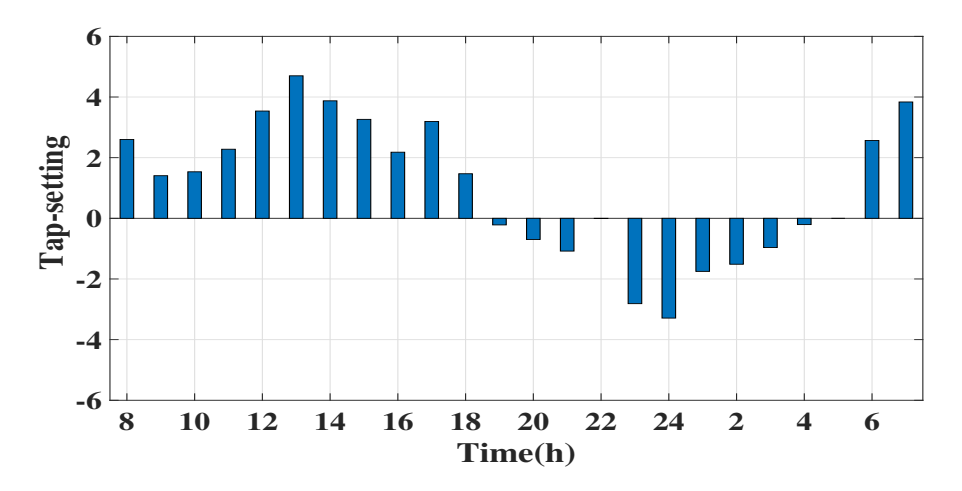


Fig. 5.5: In IEEE-33 test system tap-setting of OLTC for $24~\mathrm{h}$ time period

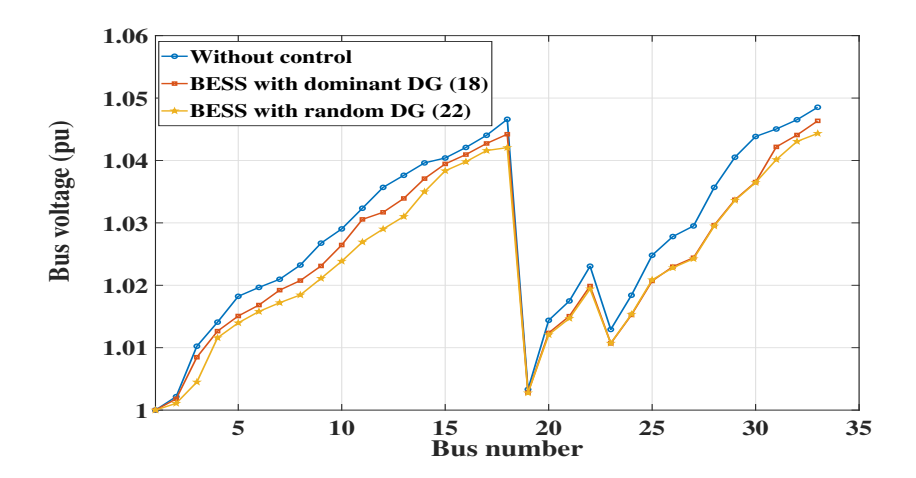


Fig. 5.6: Voltage profile of the network

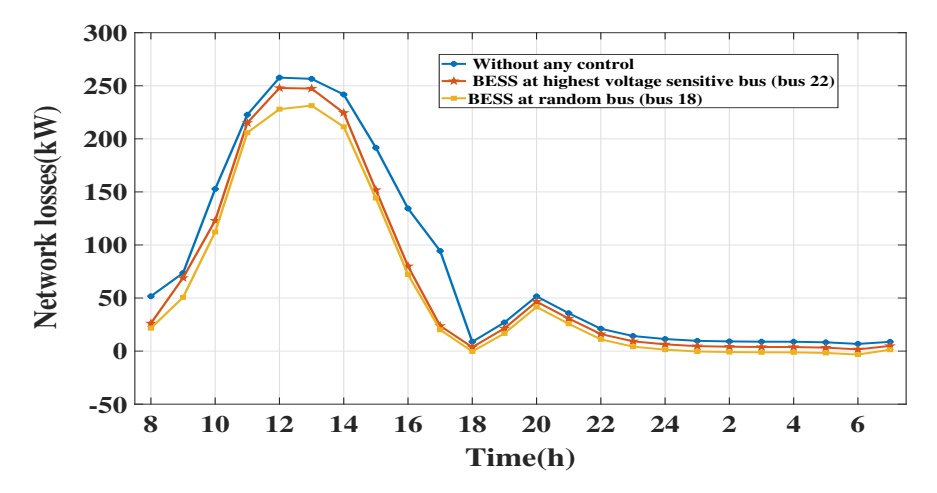


Fig. 5.7: For IEEE-33 test system losses for 24 h time period



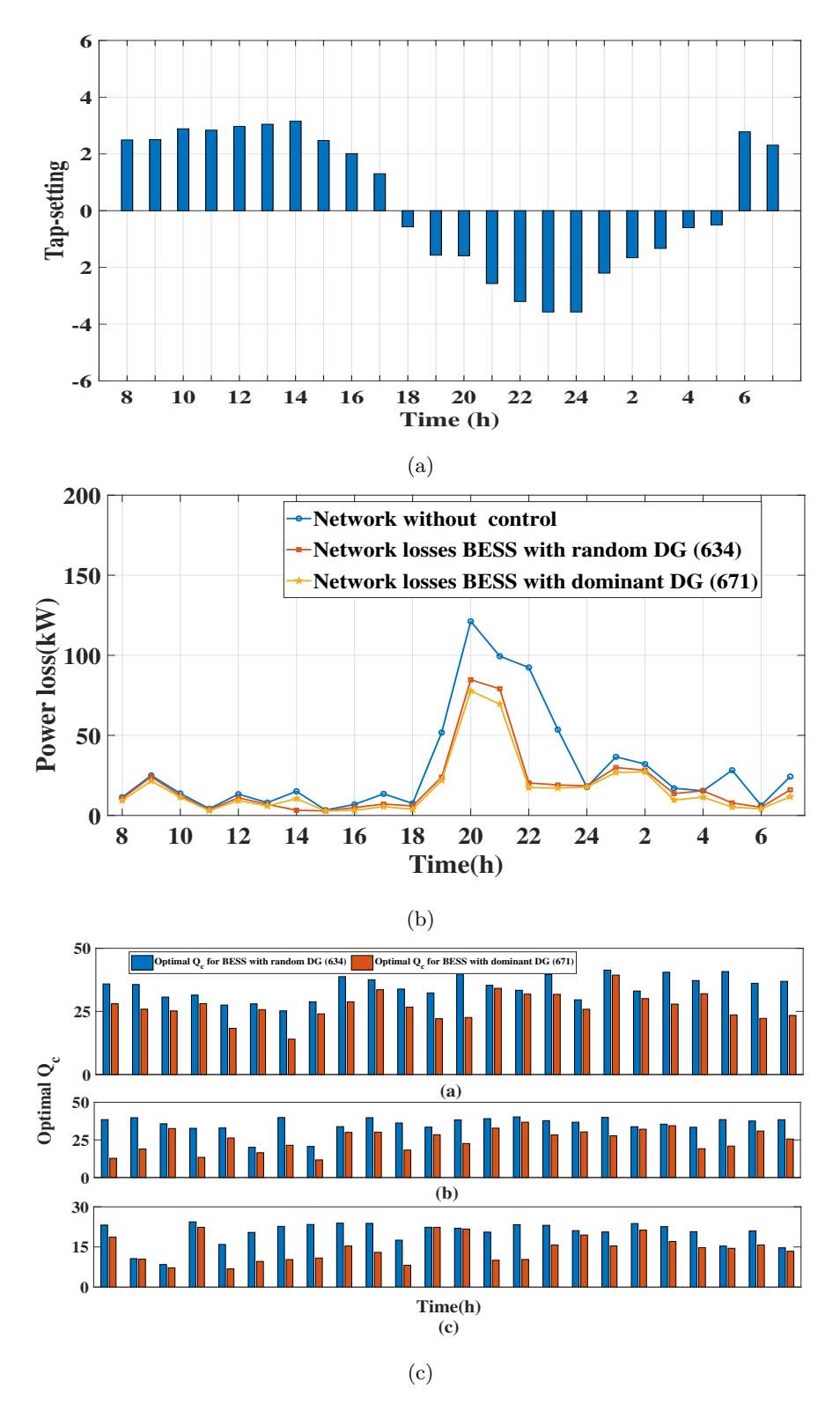


Fig. 5.8: In case of IEEE-13 (a) optimal tap setting of OLTC (b) network losses (c) optimal setting of reactive power compensator installed with bus 52 for 24 h time period

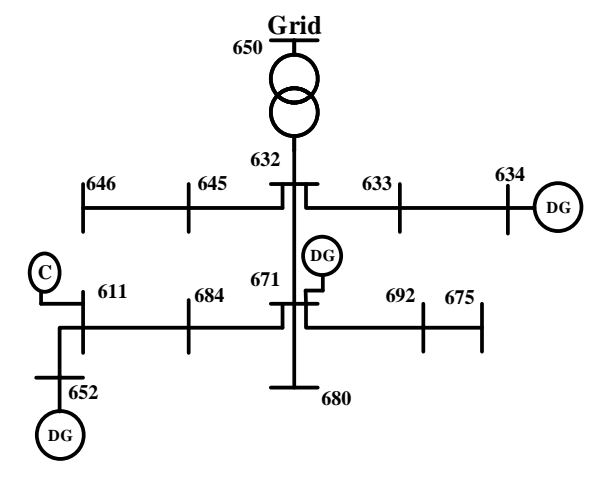


Fig. 5.9: IEEE-13 unbalanced test system

Table 5.5: Ranking of PV-DGs by Sobol index for IEEE-13 test system

Bus number	Value of Sobol index	Ranking
with PV-DG		
634	0.2143	3
652	0.2213	2
671	0.2771	1

considered for enhancing the hosting capacity, and their initial state of charge is taken as 0.45 pu. At bus 652, the reactive power compensator of the rating 50 kVAR, 50 kVAR and 30 kVAR are considered for phase -a, b and c, respectively.

5.5.2.1Discussion

In this case, enhancing the hosting capacity of the BESS with dominant PV-DGs in the network is considered. To determine the dominant PV-DGs, the sobol index has been used, as explained in section 5.3. In this case, the highest value of the sobol index is observed in bus 671, which is shown in the Table 5.5. Thus, bus 671 is considered as the optimal position for installing BESS in the network. Further, by utilizing the optimal setting of an available voltage-controlling parameter, such as an on-load tap changer with charging and discharging rate of installed BESS, the hosting capacity of the network is determined. Similarly to the IEEE-33 test system, in this case also, the hosting capacity of the network is determined in three cases, which are tabulated in Table 5.6. The cumulative hosting capacity for 13th h without any control is 3293 kW, BESS installed at bus 634 is 4178.1.1 kW and BESS installed at bus 671 is 4535.2 kW The impact of PV-DGs on bus voltage depends on common impedance sharing. Thus, PV-DG installed on bus 671 is considered to be the dominant bus. The BESS enhance the hosting capacity by mitigating the stochastic characteristics of PV-DGs by observing and releasing the active power from PV-DGs. The PV-DG installed on bus 671 has a cumulative higher impact on the voltage level on all buses than on all three buses. Thus, BESS installed on bus 671 improves the hosting capacity compared with BESS installed on bus 634. For all three cases, the voltage profile of all phases for $13^{t}h$ h is shown in Fig. 5.10. In all three cases, voltage profiles are under limits. The optimal charging-discharging power with their SOC is shown in Fig. 5.4. In Fig. 5.11-(e), (g), and (j), the charging-discharging power with their SOC is given for BESS installed at bus 634. In Fig. 5.11-(f), (h), and (k), the charging-discharging power with their SOC is given for BESS installed at bus 671. From Fig. 5.11, all the phases' charging and discharging rates are different due to their load profile. The

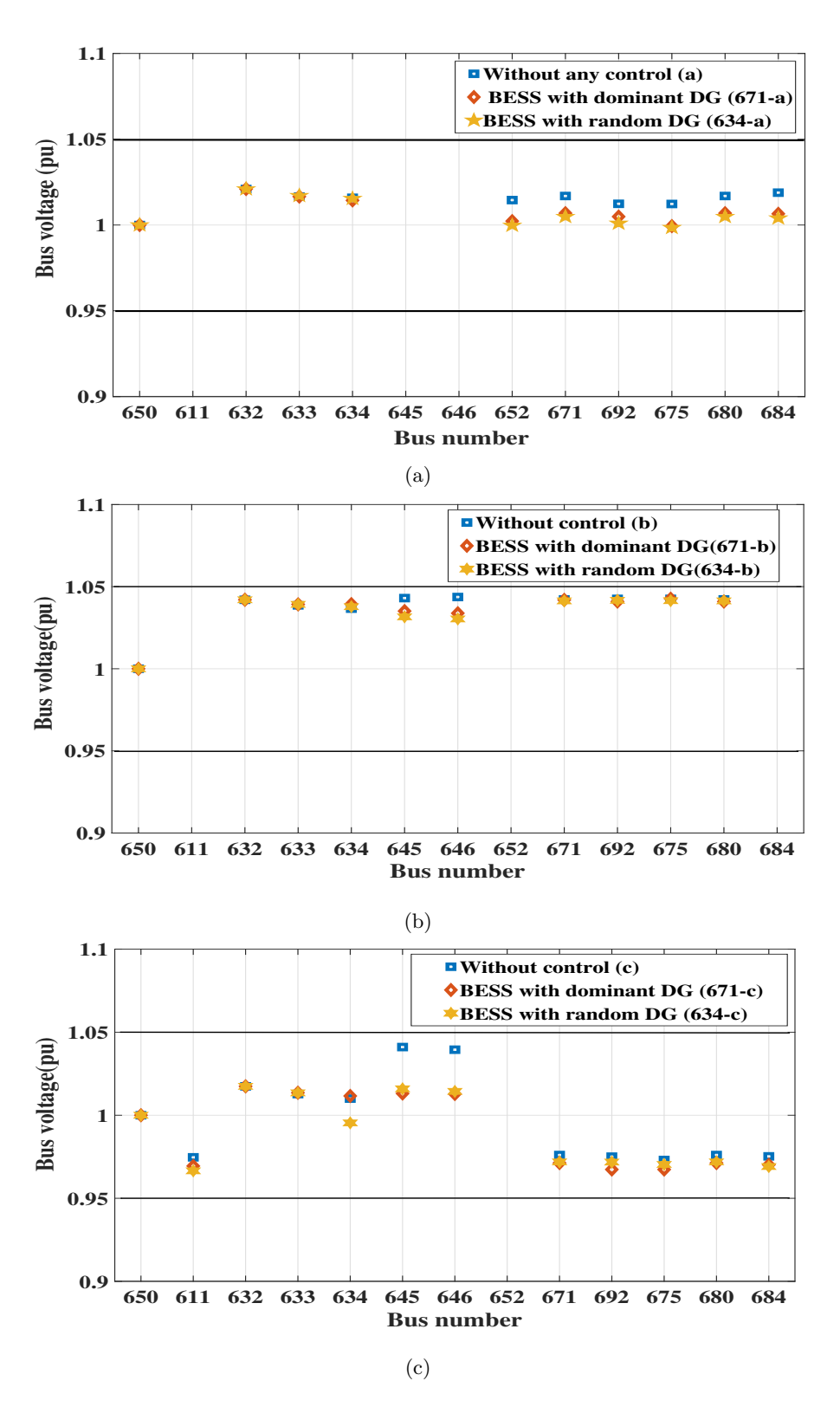


Fig. 5.10: In case of IEEE 13 test system (a) phase-(a) (b) phase-(b) (c) phase-(c) bus voltage for $13~\mathrm{h}$

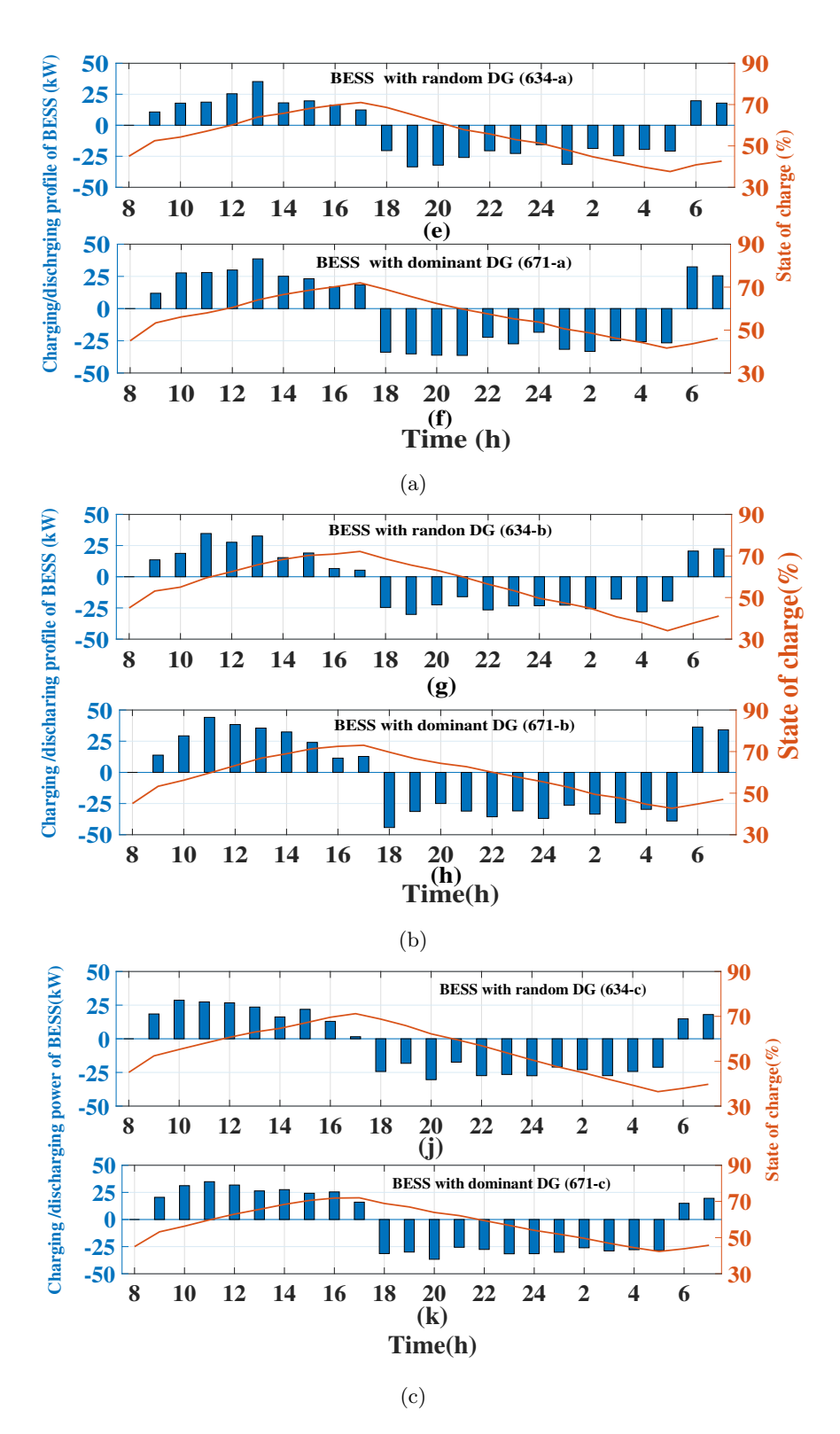


Fig. 5.11: Charging/ discharging profile of BESS installed at (a) phase-(a) of bus 634 and bus 671 (b) phase-(b) of bus 634 and bus 671 (c) phase-(c) of bus 634 and bus 671 for 24 h time period

charging-discharging rate of BESS is higher in the case of BESS installed with dominant PV-DG (Bus -671). The optimal tap setting of OLTC is shown in Fig. 5.8-(a), and the optimal setting reactive power compensator for all phases is shown in Fig. 5.8-(b). The losses of the network for all three cases are shown in Fig. 5.8-(c). It is observed that the installation of BESS with dominant PV-DG not only improves the hosting capacity of the network but also the network's losses.

Table 5.6: Comparative analysis of different approaches for enhancing hosting capacity

Test case	Hosting (Losses (kW)		
1650 Case	Bus 634	Bus 652	Bus671	Losses (KW)
Without any control	1325	1029	939	8.03
BESS at bus-634	1503	1325.1	1350	5.90
BESS at bus-671	1480	1425	1630	2.87

5.6 Conclusion

- The rising integration of PV-DGs into distribution networks drives these networks toward their operational limits. In this context, maintaining a stable voltage profile becomes challenging due to the intermittent nature of PV-DGs. As a result, the hosting capacity of the network gets reduced.
- The rising integration of PV-DGs into distribution networks drives these networks toward their operational limits. In this context, maintaining a stable voltage profile becomes challenging due to the intermittent nature of PV-DGs. As a result, the hosting capacity of the network gets reduced.
- BESS mitigates the intermittent nature of PV-DGs by observing surplus active power and releasing in time of lack of active power. However their location of placement is changing task.
- In this study, Battery Energy Storage Systems (BESS) are integrated alongside dominant PV-DGs to enhance the network's hosting capacity. The dominant PV-DGs within the network are identified using Sobol indices. Hosting capacity is then improved through optimal coordination among the charge-discharge profile of BESS with available voltage-controlling parameters in the network. To achieve this, an optimal power flow problem is solved using the M-Jaya algorithm, which determines the optimal BESS charge-discharge profile and voltage-controlling parameter settings.
- The implementation of proposed method has been done on IEEE-33 balanced and IEEE-13 unbalanced test system. From the simulation it is observed that Installation of BESS at with most dominant PV-DG bus not only enhance the hosting capacity but also reduces the losses of the network.

Chapter 6

Conclusion and Future Research

6.1 General

As the economy grows, the increasing power demand makes traditional generation methods impractical due to high costs, transmission losses, dwindling fossil fuel reserves, and environmental concerns. Renewable-Based Distributed Generation (RBDG) is seen as the best solution. Simultaneously, the rise of Electric Vehicles (EVs) in the market also increases the need for charging infrastructure. The integrated RBDGs, the number of EVs arriving at the charging station and loading in the distribution network, inherit uncertain characteristics, which causes randomly fast voltage fluctuations, sometimes leading to voltage limit violations at multiple buses in the network. Traditional method fail to maintain the voltage profile of the network due their sluggish response time. Therefore, maintaining the voltage profile in the network fast and dynamic voltage control is required. Initially, RBDGs could not control voltage profiles due to a lack of active or reactive power control. In this scenario, reinforcing networks with reactive power-compensating devices or using On-Load Tap Changers (OLTC) is employed, though these solutions are often considered costly. Progress in inverter technology now allows RBDGs to control voltage by adjusting both active and reactive power.

Active Power Curtailment (APC) and Reactive Power Compensation (RPC) are strategies used to address voltage issues. However, randomly selecting RBDGs for voltage maintenance of the network is not an economically optimal solution. Evaluating RBDG's impact on bus voltage is crucial for making fast and dynamic voltage control techniques. The voltage control technique utilizes voltage-controlling capabilities of RBDGs are classified into centralized and decentralized voltage control. The exclusive use of RBDGs, either centralized or decentralized, for maintaining the voltage profile of the network is not considered as economical solution. A hierarchical approach to voltage control is preferred, and it is implemented in multiple stages. It offers a window to coordinate decentralized DGs with all available voltage control parameters to maintain the network's voltage profile.

The stochastic nature of RBDG not only hampers the voltage profile of the network but also reduces its Hosting Capacity (HC). However, increasing power demand requires the enhancement of the network's HC. BESS mitigates the stochastic characteristics by their optimal charging and discharging power. To enhance the hosting capacity of the network, large-size BESS gives the best benefit-to-cost ratio, but their placement and evaluation of the coordination among available voltage controlling parameters is challenging. In this thesis, the research problems have been formulated by considering the above-discussed issues as follows:

- Develop a probabilistic approach to investigate the impact of distributed generation on voltage deviation in the distribution system.
- Develop a state-based probabilistic method to determine the optimal setting of voltage-controlling parameters in active distribution networks.

- Develop a dual-stage voltage control technique for solar generation-enriched active distribution network.
- Develop a techniques for enhancing the hosting capacity by placing battery energy storage systems with renewable-based generation.

6.2 Summary of contribution

The work is carried out into the thesis is about making fast and dynamic voltage control techniques to mitigate voltage issues arising in the network due to high penetration RBDGs. The high penetration of RBDG also reduces the HC of the network due their stochastic characteristics. Therefore, the placement of a BESS alongside dominant RBDG to enhance the network's HC is also investigated.

In Chapter 2, to evaluate the impact of distributed generation on the bus voltage of the network, a Principal Component Analysis (PCA) based novel Probabilistic Voltage Sensitivity Index (PVSI) is proposed. The elements of the covariance matrix are analytically derived to reduce the computation time. PVSI is implemented in MATLAB R2019b with the system configuration of Intel-Core i7-8700, CPU @ 3.20GHz. It is verified in three scenarios by considering active, reactive and complex power perturbation at DG-integrated bus on 69-bus and 141-bus distribution systems by comparing the results with the traditional Monte-Carlo Simulation (MCS) and Joint Differential Entropy (JDE) methods. From all three cases, the observation are as follows:

- PVSI gives the same rankings as traditional MCS and JDE methods while cutting computation time by 85.75% for the 69-bus system and 85.8% for the 141-bus system compared to JDE.
- Active power perturbation impacts real part of change in voltage (ΔV_O^r) more than imaginary part of change in voltage (ΔV_O^i) , whereas reactive power perturbation has a greater effect on ΔV_O^i than on ΔV_O^r . However, the impact of complex power depends on the variance of both active and reactive power perturbations.
- Due to computational advantage and accuracy, proposed *PVSI* can be implemented in formulation of decentralized voltage control.

In Chapter 3, the optimal settings for voltage-controlling parameters over a 24-hour time period are determined by considering various types of Converter Based Generations (CBGs), including solar generation, wind generation, and mixed generation, on an enhanced IEEE 33-bus system and an unbalanced IEEE 123-bus test system. The state-based probabilistic method is used to estimate the stochastic characteristics of output power from CBGs, power demand by load and the number of EVs arriving at the charging station and incorporated into the Optimal Power Flow (OPF) problem as input. Further, the M-Jaya algorithm is used to solve the OPF problem. From the simulation results, the observation are as follows:

- The optimal setting of voltage-controlling parameters not only enhances the voltage profile of the network but also reduces losses in the distribution system.
- The installation of BESS at the charging station not only improves the charging rate of EVs but also decreases losses of the network by improving the power factor of distributed generation.

- The M-Jaya algorithm achieves superior convergence for proposed objective functions without violating any operational constraints.
- The proposed work offers insights to forecast the optimal setting of available voltage controlling parameters for a given time segment, considering the intermittent nature of load and generation of the network.

In Chapter 4, a dual-stage voltage control technique is proposed to establish coordination among available voltage-controlling devices in the network and clustered renewable-based generation. In the primary stage, the optimal hourly setting of the voltage-controlling parameter for the entire 24-hour planning horizon is determined, considering the stochastic characteristics of load and generation. If the optimal hourly voltage control setting proves inadequate for maintaining the voltage profile, the Cluster Based Voltage Control (CBVC) technique is initiated in the secondary stage. At this stage, the network is segregated using entropy-based spectral clustering. This method divides the distribution network so that the available Photovoltaic Distributed Generations (PV-DGs) within each cluster can maintain the voltage profile. Subsequently, the optimal operating power of the PV-DGs is determined by independently solving the OPF problem. The effectiveness of the method is evaluated on 37-bus and modified IEEE 123-bus system by comparing the Centralized Voltage Control (CVC) method. From the simulation result, the observation are as follows:

- CBVC achieves a 70% reduction in PV-DGs operating at a lagging power factor in the 37-bus system and a 30% reduction in the modified IEEE-123 test system. As a result, CBVC reduces losses by 21.1% in the 37-bus system and by 10% in the modified IEEE 123-bus system compared to CVC.
- CBVC solves OPF on a cluster basis, thereby reducing computation time by 73.1% for the 37-bus system and 92.5% for the modified IEEE-123 test system.

In Chapter 5, a BESS is installed alongside the most dominant PV-DG to enhance the network's hosting capacity. The Sobol sensitivity index is used to determine the impact of PV-DGs on the bus voltage of the network. Furthermore, by optimizing the voltage-controlling parameters of the network and the charging and discharging of the BESS, the network's hosting capacity is significantly enhanced. The efficiency of the proposed method is evaluated using the IEEE 33 and IEEE 13 test systems. From the simulation result, the observation are as follows:

- The BESS improves not only the hosting capacity of the network but also the network's losses.
- The BESS with dominant renewable-based generation gives better hosting capacity and loss profile than the random buses.

6.3 Scope of future work

- Develop the analytic method to determine the influence the distribution generation on bus voltage in unbalanced distribution network.
- To find the correct proportionality of battery energy storage system to reduce the stochastic behavior of generations as these resource inherit the different stochastic characteristics.

• Determination of optimal solution for active and reactive power exchange between transmission and distribution system for voltage support, considering the stochastic nature of DG.

References

- [1] Leonard L Grigsby. Power system stability and control. CRC press, 2007.
- [2] Jan Machowski, Zbigniew Lubosny, Janusz W Bialek, and James R Bumby. *Power system dynamics: stability and control.* John Wiley & Sons, 2020.
- [3] Qinlin Shi, Peng Yang, Bo Tang, Jintao Lin, Guangzheng Yu, and SM Muyeen. Active distribution network type identification method of high proportion new energy power system based on source-load matching. *International Journal of Electrical Power & Energy Systems*, 153:109411, 2023.
- [4] Peng Wang, Zhenyuan Zhang, Qi Huang, Xiaotian Tang, and Wei-Jen Lee. Robustness-improved method for measurement-based equivalent modeling of active distribution network. *IEEE Transactions on Industry Applications*, 57(3):2146–2155, 2021. doi: 10.1109/TIA.2021.3057358.
- [5] M Ram, A Gulagi, D Bogdanov, and C Breyer. A 100% renewable power system across india by 2050. White paper on power system optimisation. Lappeentanta, Helsinki, 2021.
- [6] Ekta Meena Bibra, Elizabeth Connelly, Marine Gorner, Christopher Lowans, Leonardo Paoli, Jacopo Tattini, and Jacob Teter. Global ev outlook 2021: Accelerating ambitions despite the pandemic. 2021.
- [7] Heide Budde-Meiwes, Julia Drillkens, Benedikt Lunz, Jens Muennix, Susanne Rothgang, Julia Kowal, and Dirk Uwe Sauer. A review of current automotive battery technology and future prospects. Proceedings of the Institution of Mechanical Engineers, Part D: Journal of Automobile Engineering, 227(5):761-776, 2013.
- [8] Pedro MS Carvalho, Pedro F Correia, and Luís AFM Ferreira. Distributed reactive power generation control for voltage rise mitigation in distribution networks. *IEEE transactions on Power Systems*, 23(2):766–772, 2008.
- [9] Moataz Ammar and Adel M Sharaf. Optimized use of pv distributed generation in voltage regulation: A probabilistic formulation. *IEEE Transactions on Industrial Informatics*, 15 (1):247–256, 2018.
- [10] Mamdouh Abdel-Akher. Voltage stability analysis of unbalanced distribution systems using backward/forward sweep load-flow analysis method with secant predictor. *IET generation*, transmission & distribution, 7(3):309–317, 2013.
- [11] Salvador Ruiz-Romero, Antonio Colmenar-Santos, Francisco Mur-Pérez, and África López-Rey. Integration of distributed generation in the power distribution network: The need for smart grid control systems, communication and equipment for a smart city—use cases. Renewable and sustainable energy reviews, 38:223–234, 2014.
- [12] Abdelfatah Ali, Karar Mahmoud, Matti Lehtonen, et al. Enhancing hosting capacity of intermittent wind turbine systems using bi-level optimisation considering oltc and electric vehicle charging stations. *IET Renew. Power Gener.*, 14(17):3558–3567, 2020.

88 References

[13] A Rajabi, S Elphick, J David, A Pors, and D Robinson. Innovative approaches for assessing and enhancing the hosting capacity of pv-rich distribution networks: An australian perspective. *Renewable and Sustainable Energy Reviews*, 161:112365, 2022.

- [14] Xiaohu Liu, Andreas Aichhorn, Liming Liu, and Hui Li. Coordinated control of distributed energy storage system with tap changer transformers for voltage rise mitigation under high photovoltaic penetration. *IEEE Transactions on Smart Grid*, 3(2):897–906, 2012.
- [15] Yashodhan P Agalgaonkar, Bikash C Pal, and Rabih A Jabr. Distribution voltage control considering the impact of pv generation on tap changers and autonomous regulators. *IEEE Transactions on Power Systems*, 29(1):182–192, 2013.
- [16] Byungki Kim, Yang-Hyun Nam, Heesang Ko, Chul-Ho Park, Ho-Chan Kim, Kyung-Sang Ryu, and Dae-Jin Kim. Novel voltage control method of the primary feeder by the energy storage system and step voltage regulator. *Energies*, 12(17):3357, 2019.
- [17] Shibani Ghosh, Saifur Rahman, and Manisa Pipattanasomporn. Distribution voltage regulation through active power curtailment with pv inverters and solar generation forecasts. *IEEE Transactions on Sustainable Energy*, 8(1):13–22, 2016.
- [18] Liang Wu and Lin Guan. Integer quadratic programming model for dynamic var compensation considering short-term voltage stability. *IET Generation*, Transmission & Distribution, 13(5):652–661, 2019.
- [19] Fabian Tamp and Phil Ciufo. A sensitivity analysis toolkit for the simplification of my distribution network voltage management. *IEEE Transactions on Smart Grid*, 5(2):559–568, 2014.
- [20] Morris Brenna, Ettore De Berardinis, Luca Delli Carpini, Federica Foiadelli, Pietro Paulon, Paola Petroni, Gianluca Sapienza, Giorgio Scrosati, and Dario Zaninelli. Automatic distributed voltage control algorithm in smart grids applications. *IEEE Transactions on Smart Grid*, 4(2):877–885, 2012.
- [21] Morris Brenna, Ettore De Berardinis, Federica Foiadelli, Gianluca Sapienza, and Dario Zaninelli. Voltage control in smart grids: An approach based on sensitivity theory. *Journal of Electromagnetic Analysis and Applications*, 2010, 2010.
- [22] B Bakhshideh Zad, J Lobry, and François Vallee. A centralized approach for voltage control of mv distribution systems using dgs power control and a direct sensitivity analysis method. In 2016 IEEE International Energy Conference (ENERGYCON), pages 1–6. IEEE, 2016.
- [23] B Bakhshideh Zad, H Hasanvand, J Lobry, and F Vallée. Optimal reactive power control of dgs for voltage regulation of mv distribution systems using sensitivity analysis method and pso algorithm. *International Journal of Electrical Power & Energy Systems*, 68:52–60, 2015.
- [24] Vasiliki Klonari, Bashir Bakhshideh Zad, Jacques Lobry, and François Vallée. Application of voltage sensitivity analysis in a probabilistic context for characterizing low voltage network operation. In 2016 International Conference on Probabilistic Methods Applied to Power Systems (PMAPS), pages 1–7. IEEE, 2016.
- [25] G. Valverde, T. Zufferey, S. Karagiannopoulos, and G. Hug. Estimation of voltage sensitivities to power injections using smart meter data. In 2018 IEEE International Energy Conference (ENERGYCON), pages 1–6, 2018. doi: 10.1109/ENERGYCON.2018.8398841.

[26] Kumarsinh Jhala, Balasubramaniam Natarajan, and Anil Pahwa. The dominant influencer of voltage fluctuation (divf) for power distribution system. *IEEE Transactions on Power* Systems, 34(6):4847–4856, 2019.

- [27] Il-Song Kim. Sliding mode controller for the single-phase grid-connected photovoltaic system. Applied Energy, 83(10):1101–1115, 2006.
- [28] Philip J Douglass, Rodrigo Garcia-Valle, Jacob Østergaard, and Octavian Constantin Tudora. Voltage-sensitive load controllers for voltage regulation and increased load factor in distribution systems. *IEEE Transactions on Smart Grid*, 5(5):2394–2401, 2014.
- [29] Reinaldo Tonkoski, Luiz AC Lopes, and Tarek HM El-Fouly. Coordinated active power curtailment of grid connected pv inverters for overvoltage prevention. *IEEE Transactions on sustainable energy*, 2(2):139–147, 2010.
- [30] Mesut E Baran and Ismail M El-Markabi. A multiagent-based dispatching scheme for distributed generators for voltage support on distribution feeders. *IEEE Transactions on power systems*, 22(1):52–59, 2007.
- [31] Saeed Alyami, Yang Wang, Caisheng Wang, Junhui Zhao, and Bo Zhao. Adaptive real power capping method for fair overvoltage regulation of distribution networks with high penetration of pv systems. *IEEE Transactions on Smart Grid*, 5(6):2729–2738, 2014.
- [32] Andrea Ballanti, Fabrizio Pilo, Alejandro Navarro-Espinosa, and Luis F Ochoa. Assessing the benefits of pv var absorption on the hosting capacity of lv feeders. In *IEEE PES ISGT Europe 2013*, pages 1–5. IEEE, 2013.
- [33] Erhan Demirok, Pablo Casado Gonzalez, Kenn HB Frederiksen, Dezso Sera, Pedro Rodriguez, and Remus Teodorescu. Local reactive power control methods for overvoltage prevention of distributed solar inverters in low-voltage grids. *IEEE Journal of Photovoltaics*, 1(2):174–182, 2011.
- [34] Takao Tsuji, Takuhei Hashiguchi, Tadahiro Goda, Kenji Horiuchi, and Yasuhiro Kojima. Autonomous decentralized voltage profile control using multi-agent technology considering time-delay. In 2009 Transmission & Distribution Conference & Exposition: Asia and Pacific, pages 1–8. IEEE, 2009.
- [35] Li Yu, Dariusz Czarkowski, and Francisco de Leon. Optimal distributed voltage regulation for secondary networks with dgs. *IEEE Transactions on Smart Grid*, 3(2):959–967, 2012. doi: 10.1109/TSG.2012.2190308.
- [36] Bo Zhao, Zhicheng Xu, Chen Xu, Caisheng Wang, and Feng Lin. Network partition-based zonal voltage control for distribution networks with distributed pv systems. *IEEE Transactions on Smart Grid*, 9(5):4087–4098, 2018. doi: 10.1109/TSG.2017.2648779.
- [37] M Biserica, G Foggia, E Chanzy, and JC Passelergue. Network partition for coordinated control in active distribution networks. In 2013 IEEE Grenoble Conference, pages 1–5. IEEE, 2013.
- [38] Chen Chen, Jianhui Wang, Feng Qiu, and Dongbo Zhao. Resilient distribution system by microgrids formation after natural disasters. *IEEE Transactions on smart grid*, 7(2):958–966, 2015.

[39] Emiliano Dall'Anese, Sairaj V Dhople, and Georgios B Giannakis. Optimal dispatch of photovoltaic inverters in residential distribution systems. *IEEE Transactions on Sustainable Energy*, 5(2):487–497, 2014.

- [40] Ali Maknouninejad, Zhihua Qu, Johan Enslin, and Nasser Kutkut. Clustering and cooperative control of distributed generators for maintaining microgrid unified voltage profile and complex power control. In *PES T&D 2012*, pages 1–8. IEEE, 2012.
- [41] Xianzhuo Sun and Jing Qiu. Hierarchical voltage control strategy in distribution networks considering customized charging navigation of electric vehicles. *IEEE Transactions on Smart Grid*, 12(6):4752–4764, 2021.
- [42] Chen Luo, Hongbin Wu, Yiyao Zhou, Yida Qiao, and Mengyi Cai. Network partition-based hierarchical decentralised voltage control for distribution networks with distributed pv systems. *International Journal of Electrical Power & Energy Systems*, 130:106929, 2021.
- [43] Kashem M Muttaqi, An DT Le, Michael Negnevitsky, and Gerard Ledwich. A coordinated voltage control approach for coordination of oltc, voltage regulator, and dg to regulate voltage in a distribution feeder. *IEEE Transactions on Industry Applications*, 51(2):1239–1248, 2015.
- [44] Johanna Barr and Ritwik Majumder. Integration of distributed generation in the volt/var management system for active distribution networks. *IEEE Transactions on Smart Grid*, 6 (2):576–586, 2014.
- [45] Chun-Lien Su. Stochastic evaluation of voltages in distribution networks with distributed generation using detailed distribution operation models. *IEEE Transactions on Power Systems*, 25(2):786–795, 2009.
- [46] Chunlei Zhang and Xiaodong Chu. Voltage regulation strategy for active distribution network coordinating dgs, ess units and oltc. In 2017 IEEE Power & Energy Society General Meeting, pages 1–5. IEEE, 2017.
- [47] Mohamed Ebeed, Salah Kamel, and Francisco Jurado. Optimal power flow using recent optimization techniques. In *Classical and recent aspects of power system optimization*, pages 157–183. Elsevier, 2018.
- [48] R Rao. Jaya: A simple and new optimization algorithm for solving constrained and unconstrained optimization problems. *International Journal of Industrial Engineering Computations*, 7(1):19–34, 2016.
- [49] Robin Preece and Jovica V Milanović. Assessing the applicability of uncertainty importance measures for power system studies. *IEEE Transactions on Power Systems*, 31(3):2076–2084, 2015.
- [50] Motahareh Pourbehzadi, Taher Niknam, Jamshid Aghaei, Abdollah Kavousi-Fard, and Ali Dehghan. Stochastic energy management in renewable-based microgrids under correlated environment. In 2020 IEEE International Conference on Environment and Electrical Engineering and 2020 IEEE Industrial and Commercial Power Systems Europe (EEEIC/I&CPS Europe), pages 1–6. IEEE, 2020.
- [51] Mingrui Zhang and Jie Chen. Islanding and scheduling of power distribution systems with distributed generation. *IEEE Transactions on Power Systems*, 30(6):3120–3129, 2014.

[52] Mohammadreza Emarati, Mostafa Barani, Hossein Farahmand, Jamshid Aghaei, and Pedro Crespo del Granado. A two-level over-voltage control strategy in distribution networks with high pv penetration. *International Journal of Electrical Power & Energy Systems*, 130: 106763, 2021.

- [53] Seyed Ali Arefifar, Yasser Abdel-Rady I Mohamed, and Tarek El-Fouly. Optimized multiple microgrid-based clustering of active distribution systems considering communication and control requirements. *IEEE transactions on industrial electronics*, 62(2):711–723, 2014.
- [54] Amr A Munshi and A-RI Mohamed Yasser. Photovoltaic power pattern clustering based on conventional and swarm clustering methods. *Solar Energy*, 124:39–56, 2016.
- [55] Majid Nayeripour, Hossein Fallahzadeh-Abarghouei, Eberhard Waffenschmidt, and Saeed Hasanvand. Coordinated online voltage management of distributed generation using network partitioning. *Electric Power Systems Research*, 141:202–209, 2016.
- [56] Mostafa Barani, Jamshid Aghaei, Mohammad Amin Akbari, Taher Niknam, Hossein Farahmand, and Magnus Korpås. Optimal partitioning of smart distribution systems into supply-sufficient microgrids. *IEEE Transactions on Smart Grid*, 10(3):2523–2533, 2019. doi: 10.1109/TSG.2018.2803215.
- [57] Peishuai Li, Cuo Zhang, Zaijun Wu, Yan Xu, Minqiang Hu, and Zhaoyang Dong. Distributed adaptive robust voltage/var control with network partition in active distribution networks. *IEEE Transactions on Smart Grid*, 11(3):2245–2256, 2020. doi: 10.1109/TSG.2019.2950120.
- [58] Mehmet Yilmaz and Ramadan ElShatshat. Zone-oriented 2-stage distributed voltage control algorithm for active distribution networks. *Electric Power Systems Research*, 217:109127, 2023.
- [59] Math HJ Bollen and Fainan Hassan. Integration of distributed generation in the power system. John wiley & sons, 2011.
- [60] Interstate Renewable Energy Council. Solar america board for codes and standards.
- [61] Sherif M Ismael, Shady HE Abdel Aleem, Almoataz Y Abdelaziz, and Ahmed F Zobaa. State-of-the-art of hosting capacity in modern power systems with distributed generation. Renewable energy, 130:1002–1020, 2019.
- [62] Matthew Rylander, Jeff Smith, and Wes Sunderman. Streamlined method for determining distribution system hosting capacity. In 2015 IEEE Rural Electric Power Conference, pages 3–9. IEEE, 2015.
- [63] J Smith and M Rylander. Stochastic analysis to determine feeder hosting capacity for distributed solar pv. Electric Power Research Inst., Palo Alto, CA, Tech. Rep, 1026640: 0885–8950, 2012.
- [64] Anamika Dubey, Surya Santoso, and Arindam Maitra. Understanding photovoltaic hosting capacity of distribution circuits. In 2015 IEEE power & energy society general meeting, pages 1–5. IEEE, 2015.
- [65] Tobias Walla. Hosting capacity for photovoltaics in swedish distribution grids, 2012.
- [66] Ammar Arshad, Martin Lindner, and Matti Lehtonen. An analysis of photo-voltaic hosting capacity in finnish low voltage distribution networks. *Energies*, 10(11):1702, 2017.

[67] Fei Ding and Barry Mather. On distributed pv hosting capacity estimation, sensitivity study, and improvement. *IEEE Transactions on Sustainable Energy*, 8(3):1010–1020, 2016.

- [68] Shemsedin Nursebo Salih, Peiyuan Chen, Ola Carlson, and L Bertling Tjernberg. Optimizing wind power hosting capacity of distribution systems using cost benefit analysis. *IEEE Transactions on Power Delivery*, 29(3):1436–1445, 2014.
- [69] Abdelfatah Ali, Karar Mahmoud, David Raisz, and Matti Lehtonen. Probabilistic approach for hosting high pv penetration in distribution systems via optimal oversized inverter with watt-var functions. *IEEE Systems Journal*, 15(1):684–693, 2020.
- [70] Peter KC Wong, Akhtar Kalam, and Robert Barr. Modelling and analysis of practical options to improve the hosting capacity of low voltage networks for embedded photo-voltaic generation. IET Renewable Power Generation, 11(5):625–632, 2017.
- [71] Mir Hadi Athari, Zhifang Wang, and Seyed Hamid Eylas. Time-series analysis of photovoltaic distributed generation impacts on a local distributed network. In 2017 IEEE Manchester PowerTech, pages 1–6. IEEE, 2017.
- [72] Mohammadreza Vatani, Davood Solati Alkaran, Mohammad Javad Sanjari, and Gevork B Gharehpetian. Multiple distributed generation units allocation in distribution network for loss reduction based on a combination of analytical and genetic algorithm methods. *IET Generation, Transmission & Distribution*, 10(1):66–72, 2016.
- [73] Duong Quoc Hung and Nadarajah Mithulananthan. Multiple distributed generator placement in primary distribution networks for loss reduction. *IEEE Transactions on industrial electronics*, 60(4):1700–1708, 2011.
- [74] Xu Xu, Jiayong Li, Zhao Xu, Jian Zhao, and Chun Sing Lai. Enhancing photovoltaic hosting capacity—a stochastic approach to optimal planning of static var compensator devices in distribution networks. Applied energy, 238:952–962, 2019.
- [75] Jian Zhao, Jianhui Wang, Zhao Xu, Cheng Wang, Can Wan, and Chen Chen. Distribution network electric vehicle hosting capacity maximization: A chargeable region optimization model. *IEEE Transactions on Power Systems*, 32(5):4119–4130, 2017.
- [76] O Nadjemi, T Nacer, A Hamidat, and H Salhi. Optimal hybrid pv/wind energy system sizing: Application of cuckoo search algorithm for algerian dairy farms. Renewable and Sustainable Energy Reviews, 70:1352–1365, 2017.
- [77] HS Ramadan, AF Bendary, and S Nagy. Particle swarm optimization algorithm for capacitor allocation problem in distribution systems with wind turbine generators. *International Journal of Electrical Power & Energy Systems*, 84:143–152, 2017.
- [78] Abdelfatah Ali, Karar Mahmoud, David Raisz, and Matti Lehtonen. Optimal allocation of inverter-based wtgs complying with their dstatcom functionality and pev requirements. *IEEE Transactions on Vehicular Technology*, 69(5):4763–4772, 2020.
- [79] Duong Quoc Hung, Nadarajah Mithulananthan, and RC Bansal. Analytical strategies for renewable distributed generation integration considering energy loss minimization. Applied Energy, 105:75–85, 2013.

[80] John Seuss, Matthew J Reno, Robert J Broderick, and Santiago Grijalva. Improving distribution network pv hosting capacity via smart inverter reactive power support. In 2015 IEEE Power & Energy Society General Meeting, pages 1–5. IEEE, 2015.

- [81] Zahra Moravej and Amir Akhlaghi. A novel approach based on cuckoo search for dg allocation in distribution network. *International Journal of Electrical Power & Energy Systems*, 44(1): 672–679, 2013.
- [82] Munyaradzi Justice Chihota, Bernard Bekker, and Trevor Gaunt. A stochastic analytic-probabilistic approach to distributed generation hosting capacity evaluation of active feeders. *International Journal of Electrical Power & Energy Systems*, 136:107598, 2022.
- [83] Marko Kolenc, Igor Papič, and Boštjan Blažič. Assessment of maximum distributed generation penetration levels in low voltage networks using a probabilistic approach. International journal of electrical power & energy systems, 64:505–515, 2015.
- [84] Alejandro Navarro-Espinosa and Luis F Ochoa. Probabilistic impact assessment of low carbon technologies in lv distribution systems. *IEEE Transactions on Power Systems*, 31(3): 2192–2203, 2015.
- [85] Partha Kayal and CK Chanda. Optimal mix of solar and wind distributed generations considering performance improvement of electrical distribution network. *Renewable energy*, 75:173–186, 2015.
- [86] Nicholas Etherden and Math Bollen. The use of battery storage for increasing the hosting capacity of the grid for renewable electricity production. In *International Conference on Innovation for Secure and Efficient Transmission Grids:* 07/04/2014-10/04/2014, 2014.
- [87] Calum Edmunds, Stuart Galloway, James Dixon, Waqquas Bukhsh, and Ian Elders. Hosting capacity assessment of heat pumps and optimised electric vehicle charging on low voltage networks. Applied Energy, 298:117093, 2021.
- [88] Nadeeshani Jayasekara, Mohammad AS Masoum, and Peter J Wolfs. Optimal operation of distributed energy storage systems to improve distribution network load and generation hosting capability. *IEEE Transactions on sustainable energy*, 7(1):250–261, 2015.
- [89] Kumarsinh Jhala, Balasubramaniam Natarajan, and Anil Pahwa. Probabilistic voltage sensitivity analysis (pvsa)—a novel approach to quantify impact of active consumers. *IEEE Transactions on Power Systems*, 33(3):2518–2527, 2017.
- [90] John J Grainger. Power system analysis. McGraw-Hill, 1999.
- [91] Kumarsinh Jhala, Balasubramaniam Natarajan, and Anil Pahwa. Probabilistic voltage sensitivity analysis (pvsa) for random spatial distribution of active consumers. In 2018 IEEE Power & Energy Society Innovative Smart Grid Technologies Conference (ISGT), pages 1–5. IEEE, 2018.
- [92] Athanasios Papoulis and S Unnikrishna Pillai. Probability, random variables, and stochastic processes. *Tata McGraw-Hill Education*, 2002.
- [93] J. E. Jackson. A users guide to principal component analysis. New York: Wiley, 1991.
- [94] Mesut E Baran and Felix F Wu. Optimal capacitor placement on radial distribution systems. *IEEE Transactions on power Delivery*, 4(1):725–734, 1989.

[95] HM Khodr, FG Olsina, PM De Oliveira-De Jesus, and JM Yusta. Maximum savings approach for location and sizing of capacitors in distribution systems. *Electric power systems research*, 78(7):1192–1203, 2008.

- [96] . https://niwe.res.in/department_wsom_lidar_raw_data.php.
- [97] Farhad Angizeh, Ali Ghofrani, and Mohsen A Jafari. Dataset on hourly load profiles for a set of 24 facilities from industrial, commercial, and residential end-use sectors. *Mendeley Data*, 1:2020, 2020.
- [98] Maria Luisa Di Silvestre, Eleonora Riva Sanseverino, Gaetano Zizzo, and Giorgio Graditi. An optimization approach for efficient management of ev parking lots with batteries recharging facilities. *Journal of Ambient Intelligence and Humanized Computing*, 4:641–649, 2013.
- [99] MB Arias, M Kim, and S Bae. National household travel survey user's guide. *Appl. Energy*, 195:738–753, 2009.
- [100] Shubh Lakshmi and Sanjib Ganguly. Coordinated operational optimization approach for pv inverters and besss to minimize the energy loss of distribution networks. *IEEE Systems Journal*, 16(1):1228–1238, 2022. doi: 10.1109/JSYST.2020.3041787.
- [101] Sarineh Hacopian Dolatabadi, Maedeh Ghorbanian, Pierluigi Siano, and Nikos D Hatziargyriou. An enhanced ieee 33 bus benchmark test system for distribution system studies. IEEE Transactions on Power Systems, 36(3):2565–2572, 2020.
- [102] . https://cmte.ieee.org/pes-testfeeders/resources/.
- [103] Soroush Shafiee, Mahmud Fotuhi-Firuzabad, and Mohammad Rastegar. Investigating the impacts of plug-in hybrid electric vehicles on power distribution systems. *IEEE transactions on smart grid*, 4(3):1351–1360, 2013.
- [104] David J Narang and Michael Ingram. Highlights of ieee standard 1547-2018. Technical report, National Renewable Energy Lab.(NREL), Golden, CO (United States), 2019.
- [105] MNS Ke-Lin Du. Search and optimization by metaheuristics. (No Title), 2016.
- [106] Seyedali Mirjalili, Seyed Mohammad Mirjalili, and Andrew Lewis. Grey wolf optimizer. Advances in engineering software, 69:46–61, 2014.
- [107] Hany E Farag, Ehab F El-Saadany, and Ravi Seethapathy. A two ways communication-based distributed control for voltage regulation in smart distribution feeders. *IEEE Transactions* on Smart Grid, 3(1):271–281, 2011.
- [108] Md Abdul Masud, Joshua Zhexue Huang, Chenghao Wei, Jikui Wang, Imran Khan, and Ming Zhong. I-nice: A new approach for identifying the number of clusters and initial cluster centres. *Information Sciences*, 466:129–151, 2018.
- [109] Federal Highway Administration. 2009 national household travel survey user's guide, 2011.
- [110] Soroush Shafiee, Mahmud Fotuhi-Firuzabad, and Mohammad Rastegar. Investigating the impacts of plug-in hybrid electric vehicles on power distribution systems. *IEEE Transactions* on Smart Grid, 4(3):1351–1360, 2013. doi: 10.1109/TSG.2013.2251483.
- [111] Solar radiant energy over india, india meteorological dept., ministry earth sciences, new delhi, india. 2009.

[112] Ziyad M Salameh, Bogdan S Borowy, and Atia RA Amin. Photovoltaic module-site matching based on the capacity factors. *IEEE transactions on Energy conversion*, 10(2):326–332, 1995.

- [113] Shubh Lakshmi and Sanjib Ganguly. Coordinated operational optimization approach for pv inverters and besss to minimize the energy loss of distribution networks. *IEEE Systems Journal*, 16(1):1228–1238, 2020.
- [114] Andrea Saltelli, Paola Annoni, Ivano Azzini, Francesca Campolongo, Marco Ratto, and Stefano Tarantola. Variance based sensitivity analysis of model output. design and estimator for the total sensitivity index. Computer physics communications, 181(2):259–270, 2010.
- [115] . https://moeaframework.org/.
- [116] . https://cmte.ieee.org/pes-testfeeders/resources.

Chapter A

Test System Data

A.1 Test Data

A.2 141-Bus System Data

• Base Quantities: 100MVA, 12.47 kV,

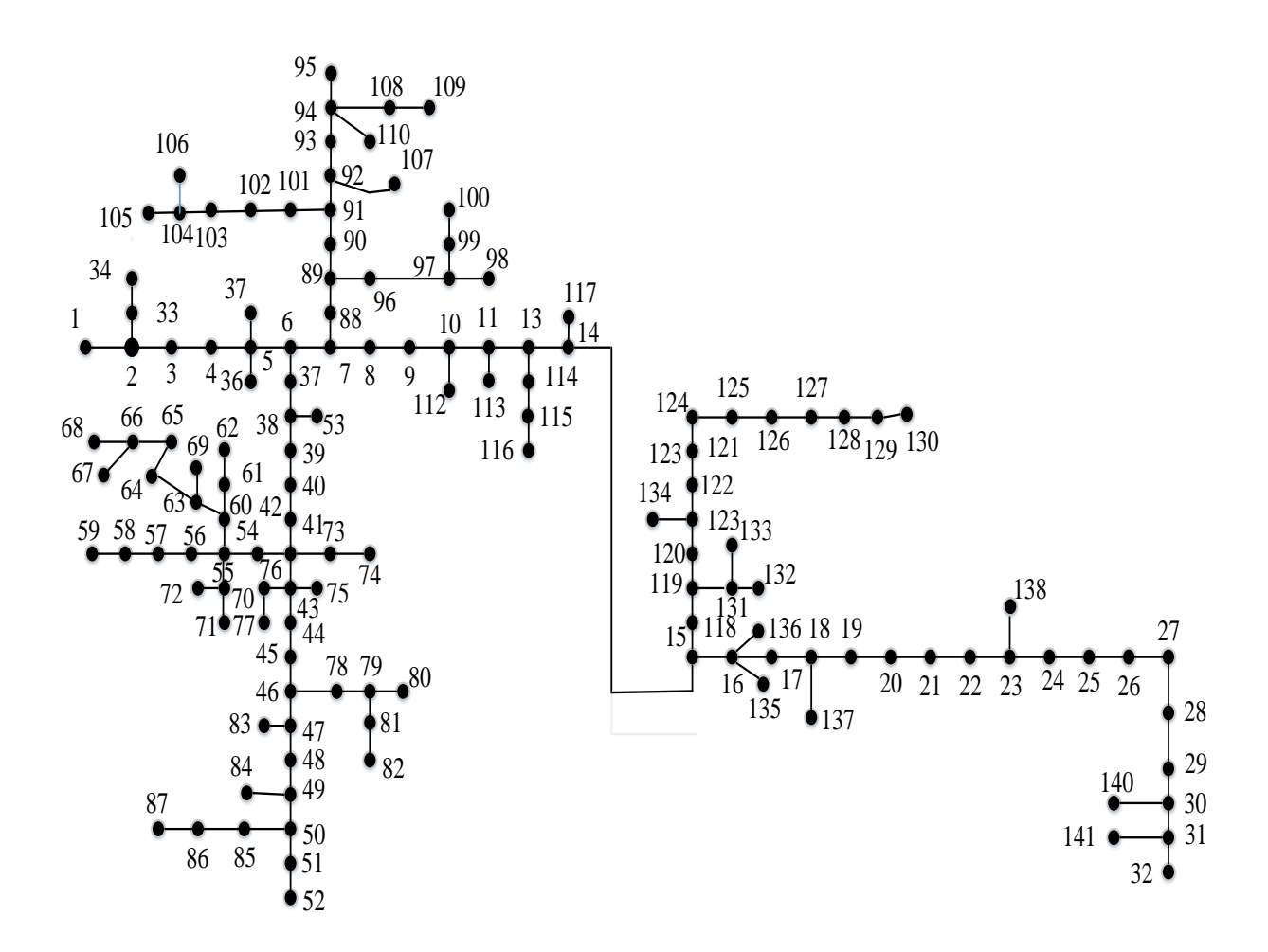


Fig. A.1: 141-bus system

Table A.1: Branch and Bus Data of 141-Bus System

From bus	To bus	R(pu)	X(pu)	Bus number	Load P(pu)	Load Q(pu)
1	2.0	0.003711	0.002630	-	P(pu)	Q(pu)
2	3.0	0.011093	0.007865	1.0	0	0
3	4.0	0.000058	0.000039	2.0	0	0
4	5.0	0.000592	0.000418	3.0	0	0
5	6.0	0.000437	0.000315	4.0	0	0
6	7.0	0.000602	0.000434	5.0	0	0
7	8.0	0.000449	0.000324	6.0	0	0
8	9.0	0.000702	0.000507	7.0	0	0
9	10.0	0.000307	0.000222	8.0	0	0
10	11.0	0.000303	0.000219	9.0	0	0
11	12.0	0.000272	0.000197	10.0	0	0
12	13.0	0.000600	0.000434	11.0	0	0
13	14.0	0.000332	0.000241	12.0	0	0
14	15.0	0.000363	0.000264	13.0	0	0
15	16.0	0.000483	0.000352	14.0	0	0
16	17.0	0.000298	0.000217	15.0	0	0
17	18.0	0.000618	0.000449	16.0	0	0
18	19.0	0.000661	0.000480	17.0	0	0
19	20.0	0.000406	0.000295	18.0	0	0
20	21.0	0.000403	0.000293	19.0	0	0
21	22.0	0.000329	0.000239	20.0	0	0
22	23.0	0.000231	0.000168	21.0	0	0
23	24.0	0.000448	0.000324	22.0	0	0
24	25.0	0.000621	0.000451	23.0	0	0
25	26.0	0.000488	0.000355	24.0	0	0
26	27.0	0.000251	0.000183	25.0	0	0
27	28.0	0.000353	0.000258	26.0	0	0
28	29.0	0.000474	0.000347	27.0	0	0
29	30.0	0.000344	0.000252	28.0	0	0
30	31.0	0.000394	0.000288	29.0	0	0

Table A.2: Branch and Bus Data of 141-Bus System

From bus	To bus	R(pu)	X(pu)	Bus number	Load P(pu)	Load Q(pu)
31	32.0	0.000347	0.000253	30.0	0	0
32	33.0	0.000536	0.000390	31.0	0	0
33	34.0	0.000389	0.000283	32.0	0	0
34	35.0	0.000513	0.000370	33.0	0	0
35	36.0	0.000548	0.000396	34.0	0	0
36	37.0	0.000571	0.000414	35.0	0	0
37	38.0	0.000638	0.000463	36.0	0	0
38	39.0	0.000472	0.000342	37.0	0	0
39	40.0	0.000414	0.000300	38.0	0	0
40	41.0	0.000434	0.000315	39.0	0	0
41	42.0	0.000388	0.000282	40.0	0	0
42	43.0	0.000273	0.000198	41.0	0	0
43	44.0	0.000353	0.000258	42.0	0	0
44	45.0	0.000446	0.000327	43.0	0	0
45	46.0	0.000406	0.000298	44.0	0	0
46	47.0	0.000564	0.000412	45.0	0	0
47	48.0	0.000637	0.000464	46.0	0	0
48	49.0	0.000572	0.000416	47.0	0	0
49	50.0	0.000398	0.000290	48.0	0	0
50	51.0	0.000552	0.000402	49.0	0	0
51	52.0	0.000436	0.000317	50.0	0	0
52	53.0	0.000366	0.000267	51.0	0	0
53	54.0	0.000438	0.000319	52.0	0	0
54	55.0	0.000414	0.000302	53.0	0	0
55	56.0	0.000581	0.000423	54.0	0	0
56	57.0	0.000638	0.000465	55.0	0	0
57	58.0	0.000465	0.000339	56.0	0	0
58	59.0	0.000603	0.000440	57.0	0	0
59	60.0	0.000581	0.000423	58.0	0	0
60	61.0	0.000500	0.000364	59.0	0	0
61	62.0	0.000563	0.000410	60.0	0	0

Table A.3: Branch and Bus Data of 141-Bus System

From bus	To bus	R(pu)	X(pu)	Bus number	Load P(pu)	Load Q(pu)
62	63.0	0.000597	0.000436	61.0	0	0
63	64.0	0.000627	0.000458	62.0	0	0
64	65.0	0.000568	0.000415	63.0	0	0
65	66.0	0.000523	0.000382	64.0	0	0
66	67.0	0.000397	0.000290	65.0	0	0
67	68.0	0.000393	0.000288	66.0	0	0
68	69.0	0.000429	0.000315	67.0	0	0
69	70.0	0.000396	0.000283	68.0	0	0
70	71.0	0.000606	0.000432	69.0	0	0
71	72.0	0.000460	0.000335	70.0	0	0
72	73.0	0.000440	0.000321	71.0	0	0
73	74.0	0.000382	0.000279	72.0	0	0
74	75.0	0.000471	0.000344	73.0	0	0
75	76.0	0.000422	0.000308	74.0	0	0
76	77.0	0.000545	0.000398	75.0	0	0
77	78.0	0.000471	0.000343	76.0	0	0
78	79.0	0.000603	0.000440	77.0	0	0
79	80.0	0.000444	0.000324	78.0	0	0
80	81.0	0.000577	0.000421	79.0	0	0
81	82.0	0.000592	0.000432	80.0	0	0
82	83.0	0.000587	0.000428	81.0	0	0
83	84.0	0.000440	0.000321	82.0	0	0
84	85.0	0.000540	0.000394	83.0	0	0
85	86.0	0.000488	0.000355	84.0	0	0
86	87.0	0.000614	0.000448	85.0	0	0
87	88.0	0.000563	0.000411	86.0	0	0
88	89.0	0.000584	0.000426	87.0	0	0
89	90.0	0.000607	0.000443	88.0	0	0
90	91.0	0.000470	0.000343	89.0	0	0
91	92.0	0.000482	0.000352	90.0	0	0

Table A.4: Branch and Bus Data of 141-Bus System

From bus	To bus	D(pu)	V(pu)	Bus number	Load P(pu)	Load Q(pu)
92	93.0	R(pu) 0.000539	X(pu) 0.000394	91.0	0	Load Q(pu)
93	94.0	0.000539	0.000394	92.0	0	0
93	95.0	0.000409	0.000489	93.0	0	0
95	96.0	0.000528	0.000386	94.0	0	0
96	97.0	0.000379	0.000277	95.0	0	0
97	98.0	0.000408	0.000297	96.0	0	0
98	99.0	0.000497	0.000362	97.0	0	0
99	100.0	0.000509	0.000372	98.0	0	0
100	101.0	0.000476	0.000348	99.0	0	0
101	102.0	0.000456	0.000333	100.0	0	0
102	103.0	0.000562	0.000410	101.0	0	0
103	104.0	0.000581	0.000424	102.0	0	0
104	105.0	0.000417	0.000304	103.0	0	0
105	106.0	0.000526	0.000386	104.0	0	0
106	107.0	0.000486	0.000355	105.0	0	0
107	108.0	0.000458	0.000335	106.0	0	0
108	109.0	0.000532	0.000388	107.0	0	0
109	110.0	0.000472	0.000344	108.0	0	0
110	111.0	0.000474	0.000347	109.0	0	0
111	112.0	0.000589	0.000433	110.0	0	0
112	113.0	0.000400	0.000294	111.0	0	0
113	114.0	0.000533	0.000391	112.0	0	0
114	115.0	0.000386	0.000283	113.0	0	0
115	116.0	0.000395	0.000290	114.0	0	0
116	117.0	0.000517	0.000379	115.0	0	0
117	118.0	0.000595	0.000436	116.0	0	0
118	119.0	0.000565	0.000414	117.0	0	0
119	120.0	0.000621	0.000455	118.0	0	0
120	121.0	0.000405	0.000297	119.0	0	0
121	122.0	0.000361	0.000265	120.0	0	0
			1	I.		

Table A.5: Branch and Bus Data of 141-Bus System

From bus	To bus	R(pu)	X(pu)	Bus number	Load P(pu)	Load Q(pu)
122	123.0	0.000455	0.000334	121.0	0	0
123	124.0	0.000394	0.000288	122.0	0	0
124	125.0	0.000370	0.000270	123.0	0	0
125	126.0	0.000523	0.000382	124.0	0	0
126	127.0	0.000536	0.000390	125.0	0	0
127	128.0	0.000390	0.000283	126.0	0	0
128	129.0	0.000452	0.000334	127.0	0	0
129	130.0	0.000592	0.000437	128.0	0	0
130	131.0	0.000364	0.000269	129.0	0	0
131	132.0	0.000404	0.000298	130.0	0	0
132	133.0	0.000519	0.000380	131.0	0	0
133	134.0	0.000510	0.000373	132.0	0	0
134	135.0	0.000541	0.000395	133.0	0	0
135	136.0	0.000569	0.000415	134.0	0	0
136	137.0	0.000472	0.000344	135.0	0	0
137	138.0	0.000618	0.000449	136.0	0	0
138	139.0	0.000399	0.000290	137.0	0	0
139	140.0	0.000495	0.000362	138.0	0	0
140	141.0	0.003756	0.002662	139.0	0.0425	0.026339
				140.0	0.1275	0.079017
				141.0	0.06375	0.039509

Chapter B

Appendix List of Publications

List of Publications

Journal

- Digamber Kumar, Bibhu Prasad Padhy, "Probabilistic approach to investigate the impact of distributed generation on voltage deviation in distribution system," Electrical Engineering 105, no. 5 (2023): 2621-2636.
- Digamber Kumar, Bibhu Prasad Padhy, "Optimal Selection of Voltage Controlling Parameter in Uncertain Active Distribution Network," in IEEE Transactions on Industry Applications, vol. 60, no. 1, pp. 1576-1588.
- Digamber Kumar, Bibhu Prasad Padhy, "Dual-Stage Cluster-Based Voltage Control For Active Distribution Network With High Penetration of Photovoltaic Distributed," Transactions on Industry Applications (Under Review).
- Digamber Kumar, Bibhu Prasad Padhy, "Partition of Active Distribution Network Using Probabilistic voltage sensitive index by Spectral Clustering," Journal of Modern Power Systems and Clean Energy (Under Review).
- D. Kumar and B. P. Padhy, "Improvement of hosting capacity of active distribution network utilizing optimal placement of BESS," Electric Power Systems Research (Under Review).

Conference Proceeding

- D. Kumar and B. Prasad, "Optimal Selection of Voltage Controlling Parameter in Uncertain Active Distribution Network," 2022 4th International Conference on Energy, Power and Environment (ICEPE), Shillong, India, 2022, pp. 1-6,
- D. Kumar and B. P. Padhy, "Entropy Based Spectral Clustering For Distribution Network With High Penetration of DGs," 2022 22nd National Power Systems Conference (NPSC), New Delhi, India, 2022, pp. 53-58

• D. Kumar and B. P. Padhy, "Group-Based Voltage Control For Distribution System With High Penetration of PVs," 2023 IEEE 3rd International Conference on Smart Technologies for Power, Energy and Control (STPEC), Bhubaneswar, India, 2023, pp. 1-6.